Ecole Centrale de Nantes

MASTER AUTOMATIQUE, ROBOTIQUE, ET INFORMATIQUE APLIQUÉE

"Robotique Avancée"

2012/2013

Thesis Report

Presented by

Marteen Samuel

September, 2013

Stiffness Analysis of The 2-DOF Translation Parallel Manipulator

Jury

Evaluators:	Wisama KHALIL	Professor of Ecole Centrale de Nantes, Nantes
	Philippe WENGER	CNRS Research Director, IRCCyN, Nantes
Supervisors:	Stéphane CARO	CNRS Researcher, IRCCyN, Nantes
	Sébastien BRIOT	CNRS Researcher, IRCCyN, Nantes

Laboratory: Institut de Recherche en Communications et Cybernétique de Nantes

Contents

List of Figures

List of Tables

Abstract

This master thesis deals with the comparison of the planar parallel manipulators in the term of their stiffness. The manipulators under study are the 2-DOF planar parallel manipulators, i.e., the RRRRR and the RPRPR, and the 3-DOF planar parallel manipulators, i.e., the 3-RRR, the 3-RPR, the 3-RPR. The stiffness matrix of each manipulator is calculated based on the Virtual Joint Modeling (VJM) method.

An optimization problem is proposed to determine optimum geometric parameters of the parallel manipulators which minimize the mass in motion and compactness under several specification factors, such as the size of regular dexterous workspace, the deformations, and the passive joint reactions.

The optimal design parameters are used to calculate manipulator's displacements. The results are compared to find the best architecture of planar parallel manipulator that has the best stiffness.

Keywords: Parallel manipulators, Stiffness analysis, Virtual Joint Modeling (VJM) method

Introduction

Context

Over the last decades, robots have become an integral part of industrial sectors, especially in manufacturing process. Based on their mechanical structure, robots are divided into two: the classical structure called serial manipulator and the parallel manipulator. Robots with serial structure can be modeled as an open-loop kinematic chain with several rigid bodies linked together in series by either revolute or prismatic joints driven by actuators [9]. Generally, one end of the chain is attached to a supporting base while the other end is free and attached with a tool to perform tasks or manipulate objects. Meanwhile, a parallel structure robot is defined as a closed-loop kinematic chain whose base and end-effector are connected by several kinematic chains [14].

According to [11], paradigm of parallel robot is defined as hexapod-type robot that has 6-DOF. However, the machine industries recently discover the potential applications of parallel robots with less than 6-DOF called lower mobility parallel robot [10]. These type of robots are very useful to handle simple tasks, such as pick-and-place operation. A lower mobility parallel manipulator has become very interesting topic since it has simple architecture and control system which are related to better speed performance, lower manufacturing and operating cost, and lighter in the total mass.

Nowadays, speed machining, stiffness, acceleration capacities, and payload to weight ratio have become crucial factors in manufacturing process. However, most of serial robots cannot meet those factors. Due to this reason, parallel robots have become a better solution since they offer higher rigidity/stiffness and lower mass/inertia parameters [16]. These features are induced by their specific kinematic structure, which not only resists kinematic chain error manipulation but also allows convenience actuators placement nearer the base [17].

Stiffness analysis has become important evaluation factor since it represents the position and orientation robot accuracy due to external forces and torques. Moreover, [16] defined the stiffness analysis as an evaluation method of the effect of applied external forces and torques on the compliance end-effector displacement, which numerically is defined as "stiffness matrix" K. This matrix gives the relation between displacement

(both translation and rotation displacement) and the static forces/torques causing the transition.

There are several approaches exist for computation of the stiffness matrix, such as the finite element analysis (FEA), the matrix structural analysis (MSA), and the virtual joint method (VJM). However, the stiffness analysis method implemented in this thesis is the virtual joint method taken from the paper of [16]. The method is based on the expansion of the traditional rigid body by adding virtual joints, which describe the elastic deformation of the manipulator components.

The aims of this master thesis are to analyze the stiffness models and to determine optimum structural and geometry parameters of five lower mobility parallel manipulators. The manipulators are divided into two different categories based on number of their degree of freedom. The first category is 2-DOF parallel manipulator that consists of $\underline{\text{R}}\text{RRR}\underline{\text{R}}$ and $\text{R}\underline{\text{P}}\text{R}\underline{\text{P}}\text{R}$ robots. The second category is 3-DOF parallel manipulator that consists of 3-$\underline{\text{R}}$RR, 3-$\underline{\text{R}}$PR, and 3-R$\underline{\text{P}}$R. In addition, at the end of this thesis a stiffness comparison is also conducted to determine the best structure among them.

Organization of the Thesis Report

This thesis report includes mainly four chapters. The first chapter provides the theoretical background about parallel manipulator, their general characteristics, and their types. This chapter also includes the stiffness analysis, especially a details description about virtual joint modeling method which will be used in this research.

The second chapter reviews the manipulator architecture of the five planar parallel manipulators which are under study in this thesis. The inverse geometric models for each manipulator are also explained in this chapter.

The third chapter explains about implementation of Virtual Joint Model (VJM) method for calculating stiffness matrix of each manipulator. At the end of this chapter, The comparisons between the output of VJM model and the RDM6 software for each manipulator are given.

The fourth chapter describes the design optimization problems of each manipulator under study. This chapter introduces the details information regarding objective functions, design parameters and constrain functions. In addition, the optimization results and the comparison results are provided at the end of this chapter.

Eventually, the last chapter presents the important points about this thesis report as the conclusion.

Chapter 1

Theoretical Background

In general, a manipulator is an agent used to *manipulate* objects. The word manipulating means to move, to arrange, or to change something from its initial condition/position. If those two definitions are combined the term of manipulator can be defined as an agent used to change initial condition/position an object. In addition, IFToMM defines a manipulator in the term of robot kinematics as a device for gripping and controlling movement of an object [11].

A manipulator is generated either in the form of serial or parallel based on its structural configuration. A serial manipulator is a manipulator constitutes of a succession of rigid bodies, which are linked together with their successor and predecessor by 1-DOF joint [14]. A famous example of serial manipulator is SCARA robot as shown in figure 1.1. Meanwhile, a parallel manipulator is a mechanism composed by a mobile/moving platform as the end effector and a fixed based, which are linked together by several independent close loop kinematics chains called legs [14], as illustrate in figure 1.2.

Fig. 1.1: Epson SCARA Robot(courtesy Epson)

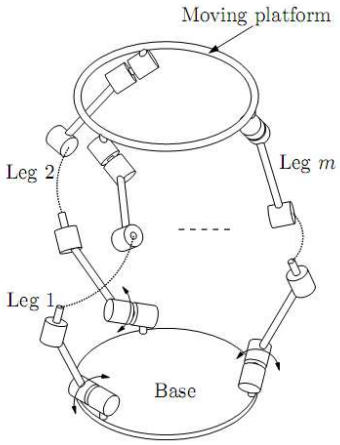

Fig. 1.2: Parallel Kinematic Chains

1.1 Types of Parallel Manipulator

There are three types of parallel manipulator based on its movement:

- *Planar parallel manipulator*: This type of manipulator is composed of a moving platform with 3-DOF or less that generates planar motion with respect to its base. Generally, the generated motions of this type of manipulator are two linear translations and one rotation about the normal of its moving platform plane. An example of this type of manipulator is shown in figure 1.3.

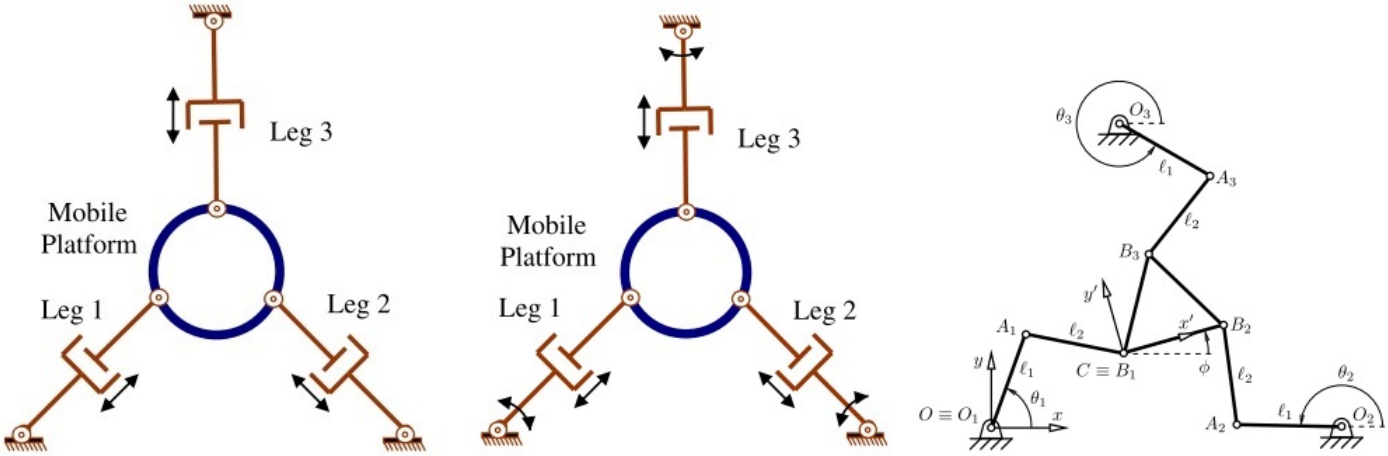

Fig. 1.3: Planar Parallel Manipulator [15],[2]

- *Spatial parallel manipulator*: This type of manipulator is composed of a moving platform which has more than or equal to three degree of freedom. Generally, a spatial parallel manipulator has the ability to move in three dimensional spaces. There are various architecture example of this kind of robot. Here, figure 1.4 is shown an example of spatial parallel manipulator.

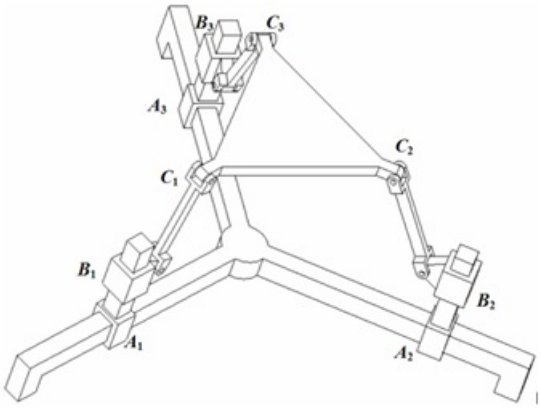

Fig. 1.4: 3-PPRR Spatial Parallel Manipulator [7]

- *Hybrid parallel manipulator*: This type of manipulator commonly is formed by combination of close and open chain mechanisms. The design purpose is to overcome the workspace limitation. An illustration of hybrid parallel manipulator is shown in figure 1.5.

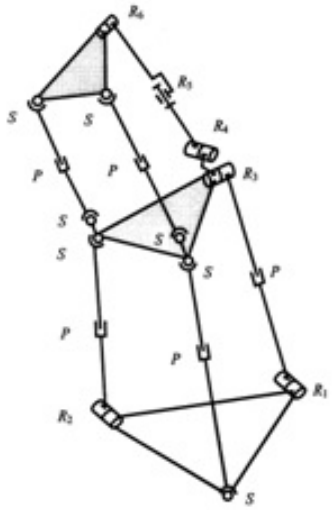

Fig. 1.5: Hybrid Parallel Manipulator [18]

1.2 Lower Mobility Parallel Manipulators

Parallel manipulators have become a better solution for solving many industrial problems, especially on machining process, due to their better stiffness, acceleration capacity, payload to weight ratio, and machining speed [16] in comparison with classical structure of serial manipulators. In fact, not all the industrial task require 6-DOF since as for some simpler tasks 2-DOF translation is sufficient. A lower mobility par-

allel manipulator which posses less than 6-DOF has become better solution because of simpler-built architecture and simpler control system.

Fig. 1.6: Delta Robot (courtesy OMRON)

One of common example of simple industrial task is pick-and-place operation. This operation is usually solved just only less than or equal to 4-DOF (three translations and one rotation). A famous designed pick-and-place manipulator is Delta robot (refer to figure 1.6). This robot has 4-DOF: three translations along x, y, and z axis and one orientation along z axis. Figure 1.7 illustrates 2D version of Delta robot designed by [12] that is built only by revolute joints that are cheaper than prismatic joint in the term of construction cost. This architecture also has low-mass links, which allows the moving platform to achieve a high acceleration.

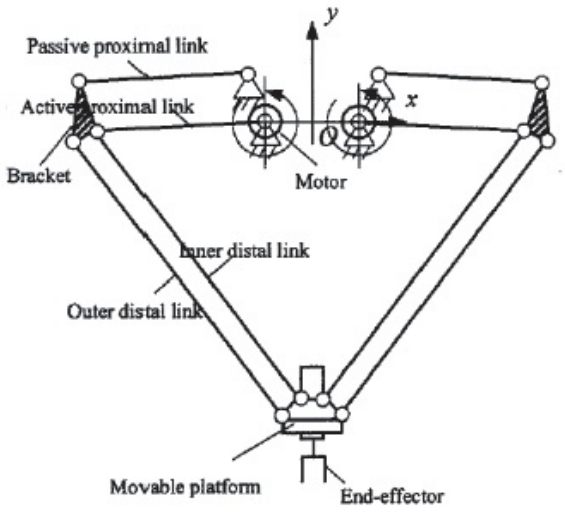

Fig. 1.7: Skecth of 2D version of Delta Robot

1.2.1 Two-DOF Parallel Manipulator

For simpler pick-and-place task, such as moving an object from one conveyor to other working places, a 2-DOF parallel manipulator is sufficient. Generally, for a 2-DOF pick-and-place task, the manipulator handles the object in x and y axis plane with at the same time maintaining the orientation of the object.

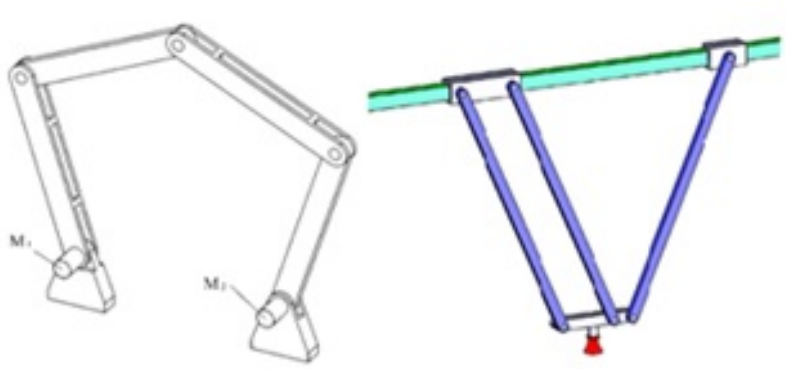

Fig. 1.8: Five-bar and Brogårdh Design of 2-DOF Planar Parallel Manipulator [5]

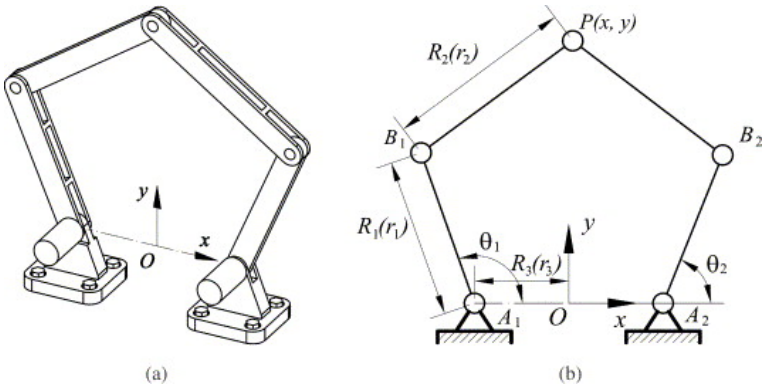

Fig. 1.9: Five-bar of 2-DOF Planar Parallel Manipulator

The most leading 2-DOF planar parallel manipulators [13] are the Five-bar mechanisms with either prismatic or revolute actuators. Figure 1.9 is a famous example of 2-DOF Five-bar planar parallel manipulator. In the case of revolute actuators, the manipulator is composed of five revolute joints, RRRRR, where the actuated joints are fixed to the base, as illustrated in figure 1.9. The output variables of this manipulator is a 2-DOF planar motion of a point on the end effector.

1.2.2 Three-DOF Parallel Manipulator

For some more advanced pick-and-place operations that are composed of 3 different types of motions, a 3-DOF parallel manipulator is needed. A 3-DOF can be built of three configuration types: 2 translation and one orientation motion (2T1R) or 2

orientations and one translation motion (2R1T) or 3 translation motions (3T). Both of them have different advantage. For 3-DOF with 2T1R operation, the manipulator is able to handle an object and not only translate it along x and z axis directions but also rotate it around z axis. For 3-DOF with 3T motions, the manipulator is able to handle an object and translate it along x, y, and z axis directions. While, for 3-DOF with 2R1T operation, the manipulator is able to handle an object, translate it along z axis direction, and rotate it in two different axis. Application example of 3-DOF translation is for rapid tracking because the robot should be able to handle the object to any position in space within its workspace. An example of 3-DOF 2T1R motion is for pick-and-place operation in which the manipulator can handle an object in the x and z planes, and change its orientation in z axis before placing it in somewhere within the workspace area, such as figure 1.10.

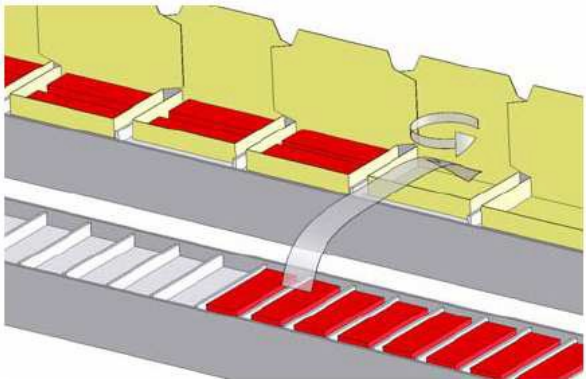

Fig. 1.10: The 2T1R Pick-and-Place Motions

Examples of planar parallel manipulator architectures with 3-DOF 2T1R are 3-RRR, 3-RPR, or even 3-PRR manipulator. Those three manipulators are distinguished by the fact that they own simple architecture and are also simple to control. But, they posses weakness to carry out a large payload whose weight is normal to the plane of motion [6]. Figure 1.11 shows an example of 3-RRR manipulator called The Agile Eye developed for rapid camera orientate by Laval University.

1.3 Stiffness Analysis of Virtual Joint Method

Stiffness analysis aims to evaluate the effect of the applied external forces and torques on the compliance displacement of the end-effector, which is numerically defined as *stiffness matrix* K. The matrix indicates the relation between displacement (both translation and rotation) and the static forces/torques causing the transition [16]. The stiffness depends on the direction of forces or torques on the manipulator configuration.

There are several approaches exist to calculate the *stiffness matrix* that depend on

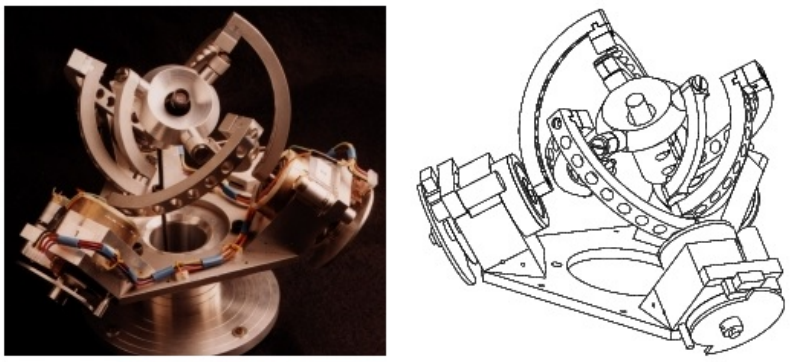

Fig. 1.11: The Agile Eye Manipulator

the modeling assumption and computational technique:

- *Finite element analysis* (FEA)
- *Matrix structural analysis* (MSA)
- *Virtual joint method* (VJM)

In this study, the calculation of *stiffness matrix* is done by a new method proposed by [16]. This method is built based on a multidimensional lumped-parameter model (VJM) that replaces the link flexibility by localize 6-DOF virtual spring that describe both the linear/rotation deflection and coupling between them.

1.3.1 Methodology

Let ${}^{j}T^{i}_{j+1}$ be denoted as a transformation matrix from frame j to frame $j+1$ for ith leg of the manipulator. Let us take Five-bar manipulator (see figure 1.12) as an example. Each kinematic chain of the $\underline{\text{R}}\text{RRR}\underline{\text{R}}$ can be considered as a serial architecture as shown in figure 1.13. The transformation matrix from origin O to the end-effector E, in rigid case is written as:

$$ {}^{0}\mathbf{T}^{i}_{E} = {}^{0}\mathbf{T}^{i}_{B}.{}^{B}\mathbf{T}^{i}_{1}.{}^{1}\mathbf{T}^{i}_{2}.{}^{2}\mathbf{T}^{i}_{3}.{}^{3}\mathbf{T}^{i}_{4}.{}^{4}\mathbf{T}^{i}_{E} \tag{1.1} $$

where i = 1,2. In this equation, R_z represents the rotation joint at z axis and the actuator is denoted as $\underline{R}_z$.

In the flexible case, deformation of kinematic chain's components will case small displacement from rigid position. Therefore, an additional term have to introduce while defining the kinematic chain's transformation matrix to describe this phenomena [16]. Let denote $\delta\mathbf{v}^{i}_{j}$ as small displacement from frame j to frame $j+1$ in 3 axes, and is

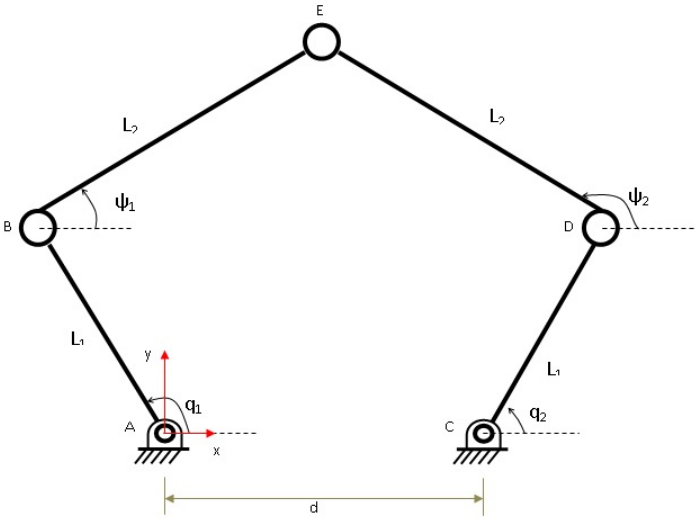

Fig. 1.12: Five-bar Manipulator Model

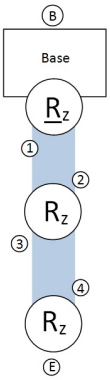

Fig. 1.13: Schematic Diagram of a Five-bar Robot

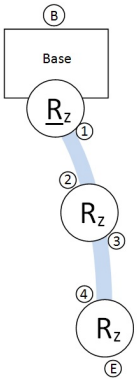

Fig. 1.14: Flexible Model of a Five-bar Robot

written as:

$$\delta \mathbf{v}_j^i = \begin{bmatrix} \delta \mathbf{p}_j^i \\ \delta \varphi_j^i \end{bmatrix} \tag{1.2}$$

where $\mathbf{p}_j^i = [p_{jx}^i, p_{jy}^i, p_{jz}^i]^T$ represents the linear displacement of frame j origin to frame *j+1* origin, and $\varphi_j^i = [\varphi_{jx}^i, \varphi_{jy}^i, \varphi_{jz}^i]^T$ represent the small rotation displacement taking frame j into frame *j+1*. Moreover, it is assumed that the displacement is close to zero where $\sin(\varphi) \approx \varphi$ and $\cos(\varphi) \approx 1$. The product of six transformation matrices (three translations and three rotations) for all the small displacement, $\mathbf{V}_j^i$, is written as:

$$\mathbf{V}_j^i = \begin{bmatrix} 1 & -\varphi_{jz}^i & \varphi_{jy}^i & p_{jx}^i \\ \varphi_{jz}^i & 1 & -\varphi_{jx}^i & p_{jy}^i \\ -\varphi_{jy}^i & \varphi_{jx}^i & 1 & p_{jz}^i \\ 0 & 0 & 0 & 1 \end{bmatrix} \tag{1.3}$$

Therefore, matrix $\mathbf{V}_j^i$ is considered as 6-DOF virtual joint with small displacement in three translations and three rotations. Then, matrix $\mathbf{V}_j^i$ is inserted between the transformation matrices where deflections happen as virtual spring model. Based on the previous kinematic chain, the locations to introduce small displacement are shown as:

1. Between frame 1 and 2: As the revolute joint is an actuator, $\mathbf{V}_{1a}^i$ is introduced to describe the displacement caused by *control loop stiffness*. This *control loop stiffness* will only influence the rotation about z axis. Hence, $\delta \mathbf{v}_{1a}^i$ can reduce to single parameter which result $\delta \mathbf{v}_{1a}^i = \varphi_{1z}$. Besides, $\mathbf{V}_{1b}^i$ is introduce to describe the displacement in three translations and rotations caused by *actuator mechanical stiffness*.

2. frame 2 and frame 3: $\mathbf{V}_2^i$ represents the translation and rotation deflection of the first link.

3. Between frame 4 and frame E: Similar to the first link , the second link deflections are describe by $\mathbf{V}_4^i$ introduced into the kinematic chain.

Hence, the new transformation matrix for the flexible model can be written as:

$${}^0\mathbf{T}_E^i = {}^0\mathbf{T}_B^i . {}^B\mathbf{T}_1^i . \mathbf{V}_1^i . {}^{1'}\mathbf{T}_2^i . \mathbf{V}_2^i . {}^{2'}\mathbf{T}_3^i . {}^3\mathbf{T}_4^i . \mathbf{V}_4^i . {}^{4'}\mathbf{T}_E^i \tag{1.4}$$

where $\mathbf{V}_1^i = \mathbf{V}_{1a}^i . \mathbf{V}_{1b}^i$

1.3.2 Differential Kinematic Model

Differential kinematic model describing relations between the end-effector location and small variations in the joint variables [16]. The general equation of differential kinematic model for each ith kinematic chain is:

$$\delta \mathbf{t}_i = \mathbf{J}^i_\theta . \delta \boldsymbol{\theta}_i + \boldsymbol{J}^i_q . \delta \boldsymbol{q}_i \tag{1.5}$$

where $\delta \mathbf{t}_i = [\delta \mathbf{p}^i_E, \delta \varphi^i_E]^T$ represents end-effector translation, $\delta \mathbf{p}^i_E = [\delta p^i_{E_x}, \delta p^i_{E_y}, \delta p^i_{E_z}]^T$, and rotation, $\delta \boldsymbol{\varphi}^i_E = [\delta \varphi^i_{E_x}, \delta \varphi^i_{E_y}, \delta \varphi^i_{E_z}]^T$, displacement with respect to the Cartesian axes. All passive joints variations in a kinematic chain are located in $\boldsymbol{q}_i$. The actuated joint is represent by displacement variables in $\mathbf{J}^i_\theta$.

1.3.3 Displacement Characteristic

The deformation of the link or the control stiffness of the actuator results in the frame displacements. These displacements are modeled individually by its response to the applied force. In general, the *Hooke's Law* defines:

$$F = K \ . \ x \tag{1.6}$$

where F is external forces, K is stiffness matrix, and x is displacement. When the displacement is expressed as a functional of forces, then compliance coefficient, $\mathbf{C}$, is introduced, and is equal to the inverse of stiffness, $\mathbf{K}^{-1}$. The compliance matrices of the intermediate legs and the ith link of the moving platform are calculated by means of the stiffness model of a cantilever beam, namely

$$K^{i-1} = \begin{bmatrix} L/EA & 0 & 0 & 0 & 0 & 0 \\ 0 & L^2/3LI_z & 0 & 0 & 0 & L^2/2LI_z \\ 0 & 0 & L^3/3LI_y & 0 & -L^2/2LI_y & 0 \\ 0 & 0 & 0 & L/GI_x & 0 & 0 \\ 0 & 0 & -L^2/2LI_y & 0 & L/EI_y & 0 \\ 0 & L^2/2LI_z & 0 & 0 & 0 & L/EI_z \end{bmatrix} \tag{1.7}$$

L is the length of the beam. A is the cross section area of the beam. $I_z = I_y$ is the polar moment of inertia about y and z axes. $I_x = I_z + I_y$ is the polar moment of inertia about the longitudinal axis of the beam. E is the Young modulus of the material and G is its shear modulus.

1.3.4 Kineostatic and Stiffness Model

Equation 1.6 can be interpreted as the definition of virtual forces within the kinematic chain. Consider the Five-bar manipulator's leg, the virtual reactions at each location of frame displacement are expressed as:

$$\begin{aligned} \tau^i_{\theta_1} &= K^i_{ctr}.\delta v^i_{1a} \\ [\tau^i_{\theta_2}, \ldots, \tau^i_{\theta_7}]^T &= \boldsymbol{K}^i_{act}.\delta \boldsymbol{v}^i_{1b} \\ [\tau^i_{\theta_8}, \ldots, \tau^i_{\theta_{13}}]^T &= \boldsymbol{K}^i_{l1}.\delta \boldsymbol{v}^i_{2} \\ [\tau^i_{\theta_{14}}, \ldots, \tau^i_{\theta_{19}}]^T &= \boldsymbol{K}^i_{l2}.\delta \boldsymbol{v}^i_{3} \end{aligned} \tag{1.8}$$

$\boldsymbol{K}^i_{act}$, $\boldsymbol{K}^i_{l1}$, $\boldsymbol{K}^i_{l2}$ are 6x6 matrices. K^i_{ctr} and $\boldsymbol{K}^i_{act}$ are the control loop stiffness and actuator mechanical stiffness respectively while $\boldsymbol{K}^i_{l1}$ and $\boldsymbol{K}^i_{l2}$ are the link stiffness. For convenience, the virtual reactions for each component are collected into:

$$\boldsymbol{\tau}^i_\theta = \mathbf{K}^i_\theta.\delta\theta^i \tag{1.9}$$

where $\mathbf{K}^i_\theta = diag(K^i_{ctr}, \boldsymbol{K}^i_{act}, \boldsymbol{K}^i_{l1}, \boldsymbol{K}^i_{l2})$ and $\boldsymbol{\tau}^i_\theta = [\tau^i_{\theta_1}, \ldots, \tau^i_{\theta_{19}}]^T$. Similarly, for passive joints within the same kinematic chain, the passive reactions are expressed as:

$$\boldsymbol{\tau}^i_q = \tau^i_{q1} = 0 \tag{1.10}$$

Assume that forces $\mathbf{f}^i$ is applied at the end of the kinematic chain and result in a displacement $\delta\mathbf{x}^i$. Then the work done by the external forces is equal to the virtual work done by virtual reactions, since there is no reaction from passive joint. Hence, the magnitude of work done can be expressed as:

$$\begin{aligned} \mathbf{f}^{i^T}.\delta\mathbf{x}^i &= \boldsymbol{\tau}^{i^T}_\theta.\delta\boldsymbol{\theta}^i \\ (\mathbf{f}^{i^T}\mathbf{J}^i_\theta).\delta\boldsymbol{\theta}^i + (\mathbf{f}^{i^T}\mathbf{J}^i_q).\delta\mathbf{q}^i &= \boldsymbol{\tau}^{i^T}_\theta.\delta\boldsymbol{\theta}^i \end{aligned} \tag{1.11}$$

Since there are no reaction in passive joints, the equilibrium condition may written as:

$$\begin{aligned} \mathbf{J}^i_\theta\mathbf{f}^{i^T} &= \boldsymbol{\tau}^{i^T}_\theta \\ \mathbf{J}^i_q\mathbf{f}^{i^T} &= \mathbf{0} \end{aligned} \tag{1.12}$$

Hence, the elastostatic model is completed with four matrix equations that consist of equation 1.5, equation 1.8, equation 1.10, and equation 1.12, where $\mathbf{f}^i$ or $\delta\mathbf{x}^i$ are treated as known, while other variables are unknown. A unique solution for the system given $\mathbf{f}^i$ might not possible as the kinematic chain is separated from the parallel manipulator, and gains some degree of freedoms. However, when$_\delta\mathbf{x}^i$ is known, both external forces,

$\mathbf{f}^i$, and internal variables $\boldsymbol{\tau}_\theta^i, \delta\boldsymbol{\theta}^i$, and $\delta\mathbf{q}^i$, can be calculated

The model can be reduced into two equations by eliminating the $\delta\boldsymbol{\theta}^i$ using equation 1.5, equation 1.8, and equation 1.12. The system equations are rewritten as:

$$\begin{bmatrix} \mathbf{S}_\theta^i & \mathbf{J}_q^i \\ \mathbf{J}_q^{iT} & \mathbf{0} \end{bmatrix} \begin{bmatrix} \mathbf{f}^i \\ \delta\mathbf{q}^i \end{bmatrix} = \begin{bmatrix} \delta\mathbf{x}^i \\ \mathbf{0} \end{bmatrix} \tag{1.13}$$

where $\mathbf{S}_\theta^i = \mathbf{J}_\theta^i[\mathbf{K}_\theta]^{-1}\mathbf{J}_\theta^{iT}$. Consequently, inverting the first left-hand side matrix gives the Cartesian stiffness of the kinematic chain, $\mathbf{K}_C^i$, and the passive joint displacement, $\delta\mathbf{q}$ of the kinematic chain. Let $\mathbf{H}^i$ be denoted as the result of inverting the first left-hand side matrix. The Cartesian stiffness is a 6x6 sub-matrix located at top left hand corner of $\mathbf{H}^i$ matrix, which corresponded to $\mathbf{S}_\theta^i$ location. Inverse of the $\mathbf{H}^i$ matrix depends on the rank of matrix $\mathbf{J}_q$. Matrix $\mathbf{J}_\theta$ is non-singular if six displacement variables are introduced in at least one location. Hence, when $\mathbf{J}_q$ is singular, it physically means that the kinematic chain is in singular configuration resulting no unique solution for the passive joint, $\mathbf{q}^i$.

After obtaining the Cartesian stiffness matrix, $\mathbf{K}_C^i$ for all manipulator's legs individually, the stiffness for the entire manipulator is determine as the summation of all kinematic chain stiffness matrices

$$\mathbf{K}_m = \sum_{i=1}^{n} \mathbf{K}_C^i \tag{1.14}$$

where n is the number of manipulator's legs.

Chapter 2

Manipulators Architecture

There are five manipulators under study which are distinguished by their number of DOF. The first group is the manipulators with 2-DOF and the second group is the manipulators with 3-DOF. The 2-DOF manipulators are RRRRR and RPRPR. The 3-DOF manipulators are 3-RRR, 3-RPR, and 3-RPR. The goals of this chapter are to provide explanation of manipulators architectures and their inverse geometric models.

2.1 Architecture of RRRRR

There are in total five revolute joints are installed in this manipulator (refer to figure 2.1). From five revolute joints, two of them are attached to the base (Point A and C) as the actuators. The others are considered as passive revolute joints. This manipulator is intended to position the end effector located in point E in the plane of motion, the xy plane.

The inputs of this manipulator are rotation angle of two revolute joints q_1 and q_2. Moreover, the Cartesian coordinates of point E, i.e., x_E and y_E are the output variables. The actuators are placed aligned along the x axis of the reference frame. Distance between the two actuators is denoted as d. Rotation angles of the passive joints are denoted as Ψ_1, Ψ_2, and Ψ_3. Point O is the origin of reference frame and overlapping with point A.

Several important parameters describing the manipulator geometry according to figure 2.1:

- L_1: length of first intermediate links, i.e., L_1 = AB = CD;
- L_2: length of second intermediate links, i.e., L_2 = BE = DE;
- r_{out}: the cross section outer radius for both first and second intermediate links;
- r_{in}: the cross section inner radius for both first and second intermediate links;

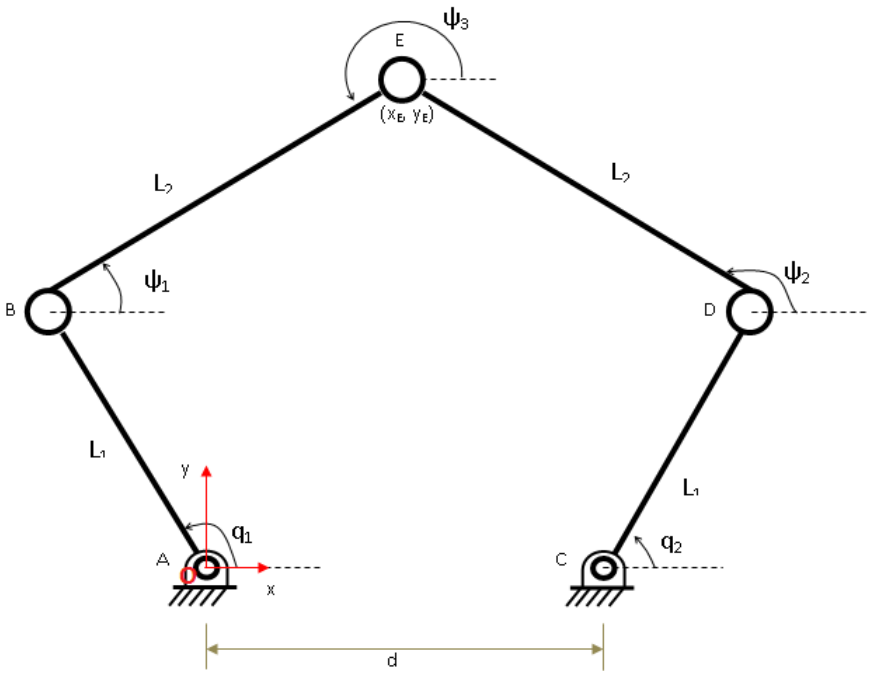

Fig. 2.1: RRRRR Manipulator Geometry Model

2.1.1 Inverse Geometric Model of RRRRR Manipulator

Based on RRRRR model in figure 2.1, the close loop vector equations can be written as:

$$\vec{OE} = \vec{OA} + \vec{AB} + \vec{BE} \tag{2.1}$$

$$\vec{OE} = \vec{OC} + \vec{CD} + \vec{DE} \tag{2.2}$$

Equation 2.1 and equation 2.2 can be expressed algebraically as:

$$\begin{pmatrix} x_E \\ y_E \end{pmatrix} = \begin{pmatrix} x_A \\ y_A \end{pmatrix} + \begin{pmatrix} L_1 \cos q_1 \\ L_1 \sin q_1 \end{pmatrix} + \begin{pmatrix} L_2 \cos \Psi_1 \\ L_2 \sin \Psi_1 \end{pmatrix} \tag{2.3}$$

$$\begin{pmatrix} x_E \\ y_E \end{pmatrix} = \begin{pmatrix} x_C \\ y_C \end{pmatrix} + \begin{pmatrix} L_1 \cos q_2 \\ L_1 \sin q_2 \end{pmatrix} + \begin{pmatrix} L_2 \cos \Psi_2 \\ L_2 \sin \Psi_2 \end{pmatrix} \tag{2.4}$$

Coordinate of point A is (0, 0) because it overlaps with the origin point of reference frame. On the other hand, coordinate of point C is (d, 0).

The inverse geometric models are expressed as follow:

$$q_1 = 2 \tan^{-1} \left(\frac{-B_1 \pm \sqrt{A_1^2 + B_1^2 + C_1^2}}{C_1 - A_1} \right) \tag{2.5}$$

with,

$$A_1 = -2x_E L_1$$
$$B_1 = -2y_E L_1$$
$$C_1 = x_E^2 + y_E^2 + L_1^2 - L_2^2$$

$$q_2 = 2\tan^{-1}\left(\frac{-B_2 \pm \sqrt{A_2^2 + B_2^2 + C_2^2}}{C_2 - A_2}\right) \tag{2.6}$$

with,

$$A_2 = -2(d - x_E)L_1$$
$$B_2 = -2y_E L_1$$
$$C_2 = x_E^2 + y_E^2 + L_1^2 - L_2^2 - 2x_E d$$

It should be noted that if $A_i^2 + B_i^2 \leq C_i^2, i = 1, 2$, the system can not assembly.

2.2 RPRPR Architecture

A RPRPR manipulator is composed by two prismatic joints and three revolute joints as shown in figure 2.2. The prismatic joints are acted as the actuators. From three revolute joints, two of them are attached to the base (Point A and C), and the last is acted as the end-effector (Point C). The plane of motion of this manipulator is in the xy plane.

The displacements of the two prismatic joints, i.e., r_1 and r_2 are the input variables whereas the Cartesian coordinates of point E, i.e., x_E and y_E is the output variable. The revolute joints attached to the base are placed aligned along the x axis of reference frame. Distance between them is denoted as d. Rotation angles of the passive joints are denoted as θ_1, θ_2, and θ_3. Point O is the origin of reference frame.

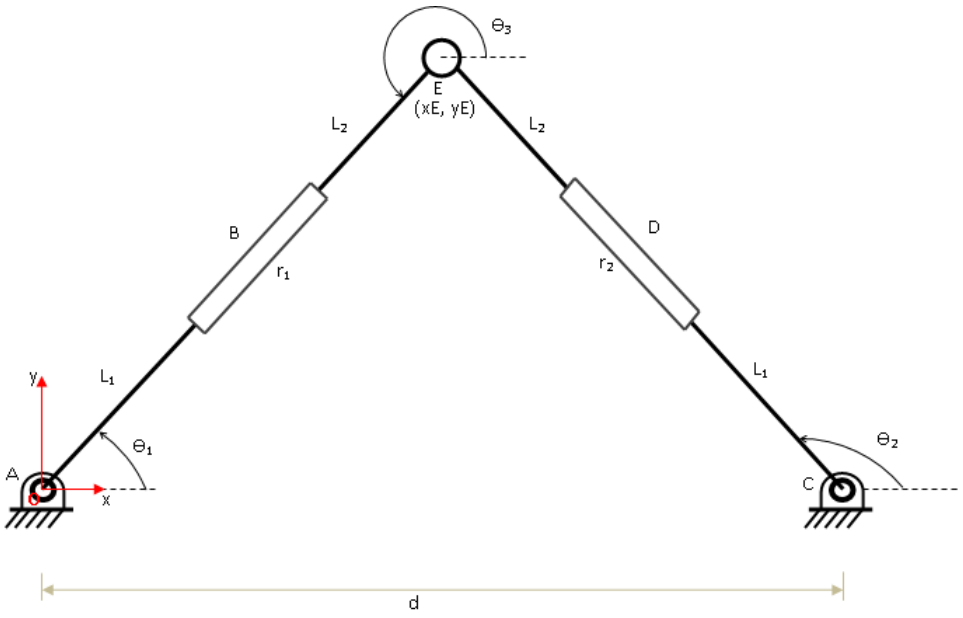

Fig. 2.2: RPRPR Manipulator Geometry Model

The parameters describing manipulator geometry are:

- L_1: length of first intermediate links, i.e., L_1 = AB - $(\frac{r_1}{2})$ = CD - $(\frac{r_2}{2})$;
- L_2: length of second intermediate links, i.e., L_2 = BE - $(\frac{r_1}{2})$ = DE - $(\frac{r_2}{2})$;
- r_{out}: the cross section outer radius of both intermediate links;
- r_{in}: the cross section inner radius of both intermediate links

2.2.1 Inverse Geometric Model of RPRPR Manipulator

As shown in figure 2.2, the close loop vector equations of this manipulator can be written as:

$$\vec{OE} = \vec{OA} + \vec{AB} + \vec{BE} \tag{2.7}$$

$$\vec{OE} = \vec{OC} + \vec{CD} + \vec{DE} \tag{2.8}$$

Equation 2.7 and equation 2.8 can be expressed algebraically as:

$$\begin{pmatrix} x_E \\ y_E \end{pmatrix} = \begin{pmatrix} L_{T_1} & \cos\theta_1 \\ L_{T_1} & \sin\theta_1 \end{pmatrix} \tag{2.9}$$

$$\begin{pmatrix} x_E \\ y_E \end{pmatrix} = \begin{pmatrix} d \\ 0 \end{pmatrix} + \begin{pmatrix} L_{T_2} & \cos\theta_2 \\ L_{T_2} & \sin\theta_2 \end{pmatrix} \tag{2.10}$$

with,

$$L_{T_1} = L_1 + L_2 + r_1$$
$$L_{T_2} = L_1 + L_2 + r_2$$

The inverse geometric models of R$\underline{\text{P}}$R$\underline{\text{P}}$R are expressed as follow:

$$r_1 = \sqrt{x_E^2 + y_E^2} \; - (L_1 + L_2) \tag{2.11}$$

$$r_2 = \sqrt{(x_E - d)^2 + y_E^2} \; - (L_1 + L_2) \tag{2.12}$$

2.3 3-$\underline{\text{R}}$RR Architecture

The 3-$\underline{\text{R}}$RR manipulator with three identical chains is shown in figure 2.3. Each of the kinematic chains is the RRR-type and consists of three revolute joints. The first revolute joints of each legs are acted as actuators and attached to the base at point P, Q, and R. This manipulator is intended to position and to orient the equilateral triangle-shaped platform ABC in the plane of motion. The geometric center of the moving platform ABC is denoted by P, which is the operation point of the manipulator.

The rotation angles of the three actuate revolute joints, i.e., θ_1, θ_2, and θ_3, are the input variables while the Cartesian coordinates of point P, i.e., x_p and y_p, and the orientation of the moving platform, i.e., Φ, are the output variables. The base-platform is also an equilateral triangle with vertices P, Q, and R. Point O is the origin of reference frame. Below are the parameters describing the 3-$\underline{\text{R}}$RR manipulator geometry:

- L_1: length of first intermediate links, i.e., L_1 = PD = QE = RF;
- L_2: length of second intermediate links, i.e., L_2 = DA = EB = FC;
- a: a side length of the triangle-shaped base platform PQR, i.e., a = PQ = QR = RP;
- h: a side length of the triangle-shaped end-effector platform ABC, i.e., h = AB = BC = CA;
- r_{out}: the cross section outer radius of both first and second intermediate links;
- r_{in}: the cross section inner radius of both first and second intermediate links;
- r_{Tool}: the cross section radius of end-effector platform link

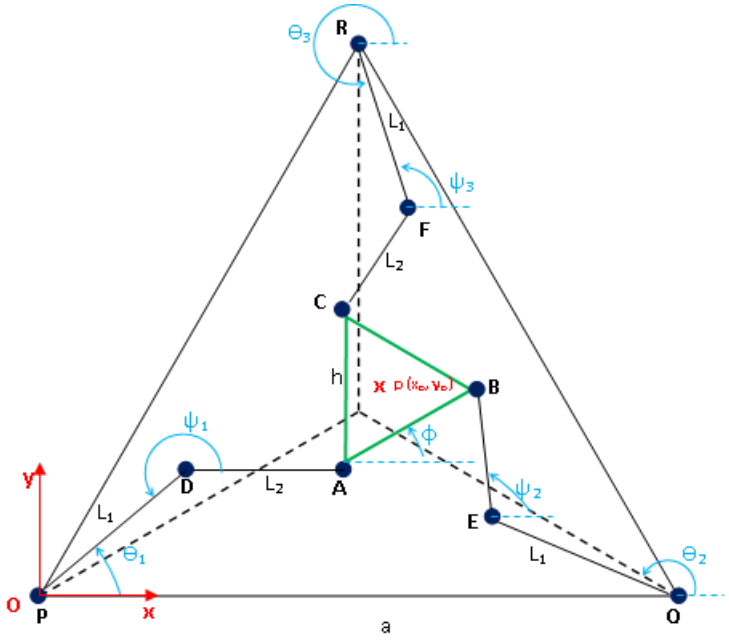

Fig. 2.3: 3-RRR Manipulator Geometry Model

2.3.1 Inverse Geometric Model of 3-RRR Manipulator

Knowing the geometric parameters of the mechanism, i.e., L_1, L_2, a, and h, its Inverse Geometric Model (IGM) gives relation between the actuators displacement,θ_1, θ_2, and θ_3, and the moving platform pose, i.e., x_p, y_p, and Φ.

Having the value of the moving platform pose, the coordinates of the vertices A, B, and C can be expressed as following:

$$\begin{cases} x_A = x_p - \frac{h}{\sqrt{3}} \cos(\phi + \frac{\pi}{6}) \\ y_A = y_p - \frac{h}{\sqrt{3}} \sin(\phi + \frac{\pi}{6}) \end{cases} \tag{2.13}$$

$$\begin{cases} x_B = x_A + h \cos\phi \\ y_B = y_A + h \sin\phi \end{cases} \tag{2.14}$$

$$\begin{cases} x_C = x_A + h \cos(\phi + \frac{\pi}{3}) \\ y_C = y_A + h \sin(\phi + \frac{\pi}{3}) \end{cases} \tag{2.15}$$

The close loop vector equations of this manipulator can be written as:

$$\vec{OA} = \vec{OP} + \vec{PD} + \vec{DA} \tag{2.16}$$

$$\vec{OB} = \vec{OQ} + \vec{QE} + \vec{EB} \tag{2.17}$$

$$\vec{OC} = \vec{OR} + \vec{RF} + \vec{FC} \tag{2.18}$$

Equations 2.16, equation 2.17, and equation 2.18 can be expressed algebraically as:

$$\begin{pmatrix} x_A \\ y_A \end{pmatrix} = \begin{pmatrix} x_p \\ y_p \end{pmatrix} + \begin{pmatrix} L_1 \cos\theta_1 \\ L_1 \sin\theta_1 \end{pmatrix} + \begin{pmatrix} L_2 \cos(\theta_1 + \Psi_1) \\ L_2 \sin(\theta_1 + \Psi_1) \end{pmatrix} \tag{2.19}$$

$$\begin{pmatrix} x_B \\ y_B \end{pmatrix} = \begin{pmatrix} x_Q \\ y_Q \end{pmatrix} + \begin{pmatrix} L_1 \cos\theta_2 \\ L_1 \sin\theta_2 \end{pmatrix} + \begin{pmatrix} L_2 \cos(\theta_2 + \Psi_2) \\ L_2 \sin(\theta_2 + \Psi_2) \end{pmatrix} \tag{2.20}$$

$$\begin{pmatrix} x_C \\ y_C \end{pmatrix} = \begin{pmatrix} x_R \\ y_R \end{pmatrix} + \begin{pmatrix} L_1 \cos\theta_3 \\ L_1 \sin\theta_3 \end{pmatrix} + \begin{pmatrix} L_2 \cos(\theta_3 + \Psi_3) \\ L_2 \sin(\theta_3 + \Psi_3) \end{pmatrix} \tag{2.21}$$

with

$$\begin{pmatrix} x_Q \\ y_Q \end{pmatrix} = \begin{pmatrix} a \\ 0 \end{pmatrix}$$

$$\begin{pmatrix} x_R \\ y_R \end{pmatrix} = \begin{pmatrix} a\ \cos(\frac{\pi}{3}) \\ a\ \sin(\frac{\pi}{3}) \end{pmatrix}$$

The inverse geometric models of 3-RRR manipulator are expressed as:

$$\theta_1 = 2\tan^{-1}\left(\frac{-B_1\ \pm\ \sqrt{A_1^2 + B_1^2 + C_1^2}}{C_1 - A_1}\right) \tag{2.22}$$

with,

$$A_1 = -2x_A L_1$$
$$B_1 = -2y_A L_1$$
$$C_1 = x_A^2 + y_A^2 + L_1^2 - L_2^2$$

$$\theta_2 = 2\tan^{-1}\left(\frac{-B_2\ \pm\ \sqrt{A_2^2 + B_2^2 + C_2^2}}{C_2 - A_2}\right) \tag{2.23}$$

with,

$$A_2 = -2L_1(x_B - x_Q)$$
$$B_2 = -2L_1(y_B - y_Q)$$
$$C_2 = x_B^2 + y_B^2 + L_1^2 - L_2^2 + x_Q^2 + y_Q^2 - 2(x_B x_Q + y_B y_Q)$$

$$\theta_3 = 2\tan^{-1}\left(\frac{-B_3 \pm \sqrt{A_3^2 + B_3^2 + C_3^2}}{C_3 - A_3}\right) \tag{2.24}$$

with,

$$\begin{aligned} A_3 &= -2L_1(x_C - x_R) \\ B_3 &= -2L_1(y_C - y_R) \\ C_3 &= x_C^2 + y_C^2 + L_1^2 - L_2^2 + x_R^2 + y_R^2 - 2(x_C x_R + y_C y_R) \end{aligned}$$

For equations 2.22, 2.23, and 2.24, the following constraint should be satisfied

$$\forall x, y, s.t.\ A_i^2 + B_i^2 \geq C_i^2, i = 1, 2, 3$$

2.4 3-RPR Architecture

The geometric model of the 3-RPR manipulator is shown in figure 2.4. The manipulator has three identical chains. Each chain is the RPR-type and consist of one prismatic joint and two revolute joints. The first revolute joints of each chain are actuated and attached to the base at point P, Q, and R. This manipulator has 3-DOF which are two translations and one orientation in the plane of motion. The shape of both the base and the end-effector platforms is the equilateral triangle.

The rotation angles of the three actuated revolute joints attached to the base are denoted as θ_1, θ_2, and θ_3. These rotation angles are the input variables of this manipulator. While, the output variables are the Cartesian coordinate of point P, i.e., x_p, and y_p, and orientation of the moving platform, i.e., Φ. Points P, Q, and R are the vertices of triangle-shape base platform, and points A, B, and C are the vertices of triangle-shape end-effector platform. Point O is the origin of reference frame.

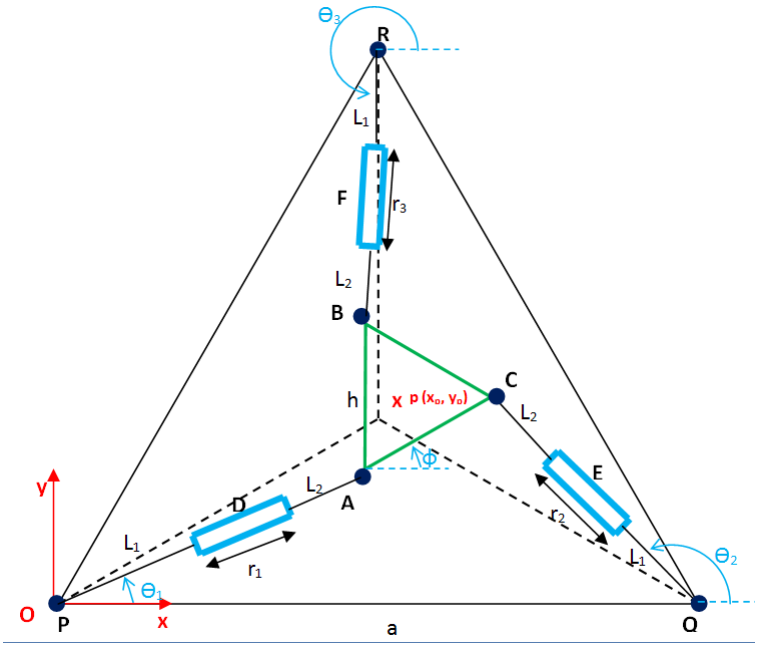

Fig. 2.4: 3-RPR Manipulator Geometry Model

Here are the parameters describing manipulator geometry:

- L_1: length of first intermediate links, i.e., L_1 = PD - $(\frac{r_1}{2})$ = QE - $(\frac{r_2}{2})$ = RF - $(\frac{r_3}{2})$;
- L_2: length of second intermediate links, i.e., L_2 = DA - $(\frac{r_1}{2})$ = EB - $(\frac{r_2}{2})$ = FC - $(\frac{r_3}{2})$;
- a: a side length of the triangle-shaped base platform PQR, i.e., a = PQ = QR = RP;
- h: a side length of the triangle-shaped end-effector platform ABC, i.e., h = AB = BC = CA;
- r_{out}: the cross section outer radius of first intermediate links;
- r_{in}: the cross section inner radius of first intermediate links and at the same time the cross section radius of prismatic joints and second intermediate links;
- r_{Tool}: the cross section radius of end-effector platform link

2.4.1 Inverse Geometry Model of 3-RPR Manipulator

Knowing the pose of moving platform, x_p, y_p, and Φ, we intend to calculate the actuated joints values. The coordinates of point A, B, and C can be calculated by applying the

equation 2.13, 2.14, and 2.15. Then, the close loop vector equations can be written as:

$$\vec{OA} = \vec{OP} + \vec{PD} + \vec{DA} \tag{2.25}$$

$$\vec{OB} = \vec{OQ} + \vec{QE} + \vec{EB} \tag{2.26}$$

$$\vec{OC} = \vec{OR} + \vec{RF} + \vec{FC} \tag{2.27}$$

Equation 2.25, equation 2.26, and equation 2.27 can be expressed as:

$$\begin{pmatrix} x_A \\ y_A \end{pmatrix} = \begin{pmatrix} x_p \\ y_p \end{pmatrix} + \begin{pmatrix} L_{T_1} \cos\theta_1 \\ L_{T_1} \sin\theta_1 \end{pmatrix} \tag{2.28}$$

$$\begin{pmatrix} x_B \\ y_B \end{pmatrix} = \begin{pmatrix} x_Q \\ y_Q \end{pmatrix} + \begin{pmatrix} L_{T_2} \cos\theta_2 \\ L_{T_2} \sin\theta_2 \end{pmatrix} \tag{2.29}$$

$$\begin{pmatrix} x_C \\ y_C \end{pmatrix} = \begin{pmatrix} x_R \\ y_R \end{pmatrix} + \begin{pmatrix} L_{T_3} \cos\theta_3 \\ L_{T_3} \sin\theta_3 \end{pmatrix} \tag{2.30}$$

where

$$\begin{aligned} x_Q &= a \\ y_Q &= 0 \\ x_R &= a \ \cos(\frac{\pi}{3}) \\ y_R &= a \ \sin(\frac{\pi}{3}) \\ L_{T_1} &= L_1 + L_2 + r_1 \\ L_{T_2} &= L_1 + L_2 + r_2 \\ L_{T_3} &= L_1 + L_2 + r_3 \end{aligned}$$

The inverse geometric model of 3-RPR manipulator are expressed as:

$$\theta_1 = \tan^{-1} \left(\frac{y_A}{x_A} \right) \tag{2.31}$$

$$\theta_2 = \tan^{-1} \left(\frac{y_B - y_Q}{x_B - x_Q} \right) \tag{2.32}$$

$$\theta_3 = \tan^{-1} \left(\frac{y_C - y_R}{x_C - x_R} \right) \tag{2.33}$$

2.5 3-RPR Architecture

The architecture model of the 3-RPR manipulator is same with the 3-RPR manipulator. The different is on 3-RPR manipulator the actuators are the prismatic joints that effect the definition of the input variables. For this manipulator, the input variables are the displacement of three prismatic joints attached to the base, i.e., r_1, r_2, and r_3. The other parameters of this manipulator are exactly same with the 3-RPR manipulator.

2.5.1 Inverse Geometric Model of 3-RPR Manipulator

Since the inputs of this manipulator are the displacement of prismatic joints, the inverse geometric models of this manipulator are defined as:

$$r_1 = \sqrt{x_A^2 + y_A^2} - (L_1 + L_2) \tag{2.34}$$

$$r_2 = \sqrt{(x_B - x_Q)^2 + (y_B - y_Q)^2} - (L_1 + L_2) \tag{2.35}$$

$$r_3 = \sqrt{(x_C - x_R)^2 + (y_C - y_R)^2} - (L_1 + L_2) \tag{2.36}$$

Chapter 3

Stiffness Matrix

This chapter is concerned with the stiffness analysis of the parallel manipulators. The stiffness of the manipulators is analyzed using the Virtual Joint Modeling (VJM) presented in [16].

3.1 Stiffness Matrix of The RRRRR Manipulator

To obtain the stiffness model of the RRRRR manipulator using VJM method, we should consider its general schematic that is composed of four intermediate bars and five revolute joints as shown in figure 3.1.

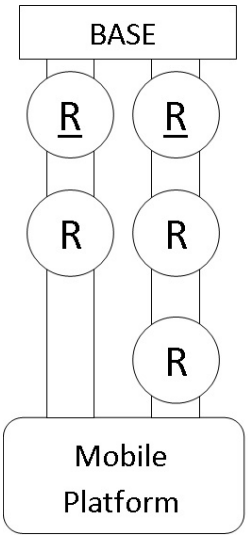

Fig. 3.1: Schematic Diagram of A RRRRR

According to the flexible model of VJM method, each kinematic chain of the RRRRR can be considered as serial structure as shown in Figure 3.2 that contains sequentially:

- a rigid link between the manipulator base and the ith actuated joint described by the constant homogeneous transformation matrix $\mathbf{T}^{i}_{Base}$;

- a 1-DOF actuated joint, defined by the homogeneous matrix function $\mathbf{V}_a(q_0^i)$ where q_0^i is the actuated coordinate;
- a 1-DOF virtual spring describing the actuator mechanical stiffness , which is defined by the homogeneous matrix function $\mathbf{V}_{s1}(\theta_0^i)$ where θ_0^i is the virtual spring coordinate;
- a first rigid leg of length L_1 linking the actuated joint and the first passive joint, which is described by the constant homogeneous transformation matrix $\mathbf{T}_{L_1}^i$;
- a 6-DOF virtual spring describing the first leg stiffness, which is defined by the homogeneous matrix function $\mathbf{V}_{s2}(\theta_1^i....\theta_6^i)$ with θ_1,θ_2, θ_3, and θ_4,θ_5, θ_6, being the virtual spring coordinates corresponding to the spring translation and rotation deflections;
- a 1-DOF passive revolute joint allowing one rotation angle q_1^i, which is described by the homogeneous matrix function $\mathbf{V}_{r1}(q_1^i)$;
- a second rigid leg of length L_2 linking the previous passive joint and the second passive joint, which is described by the constant homogeneous transformation matrix $\mathbf{T}_{L_2}^i$;
- a 6-DOF virtual spring describing the second leg stiffness, which is defined by the homogeneous matrix function $\mathbf{V}_{s3}(\theta_7^i....\theta_12^i)$ with θ_7,θ_8, θ_9, and θ_10,θ_11, θ_12, being the virtual spring coordinates corresponding to the spring translation and rotation deflections of this leg.
- a 1-DOF passive revolute joint allowing one rotation angle q_2^i, which is described by the homogeneous matrix function $\mathbf{V}_{r2}(q_2^i)$;
- a identity transformation matrix $\mathbf{T}_{End}^i$

The mathematical expression defining the end-effector location subject to variations of all defined coordinates of the ith kinematic chain can be written as follows:

$$\mathbf{T}^i = \mathbf{T}_{Base}^i\ \mathbf{V}_a(q_0^i)\ \mathbf{V}_{s1}(\theta_0^i)\ \mathbf{T}_{L_1}^i\ \mathbf{V}_{s2}(\theta_1^i....\theta_6^i)\ \mathbf{V}_{r1}(q_1^i)\ \mathbf{T}_{L_2}^i\ \mathbf{V}_{s3}(\theta_7^i....\theta_12^i)\ \mathbf{V}_{r2}(q_2^i)\ \mathbf{T}_{End}^i \tag{3.1}$$

However, for this research context the affect of actuated joint is omitted because of the RDM6 software that we use for validating our deflection results can not simulate it. So, the homogeneous matrix of $\mathbf{V}_a(q_0^i)$ and $\mathbf{V}_{s1}(\theta_0^i)$ are omitted from our transformation matrix.

The kineostatic model of the ith leg of the RRRRR can be reduced to a system of:

$$\begin{bmatrix} \mathbf{S}_\theta^i & \mathbf{J}_q^i \\ \mathbf{J}_q^{iT} & \mathbf{0} \end{bmatrix} \begin{bmatrix} \mathbf{f}^i \\ \delta\mathbf{q}^i \end{bmatrix} = \begin{bmatrix} \delta\mathbf{x}^i \\ \mathbf{0} \end{bmatrix} \tag{3.2}$$

where $\mathbf{S}_\theta^i = \mathbf{J}_\theta^i \mathbf{K}_\theta^{i^{-1}} \mathbf{J}_\theta^{i^T}$ describes the spring compliance relative to the centroid of the moving platform, and the $\mathbf{J}_q^i$ takes into account the passive joint influence on the moving platform.

The $\mathbf{K}_\theta^{i^{-1}}$ matrix , of size 12 x 12, describe the compliance of virtual springs and takes the form:

$$\mathbf{K}_\theta^{i^{-1}} = \begin{bmatrix} \mathbf{K}_{L_1}^{i^{-1}} & \mathbf{0}_{6x6} \\ \mathbf{0}_{6x6} & \mathbf{K}_{L_2}^{i^{-1}} \end{bmatrix} \tag{3.3}$$

where $\mathbf{K}_{L_1}^{i^{-1}}$ and $\mathbf{K}_{L_2}^{i^{-1}}$ are the 6 x 6 stiffness matrix of the ith of first and second leg.

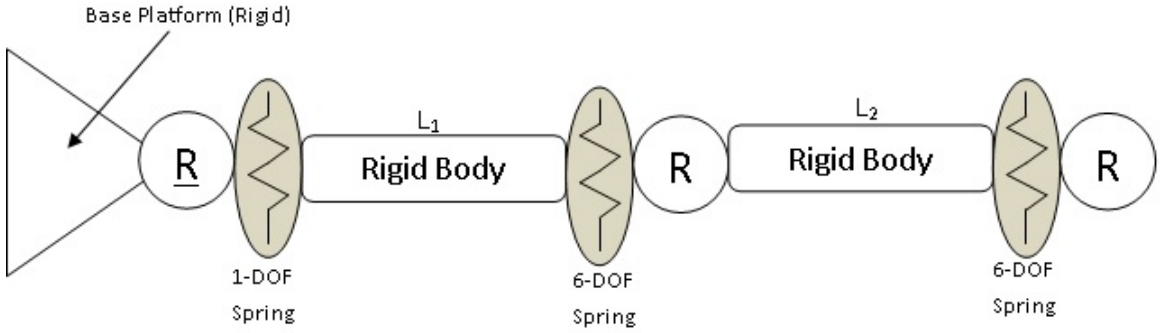

Fig. 3.2: Schematic Diagram of A RRRRR

$\mathbf{J}_\theta^i$ of size 6 x 12 is the Jacobian matrix related to the virtual springs and $\mathbf{J}_q^i$ of size 6 x 2 is the Jacobian matrix related to the passive joints.

The Cartesian stiffness matrix $\mathbf{K}$ of the RRRRR is found with a simple addition of $\mathbf{K}_i$ matrices, namely:

$$\mathbf{K} = \sum_{i=1}^{2} \mathbf{K}_i \tag{3.4}$$

3.2 Stiffness Matrix of The RPRPR Manipulator

The general schematic of the RPRPR manipulator is shown in figure 3.3. The manipulator is composed of four intermediate bars, two prismatic joints and three revolute joints. Figure 3.4 shows the flexible model of the PRPR manipulator. By considering the model, the mathematical expression defining the end-effector location

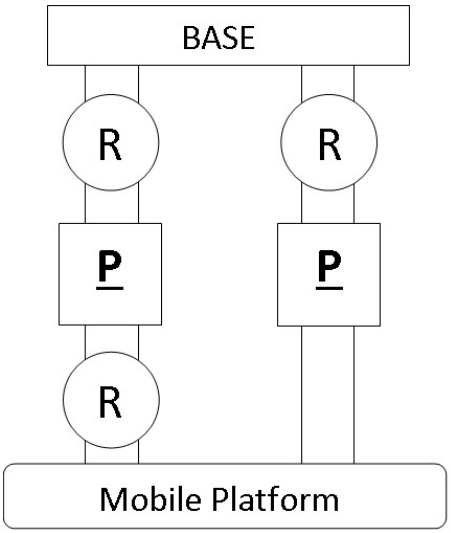

Fig. 3.3: Schematic Diagram of A PRPR

of the ith kinematic chain can be written as follow:

$$\mathbf{T}^i = \mathbf{T}^i_{Base}\ \mathbf{V}_{r1}(q^i_1)\ \mathbf{T}^i_{L_1}\ \mathbf{T}^i_{r_1}\ \mathbf{T}^i_{L_2}\ \mathbf{V}_{s1}(\theta^i_1....\theta^i_6)\ \mathbf{V}_{r2}(q^i_2)\ \mathbf{T}^i_{End} \tag{3.5}$$

where:

- $\mathbf{T}^i_{Base}$ is constant homogeneous matrix described the rigid link between manipulator base with the passive revolute joint;
- $\mathbf{V}_{r1}(q^i_1)$ describes the first 1-DOF passive revolute joint allowing one rotation angle q^i_1;
- $\mathbf{T}^i_{L_1}$ describes the first rigid link L_1 linking passive revolute joint and the actuated prismatic joint;
- $\mathbf{T}^i_{r_i}$ describes the prismatic joint of ith kinematic chain. The prismatic joint is considered as another rigid body since the RDM6 software can not simulate the effect of prismatic joint to the stiffness calculation;
- $\mathbf{T}_{L_2}$ describes the second rigid link L_2 linking the prismatic joint and the last passive revolute joint;
- $\mathbf{V}_{s1}(\theta^i_1....\theta^i_6)$ describes the summation of the first rigid body, the actuated prismatic joint, and the second rigid body stiffness.
- $\mathbf{V}_{r2}(q^i_2)$ describes the second 1-DOF passive revolute joint allowing one rotation angle q^i_2;

- $\mathbf{T}^i_{End}$ describes the transformation matrix from the last passive joint to the end-effector of the manipulator.

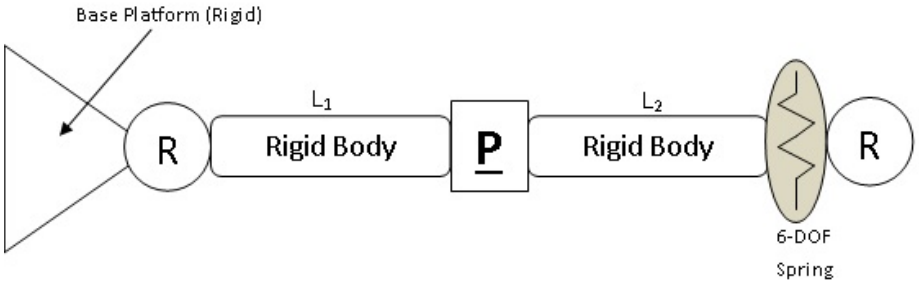

Fig. 3.4: Schematic Diagram of A RPRPR

The $\mathbf{K}^{i^{-1}}_{\theta}$ matrix , of size 6 x 6, describe the compliance of virtual springs and takes the form:

$$\mathbf{K}^{i^{-1}}_{\theta} = \mathbf{K}^{i^{-1}}_{(L_1+r_i+L_2)} \tag{3.6}$$

where $\mathbf{K}^{i^{-1}}_{(L_1+r_i+L_2)}$ is the summation of the first leg, the prismatic joint, and the second leg stiffness matrix which whose size is 6 x 6.

$\mathbf{J}^i_{\theta}$ of size 6 x 6 is the Jacobian matrix related to the virtual springs and $\mathbf{J}^i_q$ of size 6 x 2 is the Jacobian matrix related to the passive joints.

3.3 Stiffness Matrix of The 3-RRR Manipulator

The general schematic of the 3-RRR manipulator is shown in figure 3.5. The manipulator is composed of the mobile platform connected to a fixed base by three identical kinematic chains.

Figure 3.6 shows the flexible model of the 3-RPR manipulator. By considering that model, the mathematical expression defining the end-effector location of the ith kinematic chain can be written as follow:

$$\mathbf{T}^i = \mathbf{T}^i_{Base}\ \mathbf{T}^i_{act_1}\ \mathbf{T}^i_{L_1}\ \mathbf{V}_{s1}(\theta^i_1....\theta^i_6)\ \mathbf{V}_{r1}(q^i_1)\ \mathbf{T}^i_{L_2}\ \mathbf{V}_{s2}(\theta^i_7....\theta^i_{12})\ \mathbf{V}_{r2}(q^i_2)\ \mathbf{T}^i_h\ \mathbf{V}_{s3}(\theta^i_{13}....\theta^i_{18}) \tag{3.7}$$

where:

- $\mathbf{T}^i_{Base}$ is constant homogeneous matrix describing the rigid link between manipulator base with the passive revolute joint;
- $\mathbf{T}_{act_1}$ describes transformation matrix of the actuate revolute joint;
- $\mathbf{T}^i_{L_1}$ describes the first rigid link L_1 linking passive revolute joint and the actuated prismatic joint;

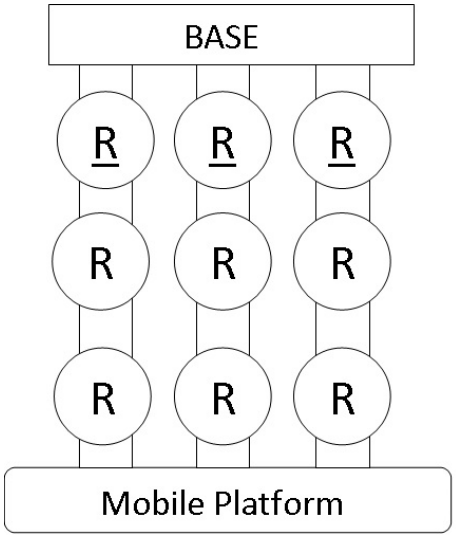

Fig. 3.5: Schematic Diagram of A 3-RRR

- $\mathbf{V}_{s1}(\theta_1^i....\theta_6^i)$ is a 6-DOF virtual spring describing the first leg stiffness;
- $\mathbf{V}_{r1}(q_1^i)$ describes the first 1-DOF passive revolute joint allowing one rotation angle q_1^i;
- $\mathbf{T}_{L_2}$ describes the second rigid link L_2 linking the prismatic joint and the last passive revolute joint;
- $\mathbf{V}_{s2}(\theta_7^i....\theta_{12}^i)$ is a 6-DOF virtual spring describing the second leg stiffness;
- $\mathbf{V}_{r2}(q_2^i)$ describes the second 1-DOF passive revolute joint allowing one rotation angle q_2^i;
- $\mathbf{T}_{End}^i$ describes the transformation matrix from the last passive joint to the end-effector of the manipulator.
- $\mathbf{T}_h^i$ describes transformation matrix of the link which is connecting the last passive revolute joint to the centroid of the moving platform.
- $\mathbf{V}_{s3}(\theta_{13}^i....\theta_{18}^i)$ is a 6-DOF virtual spring describing the end-effector platform stiffness;

The $\mathbf{K}_\theta^{i^{-1}}$ matrix , of size 18 x 18, describe the compliance of virtual springs and takes the form:

$$\mathbf{K}_\theta^{i^{-1}} = \begin{bmatrix} \mathbf{K}_{L_1}^{i^{-1}} & \mathbf{0}_{6x6} & \mathbf{0}_{6x6} \\ \mathbf{0}_{6x6} & \mathbf{K}_{L_2}^{i^{-1}} & \mathbf{0}_{6x6} \\ \mathbf{0}_{6x6} & \mathbf{0}_{6x6} & \mathbf{K}_h^{i^{-1}} \end{bmatrix} \tag{3.8}$$

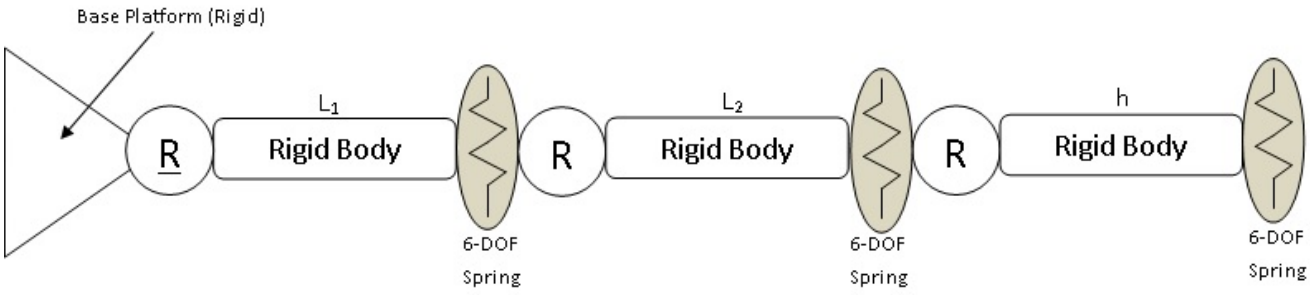

Fig. 3.6: Schematic Diagram of A 3-RRR

where $\mathbf{K}_{L_1}^{i^{-1}}$ and $\mathbf{K}_{L_2}^{i^{-1}}$ are the 6 x 6 stiffness matrix of the first and second leg of the ith kinematic chain. $\mathbf{K}_{h}^{i^{-1}}$ is the 6 x 6 stiffness matrix of the end-effector link of the ith kinematic chain.

$\mathbf{J}_{\theta}^{i}$ of size 6 x 18 is the Jacobian matrix related to the virtual springs and $\mathbf{J}_{q}^{i}$ of size 6 x 2 is the Jacobian matrix related to the passive joints.

3.4 Stiffness Matrix of The 3-RPR Manipulator

The general schematic of the 3-RPR manipulator is shown in figure 3.7. The manipulator is composed of four intermediate bars, two prismatic joints and three revolute joints.

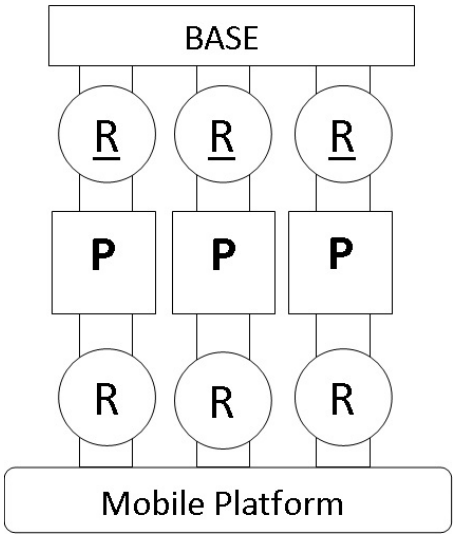

Fig. 3.7: Schematic Diagram of A 3-RPR

Figure 3.8 shows the flexible model of the 3-RPR manipulator. By considering the model, the mathematical expression defining the end-effector location of the ith kinematic chain can be written as follow:

$$\mathbf{T}^{i} = \mathbf{T}_{Base}^{i}\ \mathbf{T}_{act_1}^{i}\ \mathbf{T}_{L_1}^{i}\ \mathbf{V}_{r1}(q_1^i)\ \mathbf{T}_{L_2}^{i}\ \mathbf{V}_{r2}(q_2^i)\ \mathbf{T}_{h}^{i}\ \mathbf{V}_{s1}(\theta_1^i....\theta_6^i) \tag{3.9}$$

where:

- $\mathbf{T}^i_{Base}$ is constant homogeneous matrix describing the rigid link between manipulator base with the passive revolute joint;
- $\mathbf{T}_{act_1}$ describes transformation matrix of the actuate revolute joint;
- $\mathbf{T}^i_{L_1}$ describes the first rigid link L_1 linking passive revolute joint and the actuated prismatic joint;
- $\mathbf{V}_{r1}(q^i_1)$ describes the first 1-DOF passive revolute joint allowing one translation;
- $\mathbf{T}_{L_2}$ describes the second rigid link L_2 linking the prismatic joint and the last passive revolute joint;
- $\mathbf{V}_{r2}(q^i_2)$ describes the second 1-DOF passive revolute joint allowing one rotation angle q^i_2;
- $\mathbf{T}^i_h$ describes transformation matrix of the link which is connecting the last passive revolute joint to the centroid of the moving platform.
- $\mathbf{V}_{s1}(\theta^i_1....\theta^i_6)$ is a 6-DOF virtual spring describing the end-effector link stiffness;

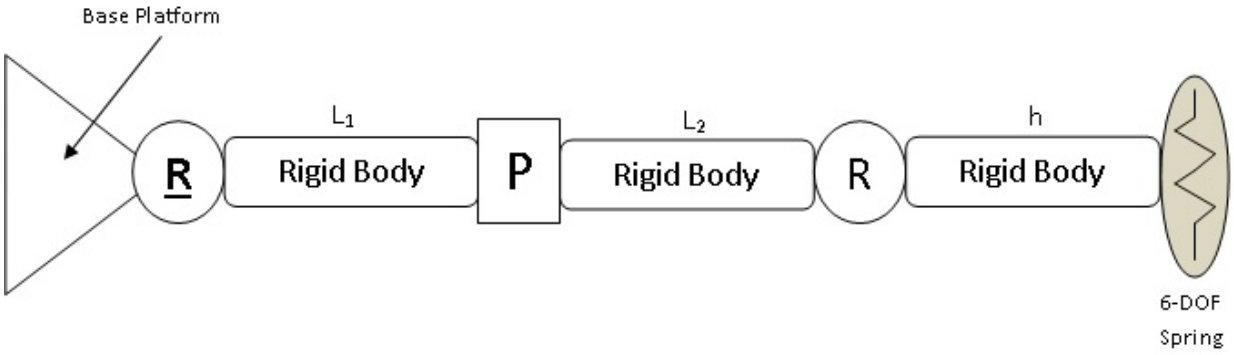

Fig. 3.8: Schematic Diagram of A 3-RPR

The $\mathbf{K}^{i^{-1}}_{\theta}$ matrix , of size 18 x 18, describe the compliance of virtual springs and takes the form:

$$\mathbf{K}^{i^{-1}}_{\theta} = \mathbf{K}^{i^{-1}}_{h} \tag{3.10}$$

where $\mathbf{K}^{i^{-1}}_{h}$ is the 6 x 6 stiffness matrix of the end-effector link of the ith kinematic chain.

$\mathbf{J}^i_{\theta}$ of size 6 x 6 is the Jacobian matrix related to the virtual springs and $\mathbf{J}^i_q$ of size 6 x 2 is the Jacobian matrix related to the passive joints.

3.5 Stiffness Matrix of The 3-RPR Manipulator

The general schematic of the 3-RPR manipulator is shown in figure 3.9. The manipulator is composed of four intermediate bars, two prismatic joints and three revolute joints.

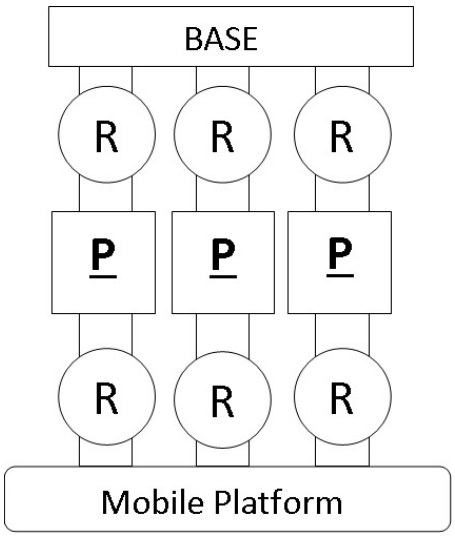

Fig. 3.9: Schematic Diagram of A 3-RPR

Figure 3.10 shows the flexible model of the 3-RPR manipulator. By considering the model, the mathematical expression defining the end-effector location of the ith kinematic chain can be written as follow:

$$\mathbf{T}^i = \mathbf{T}^i_{Base}\ \mathbf{V}_{r1}(q^i_1)\ \mathbf{T}^i_{L_1}\ \mathbf{T}^i_{r_1}\ \mathbf{T}^i_{L_2}\ \mathbf{V}_{s1}(\theta^i_1....\theta^i_6)\ \mathbf{V}_{r2}(q^i_2)\ \mathbf{T}^i_h\ \mathbf{V}_{s2}(\theta^i_7....\theta^i_{12}) \qquad (3.11)$$

where:

- $\mathbf{T}^i_{Base}$ is constant homogeneous matrix describing the rigid link between manipulator base with the passive revolute joint;
- $\mathbf{V}_{r1}(q^i_1)$ describes the first 1-DOF passive revolute joint allowing one translation;
- $\mathbf{T}^i_{L_1}$ describes the first rigid link L_1 linking the passive revolute joint and the actuated prismatic joint;
- $\mathbf{T}^i_{r_i}$ describes the prismatic joint of ith kinematic chain. The prismatic joint is considered as another rigid body since the RDM6 software can not simulate the effect of prismatic joint to the stiffness calculation;
- $\mathbf{T}_{L_2}$ describes the second rigid link L_2 linking the prismatic joint and the last passive revolute joint;

- $\mathbf{V}_{s1}(\theta_1^i....\theta_6^i)$ is a 6-DOF virtual spring describing the stiffness link composed of the first and second leg and the prismatic joint;
- $\mathbf{V}_{r2}(q_2^i)$ describes the second 1-DOF passive revolute joint allowing one rotation angle q_2^i;
- $\mathbf{T}_h^i$ describes transformation matrix of the link which is connecting the last passive revolute joint to the centroid of the moving platform.
- $\mathbf{V}_{s2}(\theta_7^i....\theta_{12}^i)$ is a 6-DOF virtual spring describing the second leg stiffness;

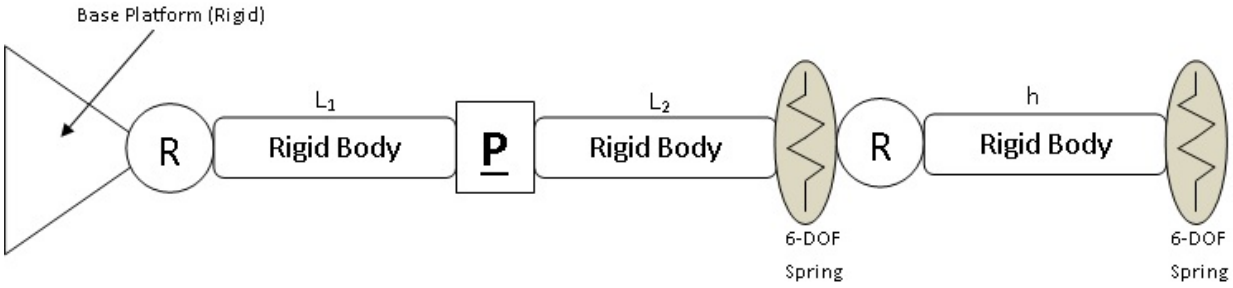

Fig. 3.10: Schematic Diagram of A 3-RPR

The $\mathbf{K}_\theta^{i^{-1}}$ matrix , of size 12 x 12, describe the compliance of virtual springs and takes the form:

$$\mathbf{K}_\theta^{i^{-1}} = \begin{bmatrix} \mathbf{K}_{(L_1+r_i+L_2)}^{i^{-1}} & \mathbf{0}_{6x6} \\ \mathbf{0}_{6x6} & \mathbf{K}_h^{i^{-1}} \end{bmatrix} \tag{3.12}$$

where $\mathbf{K}_h^{i^{-1}}$ is the 6 x 6 stiffness matrix of the end-effector link of the ith kinematic chain. $\mathbf{K}_{(L_1+r_i+L_2)}^{i^{-1}}$ is the summation of the first leg, the prismatic joint, and the second leg stiffness matrix which whose size is 6 x 6.

$\mathbf{J}_\theta^i$ of size 6 x 12 is the Jacobian matrix related to the virtual springs and $\mathbf{J}_q^i$ of size 6 x 2 is the Jacobian matrix related to the passive joints.

3.6 Stiffness Calculation and Comparison

Using the VJM model in the previous section, we developed MATLAB functions for calculating stiffness matrix. Furthermore, to verify if our models are correct, we compare our output with RDM6 software. Table below shows the output of VJM model and RDM6. As we can see, the outputs of our developed model are same with the output of RDM6.

Table 3.1: Comparison of Displacements Results Generated by the VJM Model and the RDM6 Software for RRRRR

d = 2	L1 = 1		L2 = 1.5	rf = 0.01	rl = 0.01	
RPRPR	EEpos = [0,2 1,5]					
W = [Fx Fy Fz Mx My Mz]	W = [10 0 0 0 0 0]		W = [0 -10 0 0 0 0 0]		W = [0 10 0 0 0 0 0]	
Displacement	MATLAB	RDM6	MATLAB	RDM6	MATLAB	RDM6
δ_x	1.19E-03	1.19E-03	-2.54E-04	-2.55E-04	2.54E-04	2.55E-04
δ_y	2.54E-04	2.55E-04	-6.35E-03	-6.35E-03	6.35E-03	6.35E-03
δ_z	0	0	0	0	0	0
$\delta\varphi_x$	0	0	0	0	0	0
$\delta\varphi_y$	0	0	0	0	0	0
$\delta\varphi_z$	2.16E-06	0	3.89E-03	0	3.89E-03	0

RPRPR	EEpos = [-0,6 1,65]					
W = [Fx Fy Fz Mx My Mz]	W = [10 0 0 0 0 0]		W = [0 -10 0 0 0 0 0]		W = [0 10 0 0 0 0 0]	
Displacement	MATLAB	RDM6	MATLAB	RDM6	MATLAB	RDM6
δ_x	1.03E-03	1.03E-03	-3.14E-04	-3.14E-04	3.14E-04	3.14E-04
δ_y	3.14E-04	3.14E-04	-2.57E-03	-2.57E-03	2.57E-03	2.57E-03
δ_z	0	0	0	0	0	0
$\delta\varphi_x$	0	0	0	0	0	0
$\delta\varphi_y$	0	0	0	0	0	0
$\delta\varphi_z$	-2.79E-04	0	-7.65E-04	0	-7.65E-04	0

Table 3.2: Comparison of Displacements Results Generated by the VJM Model and the RDM6 Software for RPRPR

d = 2	L1 = 1		L2 = 1.5	rf = 0.01	rl = 0.01	
RPRPR	Eepos = [0,2 2,75]					
W = [Fx Fy Fz Mx My Mz]	W = [10 0 0 0 0 0]		W = [0 -10 0 0 0 0 0]		W = [0 0 0 0 0 10]	
Displacement	MATLAB	RDM6	MATLAB	RDM6	MATLAB	RDM6
δ_x	1.91E-06	1.91E-06	9.07E-08	9.069E-08	0	0
δ_y	-9.07E-08	-9.07E-08	-2.56E-07	-2.561E-07	0	0
δ_z	1.07E-15	0	1.11E-16	0	0	0
$\delta\varphi_x$	1.03E-17	0	1.07E-18	0	0	0
$\delta\varphi_y$	0	0	0	0	0	0
$\delta\varphi_z$	-5.97E-07	0	-6.18E-08	0	6.06E-03	0

RPRPR	Eepos = [-0,5 2,9]					
W = [Fx Fy Fz Mx My Mz]	W = [10 0 0 0 0 0]		W = [0 -10 0 0 0 0 0]		W = [0 10 0 0 0 0 0]	
Displacement	MATLAB	RDM6	MATLAB	RDM6	MATLAB	RDM6
δ_x	2.28E-06	2.29E-06	-2.72E-07	-2.72E-07	0	0
δ_y	2.72E-07	2.72E-07	-2.98E-07	2.98E-07	0	0
δ_z	3.61E-15	0	-3.56E-16	0	0	0
$\delta\varphi_x$	1.36E-18	0	-1.34E-19	0	0	0
$\delta\varphi_y$	0	0	0	0	0	0
$\delta\varphi_z$	-7.49E-07	0	7.39E-08	0	5.95E-03	0

Table 3.3: Comparison of Displacements Results Generated by the VJM Model and the RDM6 Software for 3-$\underline{\overline{R}}$RR

L1 = 1 L2 = 1.5 rf = 0.01 rl = 0.01 $Base_{Width} = 7$ $EE_{width} = 2$

3-$\underline{\overline{R}}$RR	Eepos = [3.6 2.696 0.4363]					
W = [Fx Fy Fz Mx My Mz]	W = [10 0 0 0 0 0]		W = [0 -10 0 0 0 0]		W = [0 0 0 0 0 10]	
Displacement	MATLAB	RDM6	MATLAB	RDM6	MATLAB	RDM6
δ_x	2.12E-02	2.13E-02	3.02E-02	3.04E-02	3.98E-02	4.00E-02
δ_y	-3.02E-02	-3.04E-02	-5.42E-02	-5.45E-02	-6.89E-02	-6.93E-02
δ_z	0	0		0		0
$\delta\varphi_x$	0	0		0		0
$\delta\varphi_y$	0	0		0		0
$\delta\varphi_z$	3.98E-02	4.00E-02	6.89E-02	6.93E-02	9.23E-02	9.28E-02

3-$\underline{\overline{R}}$RR	Eepos = [3 2 0.3491]					
W = [Fx Fy Fz Mx My Mz]	W = [10 0 0 0 0 0]		W = [0 -10 0 0 0 0]		W = [0 0 0 0 0 10]	
Displacement	MATLAB	RDM6	MATLAB	RDM6	MATLAB	RDM6
δ_x	1.53E-02	1.58E-02	-2.58E-02	-2.70E-02	3.20E-02	3.34E-02
δ_y	2.58E-02	2.67E-02	-6.47E-02	-6.82E-02	6.97E-02	7.41E-02
δ_z	0	0	0	0	0	0
$\delta\varphi_x$	0	0	0	0	0	0
$\delta\varphi_y$	0	0	0	0	0	0
$\delta\varphi_z$	3.20E-02	3.34E-02	-6.97E-02	-7.41E-02	8.80E-02	9.22E-02

Table 3.4: Comparison of Displacements Results Generated by the VJM Model and the RDM6 Software for 3-$\underline{R}$PR and 3-$\underline{R}$PR

$EE_w = 2$ $Base_w = 7$ L1 = 1 L2 = 0,75 rf = 0.01 rl = 0.01

	Eepos = [3.5 2.5 0.3142]								
	W = [10 0 0 0 0 0]			W = [0 -10 0 0 0 0]			W = [0 0 0 0 0 10]		
	MATLAB			MATLAB			MATLAB		
Displacement	R_{act}	P_{act}	RDM6	R_{act}	P_{act}	RDM6	R_{act}	P_{act}	RDM6
δ_x	1.45E-03	3.60E-04	3.59E-04	1.91E-05	1.40E-04	1.40E-04	-1.03E-04	-9.35E-05	-9.32E-05
δ_y	-1.91E-05	-1.40E-04	-1.40E-04	-2.01E-03	-3.78E-04	-3.78E-04	-6.50E-05	-4.24E-05	-4.27E-05
δ_z	0	0	0	0	0	0	0	-1.90E-16	0
$\delta\varphi_x$	0	0	0	0	0	0	0	2.40E-18	0
$\delta\varphi_y$	0	0	0	0	0	0	0	0	0
$\delta\varphi_z$	-1.03E-04	-9.35E-05	-9.32E-05	6.50E-05	4.24E-05	4.27E-05	7.87E-04	8.22E-04	8.22E-04

	Eepos = [3.1 2.9 0.4363]								
	W = [10 0 0 0 0 0]			W = [0 -10 0 0 0 0]			W = [0 0 0 0 0 10]		
	MATLAB			MATLAB			MATLAB		
Displacement	R_{act}	P_{act}	RDM6	R_{act}	P_{act}	RDM6	R_{act}	P_{act}	RDM6
δ_x	1.03E-03	6.27E-04	6.27E-04	-3.08E-04	4.84E-04	4.83E-04	-1.26E-04	7.75E-05	7.78E-05
δ_y	3.08E-04	-4.84E-04	-4.83E-04	-1.94E-03	-8.69E-04	-8.69E-04	-4.02E-04	-3.57E-04	-3.58E-04
δ_z	0	0	0	0	0	0	0	3.50E-16	0
$\delta\varphi_x$	0	0	0	0	0	0	0	-8.60E-19	0
$\delta\varphi_y$	0	0	0	0	0	0	0	0	0
$\delta\varphi_z$	-1.26E-04	7.75E-05	7.78E-05	4.02E-04	3.57E-04	3.58E-04	8.65E-04	9.67E-04	9.67E-04

Chapter 4

Design Optimization

This chapter aims to compare the manipulators in the term of their intrinsic stiffness properties. The first comparison is for 2-DOF parallel manipulators between $\underline{R}RRR\underline{R}$ and $R\underline{P}R\underline{P}R$. The second comparison is for 3-DOF planar parallel manipulator between 3-$\underline{R}RR$, 3-$\underline{R}PR$, and 3-$R\underline{P}R$.

In order to do the comparison, each manipulator has to design under the same specifications. Moreover, in this study context the selected specifications are the fixed size of regular dexterous workspace, deformations under a certain load, and the passive joints reactions. The general specifications should be fulfilled by all the manipulators are shown in table 4.1.

Table 4.1: General Specifications for The Manipulators

Regular Workspace Size	300 mm x 300 mm
Deformation under $\mathbf{F}$ = [10, 10, 0] N and moment $\mathbf{M}$ = [0 0 1] N.m	[1, 1, 1] mm, [1, 1, 1] deg
Admissible joint reactions	10 N

4.1 Optimization Objective

The general optimization problem in this study context is to find the best design of manipulator in order to minimize its total mass in motion and compactness. The best manipulator design is determine by optimizing the geometric parameters of a manipulator. In order to achieve that goal, the workspace of the mechanism is discretized, then the considered performance and constraints are measured, evaluated, and verified for each point.

4.1.1 Mass in Motion of the Manipulators

Mass in motion of the manipulators are considered as the first objective function of this optimization problem. Mass of manipulators are function related dimension parameters such as cross-sectional area and length of links. In general, the mass in motion of a manipulator is determined by number of links, size of platform, and types of links composing a manipulator.

Therefore, the first objective function of the design optimization problem is written as:

$$f_1(\mathbf{x}) = \frac{m_t}{m_{max}} \rightarrow min \tag{4.1}$$

where $\mathbf{x}$ is the design variables vector that consists of the geometric parameters of a manipulator. m_t is total mass in motion of several manipulator's parameters. m_{max} is the maximum value of mass in motion of an evaluated manipulator.

The general mathematical expression of m_t and m_{max} are:

$$m_t = m_{pf} + a \ . \ m_b + b \ . \ m_{pj} \tag{4.2}$$

$$m_{max} = \rho \ . \ A_{max} \ . \ L_{max} \tag{4.3}$$

where m_{pf} is the mass of the platform. m_b is the mass of an intermediate bar. m_{pj} is the mass of a prismatic joint. a is the number of intermediate bars installed to the manipulator. b is number of prismatic joint installed to the manipulator. ρ is density value of used material. A_{max} is the maximum area of the calculated object. $Lmax$ is the maximum length of the calculated object.

4.1.2 Compactness of The Manipulators

The second objective function of optimization problem is compactness of the manipulator. This objective function is related to the projection size of a manipulator into the plane of motion as the manipulator is expected to be as compact as possible.

Compactness of a manipulator is defined by the rectangle-shaped area that covers the manipulator at a given configuration. As illustration, compactness of the RRRRR manipulator as shown in figure 4.1 is the grey area marked as A_{5bar}.

As it mention before, the calculated area depends on the specific manipulator's pose. Where for the case of Five-bar robot, the area is calculated when the different angles between q_1 and q_2 is equal to $\pi/2$, or we called it *home position*. The details compactness formulation of each manipulator will be explained on the next part.

Generally, the second objective function of the design optimization problem is writ-

ten as:

$$f_2(\mathbf{x}) = \frac{A_{compactness}}{A_{max}} \rightarrow min \tag{4.4}$$

where $A_{compactness}$ is the manipulator compactness area at the *home position*. A_{max} is compactness maximum value.

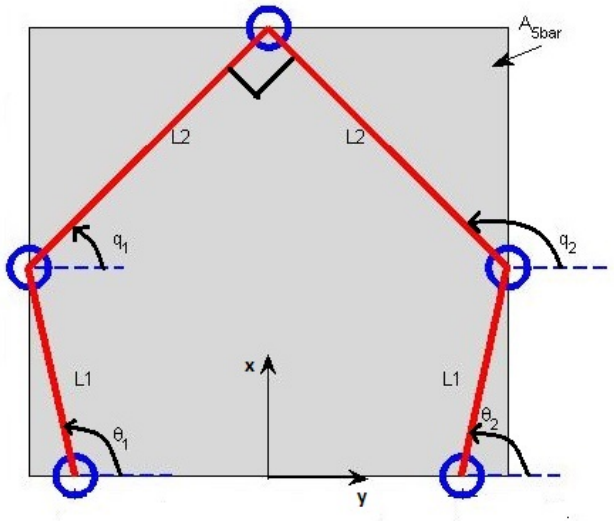

Fig. 4.1: Bounding box and home configuration of RRRRR manipulator

4.2 Design Variables

Design variables are variables which are affected the calculation of objective functions. From previous section, we knew that the objective functions are mass in motion and compactness. Based on this information the design variables can be determine generally such as length of links, cross-section type, cross-section radius, and platform size. Furthermore, the details of design variables determination will be explained independently for each manipulator in the next section.

4.3 Optimization Constraints

The optimization constraints are divided into two types: linear constraints and nonlinear constraints. Linear constraints are straight forward constraint, which usually related to geometric relation, such as cross section. Meanwhile, nonlinear constraints are function(s) of the design variable, which have certain degree of mathematical computation to obtain the constraint conditions.

The linear constraint used in this optimization problem is related to the cross-section type of the intermediate links which are spherical hollow shaped. A spherical

hollow cross-section is defined by two radius, i.e., r_{out} as the outer radius and r_{in} as the inner radius. Illustration of spherical hollow cross section can be seen in figure 4.2.

Physically, the outer radius should be greater than inner radius such that it can be written as:

$$r_{out} \geq r_{in} + c \tag{4.5}$$

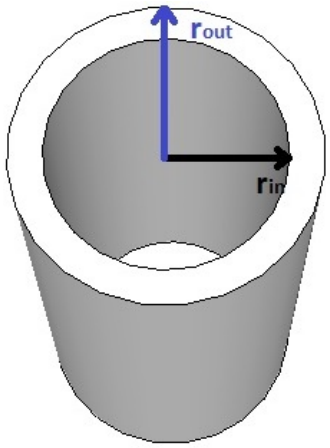

Fig. 4.2: Circular hollow link

where c is any constant value that greater than zero and rout and rin are design variable of optimization problem.

The nonlinear constraints used are the displacements of end-effector when an external wrench applied, passive joint reaction to the applied wrench, and the specified size of largest regular dexterous workspace (LRDW).

4.3.1 Largest Regular Dexterous Workspace

The largest regular dexterous workspace (LRDW) is the largest manipulator's workspace area in which the geometric and/or kinematic constraints are respected thoroughly. In the scope of this research, the design constraints/objectives that need to be respected are:

1. The assembly of the manipulator should be possible.
2. The displacement constraints.
3. The passive joints reaction constraint.

Furthermore, the minimum length and height specification of *regular workspace*, *RW*, is define as w_l and w_h, respectively. These two parameters define the minimum desired size of *regular dexterous workspace*, RDW.

$$RDW = w_l \ . \ w_h \tag{4.6}$$

Algorithm 1: Largest Dexterous Workspace Determination

Data: $\{\Omega_{ij}\}, \{G_{ij}\}$, d_x, d_y
Result: $l_{LRDW}, h_{LRDW}, (i_0, j_0)$
$\Phi_{ij} = 0$;
for $\{i = 1 \ \& \ \forall j\} \ \cup \ \{j = 1 \ \& \ \forall i\}$ **do**
  $\Phi_{ij} \ = \ \Omega_{ij}$;
end

for $i \ = \ 2 : N_0$ **do**
  for $j \ = \ 2 : N_0$ **do**
    if $\Omega_{ij} \ = \ 1$ **then**
      $\Phi_{ij} \ = \ 1 \ + \ min\{\Phi_{i-1}, \Phi_{j-1}, \Phi_{i-1,j-1}\}$
    end
  end
end

Find $d = max(\Phi_{ij} - 1)$;
$(i_0, j_0) = argmax(\Phi_{ij})$;
Retrieve from the grid $\{G_{ij}\}$ the desired square bounded by the indices $(i_0 \ - \ d, j_0 \ - \ d)$ and (i_0, j_0);
Give $l_{LRDW} \ = d_x \ . \ d$ and $h_{LRDW} \ = d_y \ . \ d$;

In order to find the largest dexterous workspace, algorithm 1 of [4] is used for the given design variables. The input of this algorithm are the workspace grid, $\{G_{ij}\}$, which includes the manipulator workspace $RDW = w_l$ x w_h and possesses uniform but different steps along the Cartesian axes, namely ($l_G = d_x.N_0$ and $h_G = d_y.N_0$), where l_G and h_G define the length and height of the workspace grid, d_x and d_z define the discretisation precision, and N_0 is the number of nodes in each direction. In addition, the 2D binary matrix $\Omega_{ij} = \{0, 1\}$ is defined to indicate if the constraints at node $\{G_{ij}\}$ are satisfied or not. $\Omega_{ij} = 1$ means the corresponding design constraints/objectives are all satisfied, and $\Omega_{ij} = 0$ otherwise. For computation convenience, $\Omega_{ij} = 0$ if $\{G_{ij}\} \notin RDW$.

Hence, the original problem it to find the largest sub-matrix inside $\{\Omega_{ij}\}$ containing non-zero value only. Moreover, the algoritm 1 utilizes an additional integer matrix $\{\Phi_{ij}\}$ that define the candidate solutions with the vertex (i,j).

The output of algorithm 1 is the length and height of manipulator's LRDW (l_{LRDW} and h_{LRDW}). Therefore, using these two values and then comparing it with the prescribe regular workspace height and length (w_l and h_l) we can define the constraint functions as

$$l_{LRDW} \ \geq w_l \tag{4.7}$$

$$h_{LRDW} \ \geq h_l \tag{4.8}$$

4.3.2 Deformation Constraints

The position and orientation deformations are assessed by using the stiffness parameters of the manipulator. Let defines δx, δy, and δz as position deformation error and $\delta\Phi_x$, $\delta\Phi_y$, and $\delta\Phi_z$ as orientation deformation error of the end-effector subjected to external forces (F_x, F_y, and F_z) and torques (τ_x, τ_y, and τ_z). The constraints related to the deformation of manipulator are defined as follows:

$$f_3(\mathbf{x}) = \begin{cases} \delta x_{min} \leq \delta x \leq \delta x_{max} \\ \delta y_{min} \leq \delta y \leq \delta y_{max} \\ \delta z_{min} \leq \delta z \leq \delta z_{max} \\ \delta\Phi_{x_{min}} \leq \delta\Phi_x \leq \delta\Phi_{x_{max}} \\ \delta\Phi_{y_{min}} \leq \delta\Phi_y \leq \delta\Phi_{y_{max}} \\ \delta\Phi_{z_{min}} \leq \delta\Phi_z \leq \delta\Phi_{z_{max}} \end{cases} \tag{4.9}$$

where $(\delta x_{max}, \delta y_{max}, \delta z_{max})$ being the maximum allowable position errors, $(\delta x_{min}, \delta y_{min}, \delta z_{min})$ the minimum allowable position error, $(\delta\Phi_{x_{max}}, \delta\Phi_{y_{max}}, \delta\Phi_{z_{max}})$ the maximum allowable orientation errors, and $(\delta\Phi_{x_{min}}, \delta\Phi_{y_{min}}, \delta\Phi_{z_{min}})$ the minimum allowable position errors of the end-effector. These deformation constraints can be expressed in term of the components of the mechanism stiffness matrix and wrench applied to the end effector. The deformation specification range is set to be:

$$\delta x_{max} = \delta y_{max} = 10^{-3} m \tag{4.10}$$

$$\delta x_{min} = \delta y_{min} = -10^{-3} m \tag{4.11}$$

$$\delta\Phi_z = 1\,\text{deg} \tag{4.12}$$

These specifications should be satisfied if forces equal to 10 N are applied to x and y axis and 1 Nm torque is applied to z axis when the manipulator is in *home position*.

4.3.3 Passive Joints Reaction Constraints

The passive joints reaction calculate the reaction(s) value of passive joints due to applied of external wrench (force(s) and moment(s)) for a given/specific manipulator's configuration. The value of passive joint i reaction forces ($\mathbf{R}_i$) should lied below an admissible reaction value(R_{adm}) since the excessively high values leading to the breakdown of the manipulator.

$$\mathbf{R}_i \leq R_{adm} \tag{4.13}$$

For guarantying that our mechanism is strong enough to resist the external wrench

equation 4.13 must be considered as one of constraint equation of this optimization design. The problem is lied on how to calculate the value of reaction forces $\mathbf{R_i}$ to guarantee the output optimize design can resist a given external wrench.

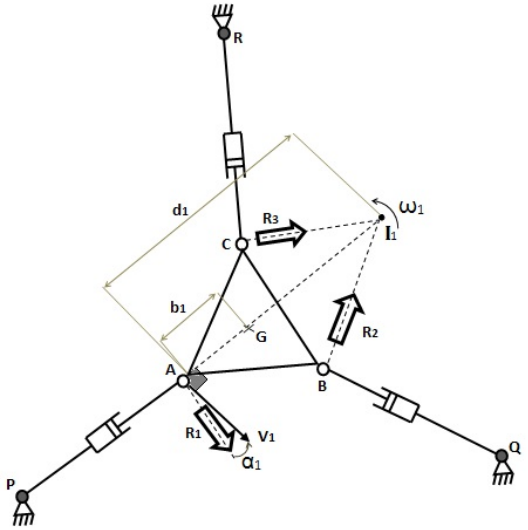

Fig. 4.3: Determination of passive joints reaction for the planar 3-RPR manipulator

According to [3], the reaction forces $\mathbf{R}_i$ in the platform passive joints (denoted as point A, B, and C in figure 4.3) is related to the external wrench, $\mathbf{w}^T = [\mathbf{f}^T; C]^T$ (f is the external force and C is the scalar value of the external moment applied on the end effector) applying the Newton-Euler equations at any point Q. For example of $3-\underline{R}PR$ manipulator in figure 4.3, the description of force and moment are

$$\mathbf{f} = \sum_{i=1}^{3} \mathbf{R}_i \tag{4.14}$$

$$C = -(\overline{\mathbf{d}}_{QA}^T \mathbf{R}_1 + \overline{\mathbf{d}}_{QB}^T \mathbf{R}_2 + \overline{\mathbf{d}}_{QC}^T \mathbf{R}_3) \tag{4.15}$$

where $\overline{\mathbf{d}}_{QA}^T$, $\overline{\mathbf{d}}_{QB}^T$, and $\overline{\mathbf{d}}_{QC}^T$ on equation 4.15are described the coordinates of vector $\overrightarrow{QA}$, $\overrightarrow{QB}$, and $\overrightarrow{QC}$ respectively. the double arrows in figure 3 show direction reaction for each passive joints. In addition, direction of reaction forces of different types of joint configurations is explained on paper of [3]. Taking into consideration of $\mathbf{R}_i = R_i\ \mathbf{r}_i$ where $\mathbf{r}_i$ is a dimensionless unit vector and $||\mathbf{R}_i|| = R_i$ then applying the Newton-Euler equations at point A, it comes that

$$\mathbf{w} = -\begin{bmatrix} \mathbf{r}_1 & \mathbf{r}_2 & \mathbf{r}_3 \\ \overline{\mathbf{d}}_{AA}^T \mathbf{r}_1 & \overline{\mathbf{d}}_{AB}^T \mathbf{r}_2 & \overline{\mathbf{d}}_{AC}^T \mathbf{r}_3 \end{bmatrix} \begin{bmatrix} R_1 \\ R_2 \\ R_3 \end{bmatrix} = -\begin{bmatrix} \mathbf{s_{w1}} & \mathbf{s_{w1}} & \mathbf{s_{w1}} \end{bmatrix} \mathbf{R} = -\mathbf{A}^T\ \mathbf{R} \tag{4.16}$$

According to [14, 8], matrix $\mathbf{A}$ at Eq. 4.16 is parallel jacobian matrix founded from differentiation close loop equations of the manipulator with respect to end effector coordinates.

The reaction forces $\mathbf{R}$ of passive joint are calculated refer to Eq. 4.16 as

$$\mathbf{R} = -\mathbf{A}^{-T}\ \mathbf{w} \tag{4.17}$$

$$\mathbf{A}^{-1} = [\mathbf{s_{t1}} \mathbf{s_{t1}} \mathbf{s_{t1}}], \quad with \ \ \mathbf{s}_{\mathbf{ti}}^T = [\mathbf{v}_i^T, \omega_i] \tag{4.18}$$

combining Eq. 4.17 and 4.18 then applying for manipulator in figure 4.3

$$\begin{bmatrix} R_1 \\ R_2 \\ R_3 \end{bmatrix} = - \begin{bmatrix} \mathbf{v}_1^T & \omega_1 \\ \mathbf{v}_2^T & \omega_2 \\ \mathbf{v}_3^T & \omega_3 \end{bmatrix} . \begin{bmatrix} \mathbf{f} \\ C + CG \end{bmatrix} \tag{4.19}$$

where R_i is reaction force on passive joints. $\mathbf{v}_i^T$ and ω_i are linear velocity vector and scalar angular velocity of each passive joints. $\mathbf{f}$ is external vector forces applied to the manipulator. C is scalar external moments applied to the manipulator, and C_G is external moments applied to point G . Taking an example of norm of R_1 of the reaction force at point A (first limb of $3 - \underline{R}PR$ manipulator)

$$\begin{aligned} R_1 &= -(\mathbf{v}_1^T\ \mathbf{f}\ +\ \omega_1\ (C\ +\ C_G)) \\ R_1 &= -(\mathbf{v}_1^T\ \mathbf{f}\ +\ \omega_1\ (C\ +\ \overline{\mathbf{d}}_{GA}^T)\ \mathbf{f}) \\ R_1 &= -((\mathbf{v}_1^T\ +\ \omega_1\ \overline{\mathbf{d}}_{GA}^T)\ \mathbf{f}\ +\ \omega_1 C) \end{aligned} \tag{4.20}$$

For a give norm f of external force $\mathbf{f}$ and a given value C of external moment, and for any direction of vector $\mathbf{f}$, the maximum value of $R_{1_{max}}$ of R_1 as:

$$R_{1_{max}} = f\ \sqrt{||\mathbf{v}_1||^2\ +\ (\ \omega_1\ b_1)^2\ -\ 2||\mathbf{v}_1||\ |\ \omega_1\ b_1|\ \cos\ \beta_1}\ +\ |\ \omega_1\ C| \tag{4.21}$$

where b_1 is distance between application point of the external wrench, G, and passive joint at point A. β_1 is angle between vector $\mathbf{v}_1$ and $\omega_1\ \overline{\mathbf{d}}_{GA}$ (see figure 4.4), where Ii is the position of the instantaneous center of rotation (ICR) of the manipulator when limb 1 is disconnected. The method to determine position of ICR is explained on [1]. Put equation 4.22 as reference and generalizing the approach to the other legs, the general equation becomes

$$R_{i_{max}} = f\ \sqrt{||\mathbf{v}_i||^2\ +\ (\ \omega_i\ b_i)^2\ -\ 2||\mathbf{v}_i||\ |\ \omega_i\ b_i|\ \cos\ \beta_i}\ +\ |\ \omega_i\ C| \tag{4.22}$$

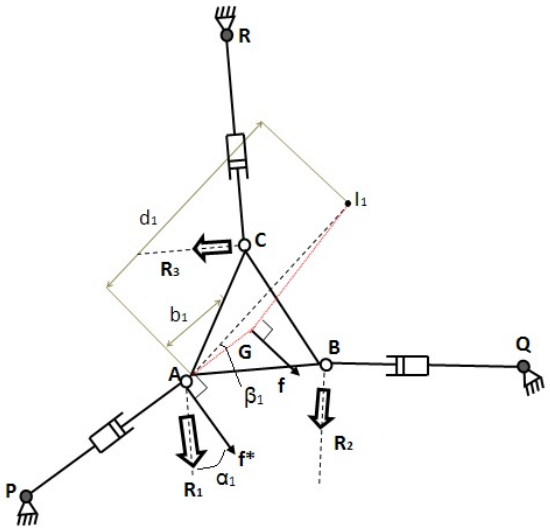

Fig. 4.4: Instantaneous system equivalent to the planar 3-RPR manipulator

Based on equation 4.22 and for a given mechanism configuration, it is possible to find admissible ranges for f and C, in order to avoid the breakdown of the platform of each passive joint location in a manipulator. Therefore, the maximum values of reaction forces of each passive joints can be verified if it was in the range of admissible value or not (refer to equation 4.13).

4.4 General Optimization Problem Statement

The general optimization problem for all the manipulators can be stated as:

Finding the optimum design parameter $\mathbf{x}$ of the five manipulators (RRRRR, RPRPR, 3-RRR, 3-RPR, and 3-RPR) in order to minimize the total mass in motion and compactness with subject to several design constraints, i.e., largest regular dexterous workspace, deformation constraints, and passive joints reaction constraints.

Mathematically, the problem is written as:

$$\begin{aligned}
minimize \quad & f_1(\mathbf{x}) &&= \tfrac{m_t}{m_{max}} \\
& f_2(\mathbf{x}) &&= \tfrac{A_{manipulator}}{A_{max}} \\
over \quad & \mathbf{x} &&= [r_{out}\ r_{in}\ r_{Tool}\ L_1\ L_2\ EE_{width}\ Base_{width}]^T \\
subject\ to \quad & g1 &&= r_{out} \geq r_{in} + 0.001 \\
& g2 &&= l_{LRDW} \geq w_l \\
& g3 &&= h_{LRDW} \geq w_h \\
& g4 &&= \delta x_{min} \leq \delta x \leq \delta x_{max} \\
& g5 &&= \delta y_{min} \leq \delta y \leq \delta y_{max} \\
& g6 &&= \delta \Phi_{z_{min}} \leq \delta \Phi_z \leq \delta \Phi_{z_{max}} \\
& g7 &&= R_{1_{max}} \leq R_{adm} \\
& g8 &&= R_{2_{max}} \leq R_{adm} \\
& && \mathbf{x}_{lb} \leq \mathbf{x} \leq \mathbf{x}_{ub}
\end{aligned} \tag{4.23}$$

where $\mathbf{x}_{lb}$ and $\mathbf{x}_{ub}$ are lower and upper bounds of $\mathbf{x}$, respectively.

4.5 Optimization Problem of RRRRR Manipulator

The objective of this optimization problem is to find optimal design variables of RRRRR manipulator that minimize its total mass in motion and compactness. Figure 4.5 shows the model with its parameters of the RRRRR used in this optimization problem.

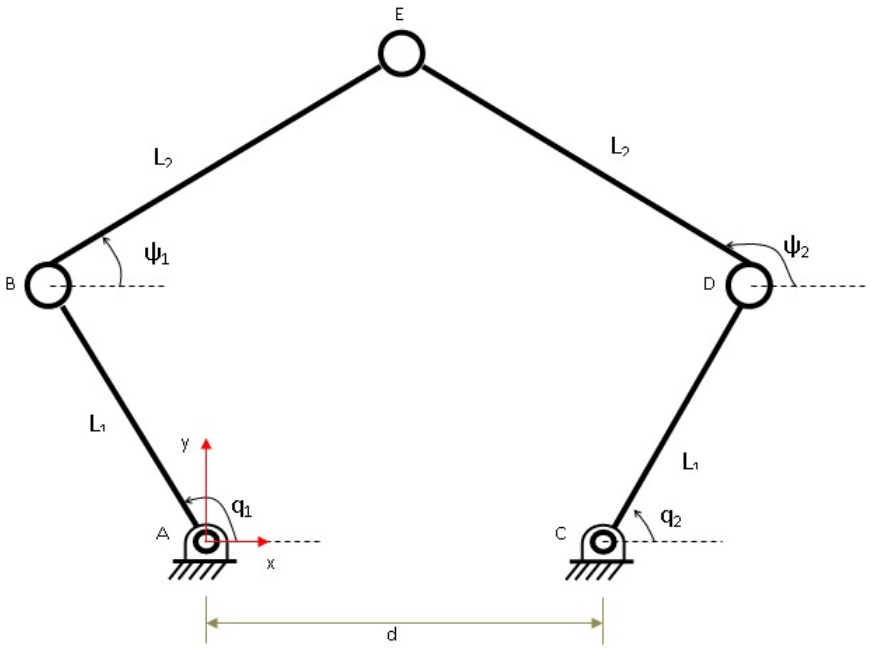

Fig. 4.5: RRRRR Model and Parameters

4.5.1 Objective Function

The first objective function of the optimization problem corresponds to the total mass in motion of the RRRRR manipulator. Mass is a function of manipulator dimensions, i.e., length of links, cross section type and area. In this case, both first and second intermediate links (L_1 and L_2) are consider to have a same type of cross section which is spherical hollow with radius $r_{out_{Li}}$ and $r_{in_{Li}}$ (for i = 1,2).

$$\begin{aligned} r_{out_{L1}} &= r_{out_{L2}} \\ r_{in_{L1}} &= r_{in_{L2}} \end{aligned} \tag{4.24}$$

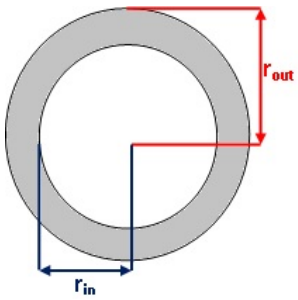

Fig. 4.6: Circular Hollow Section Model and Parameter

where r_{out_1} and r_{out_2} are outer radius of first and second intermediate links. r_{in_1} and r_{in_2} are inner radius of first and second intermediate links.

The total mass in motion of the RRRRR manipulator, m_t, is composed of the mass of two first bar, m_{L1}, and the mass of two second bar, m_{L2}. The total mass in motion calculation is:

$$m_t = 2m_{L1} \; + \; 2m_{L2} \tag{4.25}$$

with,

$$m_{L1} = \; \rho \; \pi \; (r^2_{out_{L1}} - r^2_{in_{L1}}) \; L1 \tag{4.26}$$

$$m_{L2} = \; \rho \; \pi \; (r^2_{out_{L2}} - r^2_{in_{L2}}) \; L2 \tag{4.27}$$

where ρ is density of material used, which in this case is stainless steel ($\rho = 7860$ kg/m^3). L1 and L2 are length of first and second intermediate links of the manipulator.

The second objective function corresponds to the size of projection of RRRRR into the plane of motion as the manipulator should be as compact as possible. The RRRRR compactness calculates the amount of surface area A_{RRRRR} of the rectangle-shaped bounding box as it shown as grey area in figure 4.7. The calculation is done when the manipulator is in the *home position*. In this position the value of ε is equal to $\pi/2$ and the end-effector is in the middle of point A and C.

The surface area A_{RRRRRR} is expressed as:

$$A_{RRRRRR} = bb_H \ . \ bb_L \tag{4.28}$$

where bb_H and bb_L are height and length of bounding rectangle and take the form:

$$bb_H = L_1 \ \sin(q_1) + L_2 \ \sin(\psi_1) \tag{4.29a}$$

$$bb_L = L_2 \ \cos(\psi_1) - L_2 \ \cos(\psi_2) \tag{4.29b}$$

$$q_1 = \ \arccos(-\frac{(L_2/\ \sqrt{2}) - (d/2)}{L_1}) \tag{4.29c}$$

$$\psi_1 = \pi/4 \tag{4.29d}$$

$$\psi_2 = 3\pi/4 \tag{4.29e}$$

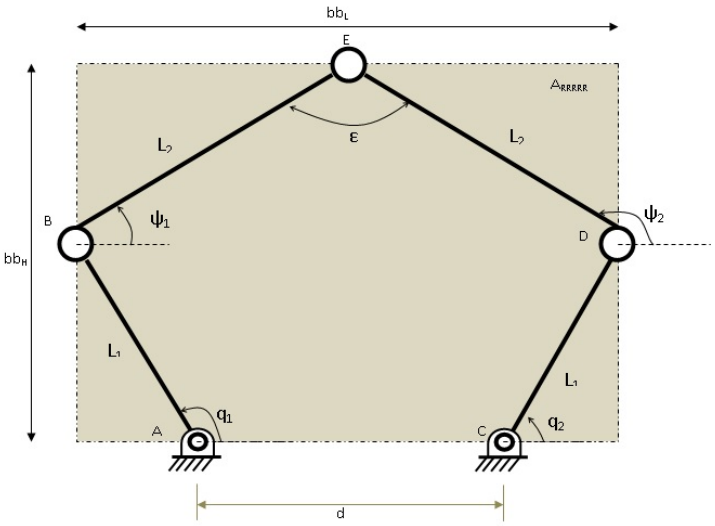

Fig. 4.7: Bounding Box of The RRRRR

4.5.2 Design Variables

The design variables of this optimization problem are the design parameters of the RRRRR that affect m_t as well as A_{RRRRRR}, namely:

$$\mathbf{x}_1 = [r_{out} \ \ r_{in} \ \ L_1 \ \ L_2]^T \tag{4.30}$$

4.5.3 Optimization Problem Formulation of RRRRR Manipulator

From tabel 4.1, the RRRRR is designed to cover a rectangular shaped workspace, called Regular Workspace (RW) of length and height equal to 300 mm (w_l and w_h).

Moreover, at the *home configuration* the maximum deformation and admissible joint reactions under external forces $\mathbf{F}$ and moments $\mathbf{M}$ should be also satisfied.

The optimization problem aims to find the design variable vector $\mathbf{x}_1$ that minimize the total mass in motion $m_{t_{RRRRRR}}$ and the surface area A_{RRRRRR} while the length and height of LRDW are bigger or equal to w_l and w_h. The deformations under external forces and moments should be less or equal to 1 mm and 1 deg, respectively. The passive joint reaction for a given external wrench should not greater than 10 N.

As a summary, the optimization problem can be written in mathematical form as:

$$\begin{aligned}
\textit{minimize} \quad & f_1(\mathbf{x}) = m_{t_{RRRRRR}} \\
& f_2(\mathbf{x}) = A_{RRRRRR} \\
\textit{over} \quad & \mathbf{x}_1 = [r_{out}\ r_{in}\ L_1\ L_2]^T \\
\textit{subject to} \quad & g1 = r_{out} \geq r_{in} + 0.001 \\
& g2 = l_{LRDW} \geq w_l \\
& g3 = h_{LRDW} \geq w_h \\
& g4 = \delta x_{min} \leq \delta x \leq \delta x_{max} \\
& g5 = \delta y_{min} \leq \delta y \leq \delta y_{max} \\
& g6 = \delta \Phi_{z_{min}} \leq \delta \Phi_z \leq \delta \Phi_{z_{max}} \\
& g7 = R_{1_{max}} \leq R_{adm} \\
& g8 = R_{2_{max}} \leq R_{adm} \\
& \mathbf{x}_{lb} \leq \mathbf{x}_1 \leq \mathbf{x}_{ub}
\end{aligned} \tag{4.31}$$

where $\mathbf{x}_{lb}$ and $\mathbf{x}_{ub}$ are lower and upper bounds of $\mathbf{x}_1$, respectively.

4.5.4 Results

The MATLAB function *fmincon* was used to solve this optimization problem. Using this function and by providing several initial parameters, the optimal set of design parameters are found. The optimal design variables of this problem and the associated mass in motion and surface are A_{RRRRRR} are given in Table 4.2. Figure 4.8 shows the optimum 2D design of the RRRRRR with its LRDW.

Table 4.2: Optimal Design Parameters of The RRRRRR

r_{out} (m)	r_{in} (m)	L_1 (m)	L_2 (m)	m_t (kg)	A_{RRRRRR} (m^2)	l_{LRDW} (m)	h_{LRDW} (m)
0.025	0.015	0.9019	0.9391	36.3223	1.9936	0.44	0.44

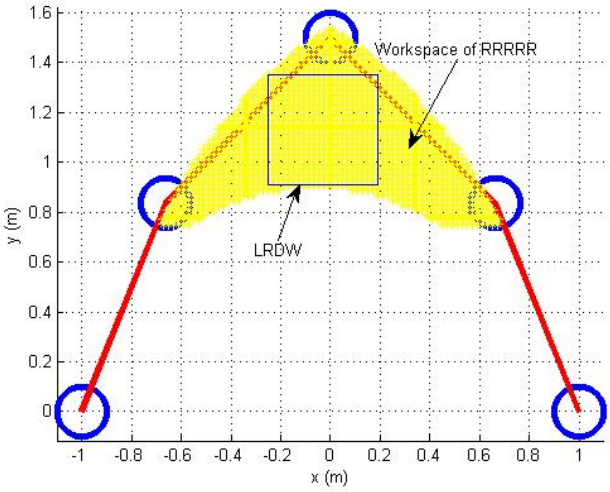

Fig. 4.8: Optimal Design of The RRRRR and Largest Regular Dexterous Workspace

4.6 Optimization Problem of RPRPR Manipulator

This optimization problem aims to find optimal design variables of the RPRPR manipulator that minimize its total mass in motion and compactness. Figure 4.9 shows the RPRPR manipulator model and its parameters.

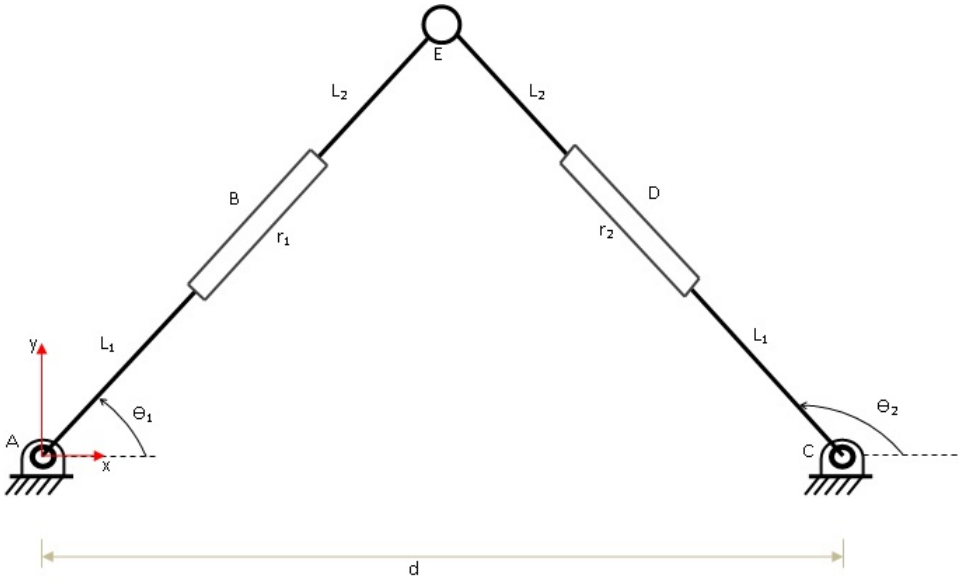

Fig. 4.9: RPRPR Model and Parameters

4.6.1 Objective Functions

Same with the RRRRR, the first objective function is to find the minimum mass of motion. The mass in motion of the RPRPR manipulator is composed by the mass of first and second intermediate links m_{L_1} and m_{L_2}, and the mass of prismatic joints, m_{r_1} and m_{r_2}.

In this problem, the cross section of first intermediate links is spherical hollow section. The cross section of second intermediate links and the passive joints are solid spherical section. It is also considered that the radius of the prismatic joints and the second intermediate links are same and equal to inner radius of the first intermediate links. This relation can be written as:

$$r_{in_{L1}} = r_{prismatic} = r_{L2} \tag{4.32}$$

Therefore, the total mass of motion of R$\underline{\text{P}}$R$\underline{\text{P}}$R manipulator is

$$m_t = 2m_{L_1} \ + \ 2m_{L_2} \ + \ m_{r_1} \ + \ m_{r_2} \tag{4.33}$$

with,

$$m_{L_1} = \rho \ \pi \ (r_{out}^2 - r_{in}^2) \ L_1 \tag{4.34}$$
$$m_{L_2} = \rho \ \pi \ r_{in}^2 \ L_2 \tag{4.35}$$
$$m_{r_1} = \rho \ \pi \ r_{in}^2 \ r_1 \tag{4.36}$$
$$m_{r_2} = \rho \ \pi \ r_{in}^2 \ r_2 \tag{4.37}$$

where ρ is material density. L_1 and L_2 are the length of first and second intermediate links. r_1 and r_2 are the length of prismatic joints. r_{out} is the outer radius of the first links. r_{in} is the inner radius of first link and also the radius of both the prismatic joints and the second intermediate links.

The second objective function corresponds to compactness of the manipulator. The goal is to minimize the surface area A_{RPRPR}. Figure 4.10 shows the area of A_{RPRPR} as the rectangle shaped bounding box. The surface area A_{RPRPR} is expressed as:

$$A_{RPRPR} = bb_H \ . \ bb_W \tag{4.38}$$

where

$$bb_H = (L_1 + L_2 + r_1) \sin\theta_1 \tag{4.39}$$
$$bb_W = (L_1 + L_2 + r_1) \cos\theta_1 \ + \ (L_1 + L_2 + r_2) \cos(\theta_2 - \frac{\pi}{2}) \tag{4.40}$$

4.6.2 Design Variables

The design variables of this optimization problem are:

$$\mathbf{x}_2 = [r_{out} \ \ r_{in} \ \ L_1 \ \ L_2]^T \tag{4.41}$$

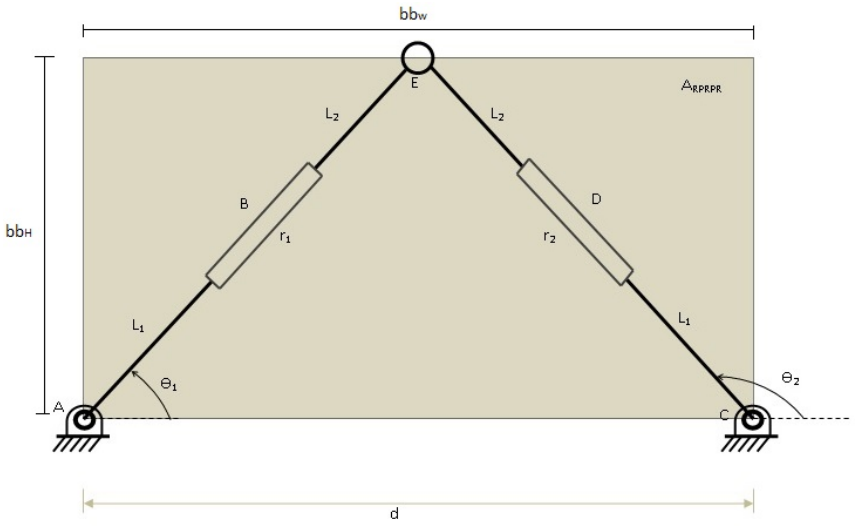

Fig. 4.10: Bounding Box of The RPRPR

4.6.3 Optimization Problem Formulation of RPRPR Manipulator

The optimization problem of RPRPR manipulator can be formulated as follows,

$$
\begin{aligned}
minimize \quad & f_1(\mathbf{x}) && = m_{t_{RPRPR}} \\
& f_2(\mathbf{x}) && = A_{RPRPR} \\
over \quad & \mathbf{x}_2 && = [r_{out}\ r_{in}\ L_1\ L_2]^T \\
subject\ to \quad & g1 && = r_{out} \geq r_{in} + 0.001 \\
& g2 && = l_{LRDW} \geq w_l \\
& g3 && = h_{LRDW} \geq w_h \\
& g4 && = \delta x_{min} \leq \delta x \leq \delta x_{max} \\
& g4 && = \delta y_{min} \leq \delta y \leq \delta y_{max} \\
& g5 && = \delta \Phi_{z_{min}} \leq \delta \Phi_z \leq \delta \Phi_{z_{max}} \\
& g6 && = R_{1_{max}} \leq R_{adm} \\
& g7 && = R_{2_{max}} \leq R_{adm} \\
& && \mathbf{x}_{lb} \leq \mathbf{x} \leq \mathbf{x}_{ub}
\end{aligned}
\tag{4.42}
$$

where $\mathbf{x}_{lb}$ and $\mathbf{x}_{ub}$ are lower and upper bounds of $\mathbf{x}_2$, respectively.

4.6.4 Results

The optimum design parameters for this optimization problem are shown in Table 4.3. Figure 4.11 shows the optimum 2D design of RPRPR with its LRDW.

Table 4.3: Optimal Design Parameters of The PRPR

r_{out} (m)	r_{in} (m)	L_1 (m)	L_2 (m)	m_t (kg)	A_{RRRRR} (m^2)	l_{LRDW} (m)	h_{LRDW} (m)
0.025	0.0012	0.4998	0.3946	15.4386	2	0.38	0.38

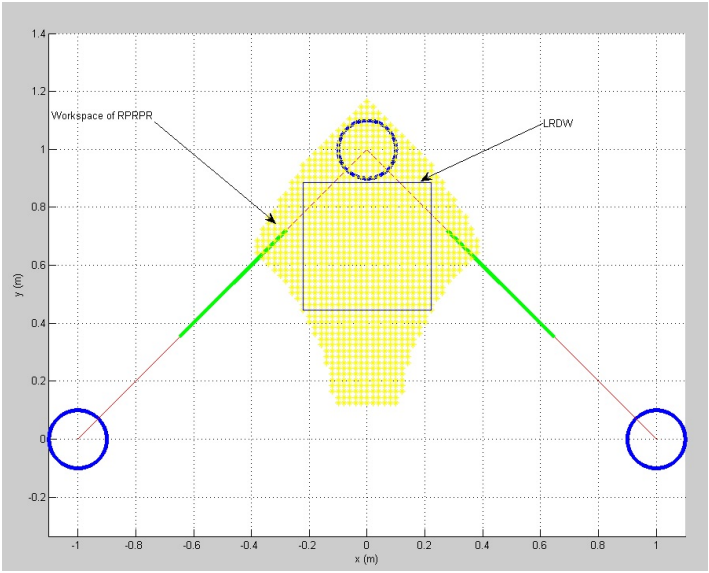

Fig. 4.11: Optimal Design of The PRPR and Largest Regular Dexterous Workspace

4.7 Optimization Problem of 3-RRR Manipulator

Optimization problem of 3-RRR manipulator is to find optimal design variables that minimize its total mass in motion and compactness. Figure 4.12 shows model and parameter of the 3-RRR manipulator.

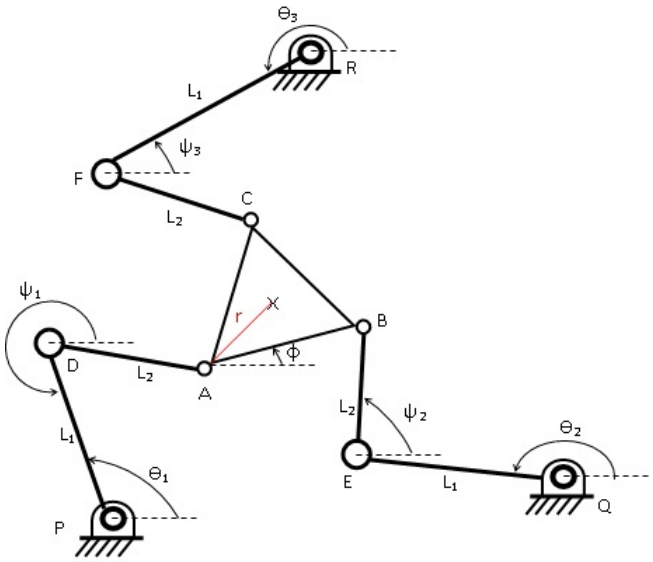

Fig. 4.12: RRRRR Model and Parameters

4.7.1 Objective Functions

Total mass in motion as the first objective function is composed of three identical leg and end effector. Each leg of 3-RRR manipulator is composed by two cylindrical links that have circular hollow type cross section. The end effector is assumed to be made up of three circular bars. Hence, total mass of motion of 3-RRR manipulator is:

$$m_t = m_{EE} + 3m_{L_1} + 3m_{L_2} \tag{4.43}$$

with,

$$m_{EE} = 3\ \rho\ \pi\ r_{Tool}^2\ r \tag{4.44}$$

$$m_{L_1} = \rho\ \pi\ (r_{out}^2 - r_{in}^2)\ L_1 \tag{4.45}$$

$$m_{L_2} = \rho\ \pi\ (r_{out}^2 - r_{in}^2)\ L_2 \tag{4.46}$$

m_{EE} is the end-effector mass composed of two components which are r_{Tool} which is radius of the end-effector bar, and r which is the length from last passive joint (point A, B, and C) to mid point of end-effector. m_{L_1} is mass of the first intermediate link. m_{L_2} is mass of the second intermediate link. Moreover, mass of first and second links are composed by three components: r_{out} as the outer radius of cross section, r_{in} as the inner radius of cross section, and L_i (i=1,2) as the length of first and second intermediate links.

The second objective function is compactness of the manipulator. Compactness of the 3-RRR is determine by the size of bounding box area, A_{3RRR} (shown at figure 4.13).

$$A_{3RRR} = bb_H\ .\ bb_W \tag{4.47}$$

where

$$bb_H = |L_2 \sin(\theta_1 + \Psi_1)| + \frac{EE_{width}\sqrt{3}}{2} + |L_2 \sin(\theta_3 + \Psi_3)| + |L_1 \cos\theta_3| \tag{4.48}$$

$$bb_W = |L_1 \cos\theta_1| + |L_2 \cos(\theta_1 + \Psi_1)| + EE_{width} + |L_2 \cos(\theta_2 + \Psi_2)| \tag{4.49}$$

$$EE_{width} = r\sqrt{3} \tag{4.50}$$

4.7.2 Design Variables

The design variables of the optimization problem are the components of vector $\mathbf{x}_3$, namely,

$$\mathbf{x}_3 = [r_{out}\ r_{in}\ r_{Tool}\ L_1\ L_2\ EE_{width}\ Base_{width}]^T \tag{4.51}$$

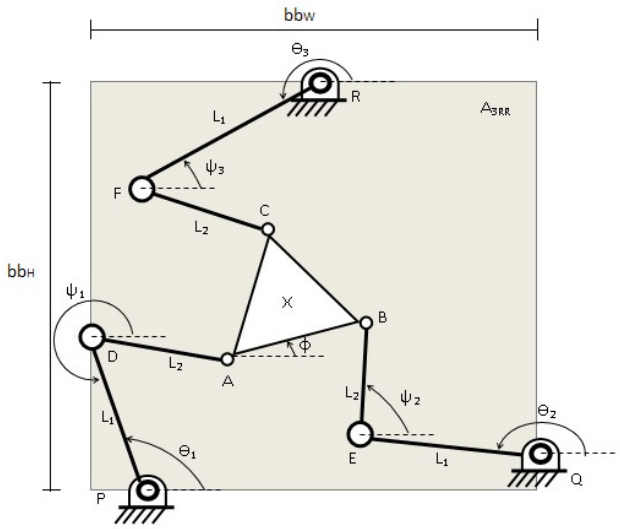

Fig. 4.13: Bounding Box of The 3-RRR Manipulator

The EE_{width} and $Base_{Width}$ are dimension of equilateral triangle shaped of the base platform and the end-effector platform, respectively.

4.7.3 Optimization Problem Formulation of 3-RRR Manipulator

The 3-RRR manipulator optimization problem can be formulated as follows,

$$
\begin{aligned}
minimize \quad & f_1(\mathbf{x}) && = m_{t_{3RRR}} \\
& f_2(\mathbf{x}) && = A_{3RRR} \\
over \quad & \mathbf{x}_3 && = [r_{out}\ r_{in}\ r_{Tool}\ L_1\ L_2\ EE_{width}\ Base_{width}]^T \\
subject\ to \quad & g1 && = r_{out} \geq r_{in} + 0.001 \\
& g2 && = l_{LRDW} \geq w_l \\
& g3 && = h_{LRDW} \geq w_h \\
& g4 && = \delta x_{min} \leq \delta x \leq \delta x_{max} \\
& g4 && = \delta y_{min} \leq \delta y \leq \delta y_{max} \\
& g5 && = \delta \Phi_{z_{min}} \leq \delta \Phi_z \leq \delta \Phi_{z_{max}} \\
& g6 && = R_{1_{max}} \leq R_{adm} \\
& g7 && = R_{2_{max}} \leq R_{adm} \\
& g8 && = R_{3_{max}} \leq R_{adm} \\
& && \mathbf{x}_{lb} \leq \mathbf{x} \leq \mathbf{x}_{ub}
\end{aligned}
\tag{4.52}
$$

where $\mathbf{x}_{lb}$ and $\mathbf{x}_{ub}$ are lower and upper bounds of $\mathbf{x}_3$, respectively.

4.7.4 Results

The optimal design parameters obtained for this optimization problem are given in Table 4.4. In addition, Table 4.5 provides value of objective functions. The 2D design of the 3-RRR manipulator with its LRDW is shown in figure 4.14.

Table 4.4: Optimal Design Parameters of The 3-RRR

r_{out} (m)	r_{in} (m)	r_{Tool} (m)	L_1 (m)	L_2 (m)	$Base_{Width}$ (m)	EE_{Width} (m)	
0.0575	0.0075	0.0431		0.635	0.615	2.5	1

Table 4.5: Objective Function Results

m_t (kg)	A_{RRRRR} (m^2)	l_{LRDW} (m)	h_{LRDW} (m)
325.789	5.8289	0.35	0.35

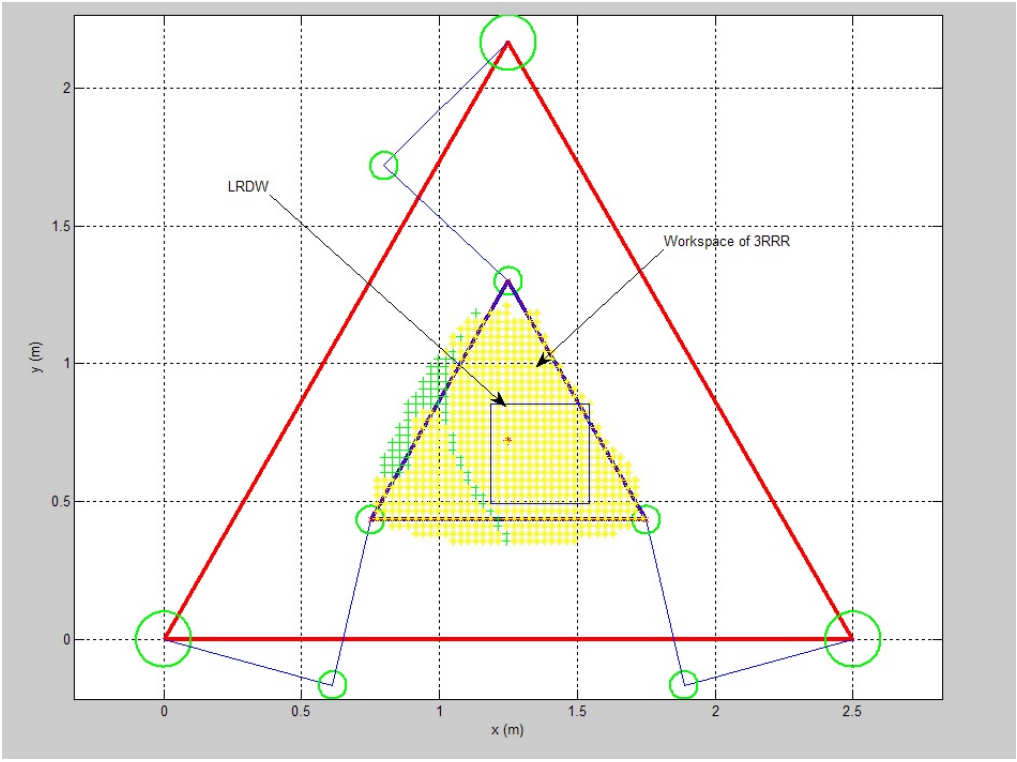

Fig. 4.14: Optimal Design of The 3-RRR and Largest Regular Dexterous Workspace

4.8 Optimization Problem of 3-RPR Manipulator

Optimization problem of 3-RPR manipulator is to find the optimal design variables that minimize its total mass in motion and compactness. Figure 4.15 shows model and parameter of the 3-RPR manipulator.

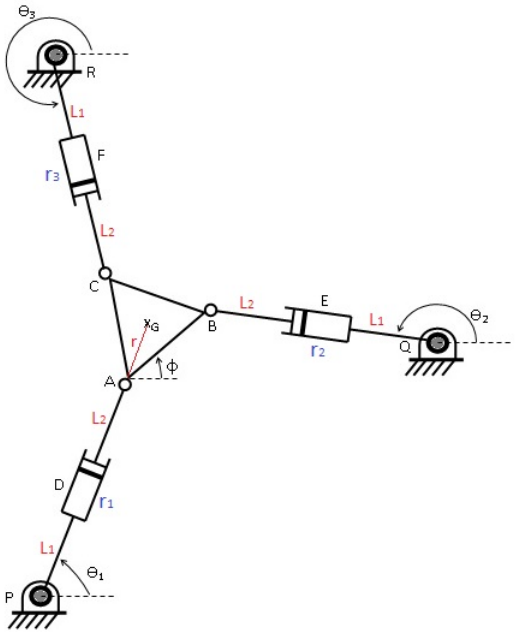

Fig. 4.15: 3-RPR Model and Parameters

4.8.1 Objective Functions

Total mass in motion as the first objective function is composed of three identical legs and a moving platform. Here, the mass of moving platform is denoted as m_{EE}. Each manipulator's leg consists of 2 bars, L_1 and L_2, and prismatic joint, r_i (i=1,..,3). In general, the total mass in motion m_t of 3-RPR is equal to

$$m_t = m_{EE} + 3m_{L_1} + 3m_{L_2} + \sum_{i=1}^{3} m_{r_i} \tag{4.53}$$

with

$$m_{EE} = 3\ \rho\ \pi\ r_{Tool}^2\ r \tag{4.54}$$

$$m_{L_1} = \rho\ \pi\ (r_{out}^2 - r_{in}^2)\ L_1 \tag{4.55}$$

$$m_{L_2} = \rho\ \pi\ r_{in}^2\ L_2 \tag{4.56}$$

$$m_{r_i} = \rho\ \pi\ r_{in}^2\ r_i \tag{4.57}$$

where r_{Tool} is radius of the end effector bars, r is the length from center point to vertices point of end-effector platform. r_{out} is the outer radius of first intermediate link. r_{in} is the inner radius of second intermediate link. L_1 is the length of first intermediate link, L_2 is length of second intermediate link, r_i is length of prismatic joints (There are three prismatic joint installed in this manipulator. One for each legs).

The second objective function is the compactness of manipulator. Compactness of manipulator is determine by the size of bounding box area A_{3RPR}.

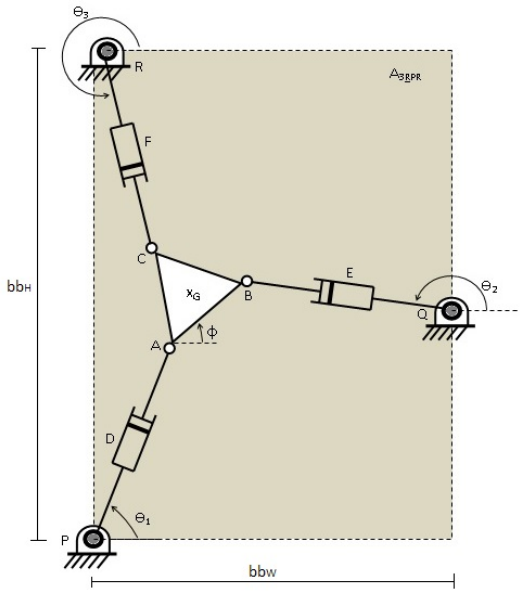

Fig. 4.16: Bounding Box of The 3-RPR Manipulator

The bounding box $A_{3\underline{R}PR}$ calculation is expressed as follow

$$A_{3\underline{R}PR} = bb_H \ . \ bb_W \tag{4.58}$$

bb_H and bb_W are the length and the height of the bounding box rectangle and take the form:

$$bb_H = |L_1 + L_2 + r_1) \sin\theta_1| + \frac{EE_{width}\sqrt{3}}{2} + |(L_1 + L_2 + r_3) \sin\theta_3| \tag{4.59}$$

$$bb_W = |L_1 + L_2 + r_1) \cos\theta_1| + EE_{width} + |L_1 + L_2 + r_2) \cos\theta_2| \tag{4.60}$$

$$EE_{width} = r\sqrt{3} \tag{4.61}$$

4.8.2 Design Variables

The decision variables of the optimization problem are the components of vector $\mathbf{x}_4$

$$\mathbf{x}_4 = [r_{out} \ r_{in} \ r_{Tool} \ L_1 \ L_2 \ EE_{width} \ Base_{width}]^T \tag{4.62}$$

4.8.3 Optimization Problem of 3-RPR Manipulator

The 3-RPR manipulator optimization problem can be formulated as follows,

$$
\begin{aligned}
\textit{minimize} \quad & f_1(\mathbf{x}) && = m_{t_{3\underline{R}PR}} \\
& f_2(\mathbf{x}) && = A_{3\underline{R}PR} \\
\textit{over} \quad & \mathbf{x}_4 && = [r_{out}\ r_{in}\ r_{Tool}\ L_1\ L_2\ EE_{width}\ Base_{width}]^T \\
\textit{subject to} \quad & g1 && = r_{out} \geq r_{in} + 0.001 \\
& g2 && = l_{LRDW} \geq w_l \\
& g3 && = h_{LRDW} \geq w_h \\
& g4 && = \delta x_{min} \leq \delta x \leq \delta x_{max} \\
& g4 && = \delta y_{min} \leq \delta y \leq \delta y_{max} \\
& g5 && = \delta \Phi_{z_{min}} \leq \delta \Phi_z \leq \delta \Phi_{z_{max}} \\
& g6 && = R_{1_{max}} \leq R_{adm} \\
& g7 && = R_{2_{max}} \leq R_{adm} \\
& g8 && = R_{3_{max}} \leq R_{adm} \\
& && \mathbf{x}_{lb} \leq \mathbf{x} \leq \mathbf{x}_{ub}
\end{aligned}
\tag{4.63}
$$

where $\mathbf{x}_{lb}$ and $\mathbf{x}_{ub}$ are lower and upper bounds of $\mathbf{x}_4$, respectively.

4.8.4 Results

The optimal design parameters and the objective function results are given in Table 4.6 and 4.7. Figure 4.17 shows the optimal 2D design of the 3-$\underline{R}$PR manipulator and its LRDW.

Table 4.6: Optimum Design Parameters of The 3-$\underline{R}$PR

r_{out} (m)	r_{in} (m)	r_{Tool} (m)	L_1 (m)	L_2 (m)	$Base_{Width}$ (m)	EE_{Width} (m)	
0.0239	0.0139	0.01	0.5	0.5	3.0785	1	

Table 4.7: Objective Results

m_t (kg)	$A_{3\underline{R}PR}$ (m^2)	l_{LRDW} (m)	h_{LRDW} (m)
57.9781	8.2073	0.42	0.42

4.9 Optimization Problem of 3-R$\underline{P}$R Manipulator

Optimization problem of 3-R$\underline{P}$R manipulator is to find the optimal design variables that minimize its total mass in motion and compactness. Figure 4.18 shows the 3-R$\underline{P}$R manipulator model and its design parameters.

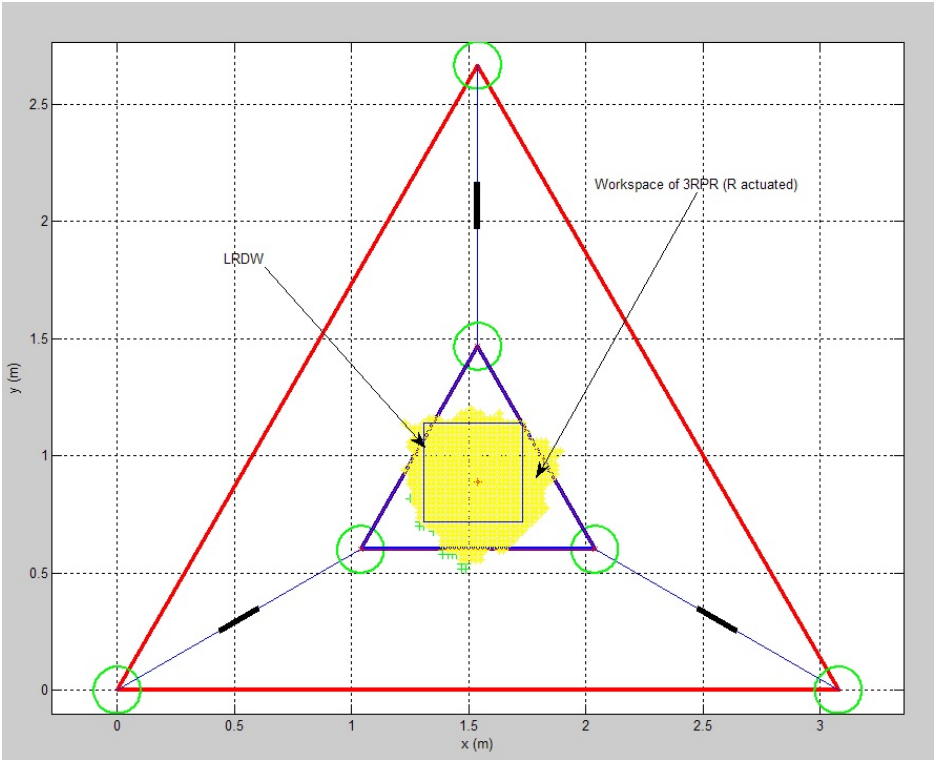

Fig. 4.17: Optimal Design of The 3-RPR and Largest Regular Dexterous Workspace

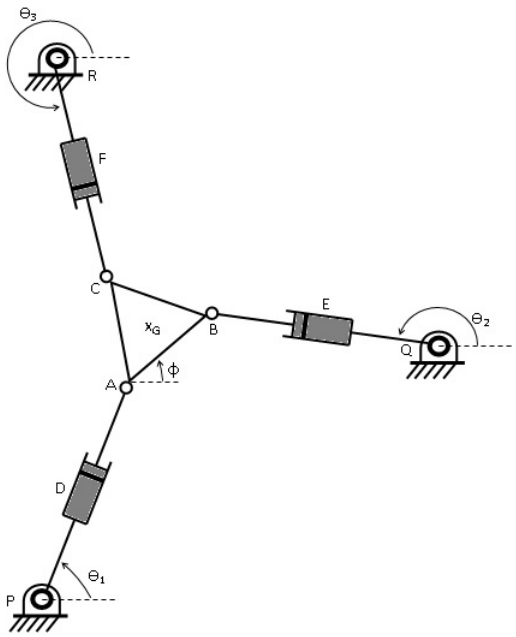

Fig. 4.18: 3-RPR Model and Parameters

4.9.1 Objective Functions

Objective functions of this optimization are similar with the other manipulators. The first is to minimize total mass in motion and the second is to minimize compactness of the robot. Due to similarity of manipulator architecture and parameters between

3-RPR and 3-RPR, the mathematical equations to calculate mass in motion and compactness of 3-RPR are not written again. One can directly refer it to the previous chapter.

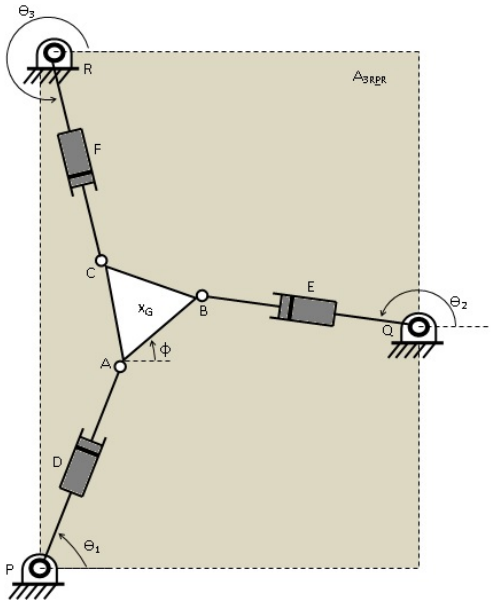

Fig. 4.19: Bounding Box of The 3-RPR Manipulator

4.9.2 Design Variables

The design variables of the optimization problem are the components of vector $\mathbf{x}_5$.

$$\mathbf{x} = [r_{out}\ r_{in}\ r_{Tool}\ L_1\ L_2\ EE_{width}\ Base_{width}]^T \tag{4.64}$$

4.9.3 Summary

The 3-RPR manipulator optimization problem can be formulated as follows,

$$\begin{aligned}
minimize \quad & f_1(\mathbf{x}) = m_{t_{3RPR}} \\
& f_2(\mathbf{x}) = A_{3RPR} \\
over \quad & \mathbf{x}_4 = [r_{out}\ r_{in}\ r_{Tool}\ L_1\ L_2\ EE_{width}\ Base_{width}]^T \\
subject\ to \quad & g1 = r_{out} \geq r_{in} + 0.001 \\
& g2 = l_{LRDW} \geq w_l \\
& g3 = h_{LRDW} \geq w_h \\
& g4 = \delta x_{min} \leq \delta x \leq \delta x_{max} \\
& g4 = \delta y_{min} \leq \delta y \leq \delta y_{max} \\
& g5 = \delta \Phi_{z_{min}} \leq \delta \Phi_z \leq \delta \Phi_{z_{max}} \\
& g6 = R_{1_{max}} \leq R_{adm} \\
& g7 = R_{2_{max}} \leq R_{adm} \\
& g8 = R_{3_{max}} \leq R_{adm} \\
& \mathbf{x}_{lb} \leq \mathbf{x} \leq \mathbf{x}_{ub}
\end{aligned} \tag{4.65}$$

where $\mathbf{x}_{lb}$ and $\mathbf{x}_{ub}$ are lower and upper bounds of $\mathbf{x}_5$, respectively.

4.9.4 Results

The optimal design parameters result obtained form *fmincon* function in MATLAB with several starting points are shown in table 4.8. Table 4.9 shows the results of mass in motion and compactness calculation for a given optimum parameters. The corresponding 2D optimum desing of the 3-RPR and LRDW are depict in figure 4.20.

Table 4.8: Optimum Design Parameters of The 3-RPR

rout (m)	rin (m)	rTool (m)	L1 (m)	L2 (m)	BaseWidth	EEWidth
0.0175	0.0075	0.01	0.5015	0.5154	3.0785	1

Table 4.9: Objective Results

mt (kg)	ARRRRR (m2)	lLRDW (m)	hLRDW (m)
46.1527	8.2073	0.44	0.44

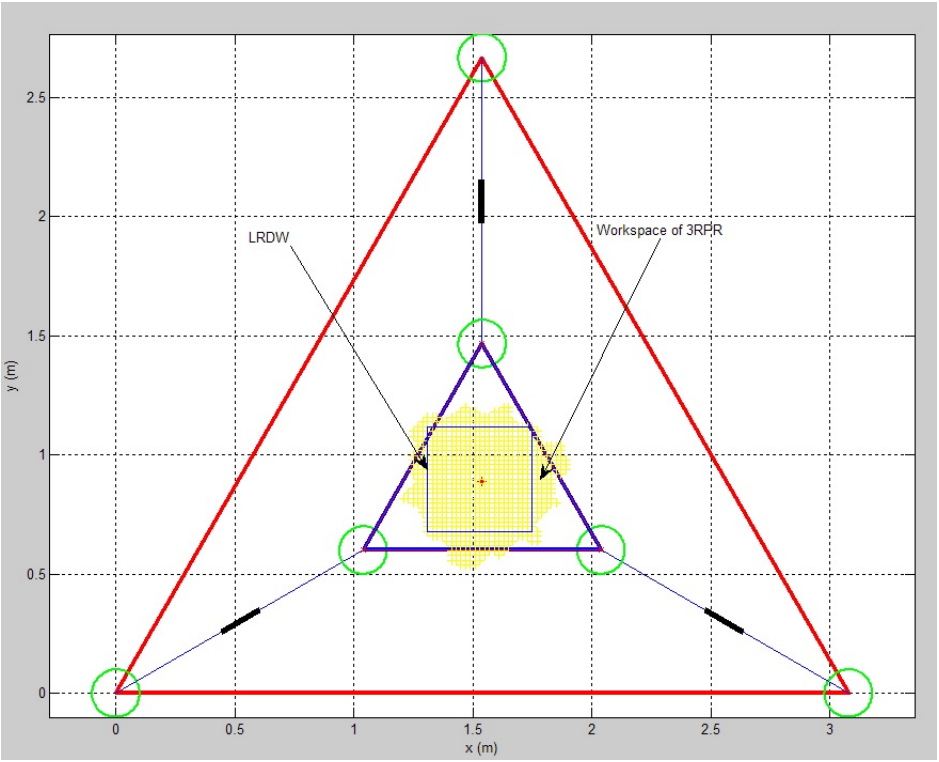

Fig. 4.20: Optimal Design of The 3-RPR and Largest Regular Dexterous Workspace

4.10 Displacement Comparison of 2-DOF Planar Parallel Manipulator

In this section, a comparison between the RRRRR and the RPRPR manipulator in the term of displacements factor is done. The purpose of this comparison is to determine which manipulator's architecture has a better stiffness.

To do the comparison, the external forces, in the magnitude of 10 N, and moments, in the magnitude of 1 Nm, are applied to the end-effector of the optimum design of the manipulators. The comparison is also performed in several locations within the workspace of the manipulators. The determination of test locations is important part because we should guarantee that those locations are reachable by both the manipulators before performing displacement analysis.

The determination of testing locations is performed by finding intersection area in the workspace of both manipulators. In figure 4.8 and figure 4.11, the workspace area of RRRRR and RPRPR are denoted by yellow area. By intersecting the workspace area of both manipulator we are able to choose several test points.

Table 4.10 and 4.11 shows displacement analysis for for 4 testing points. Table 4.12 and 4.13 informs mean and maximum displacement for both manipulators.

According to data on table 4.12, the RRRRR manipulator has bigger displacement value than the RPRPR manipulator for both linear displacement and rotation angle.

The similar condition is found for the mean linear displacement and rotation angle of the RRRRR manipulator. Therefore, the RPRPR manipulator has a better architecture than the RRRRR manipulator in the term of stiffness since it has lower value for both linear displacement and rotation angle.

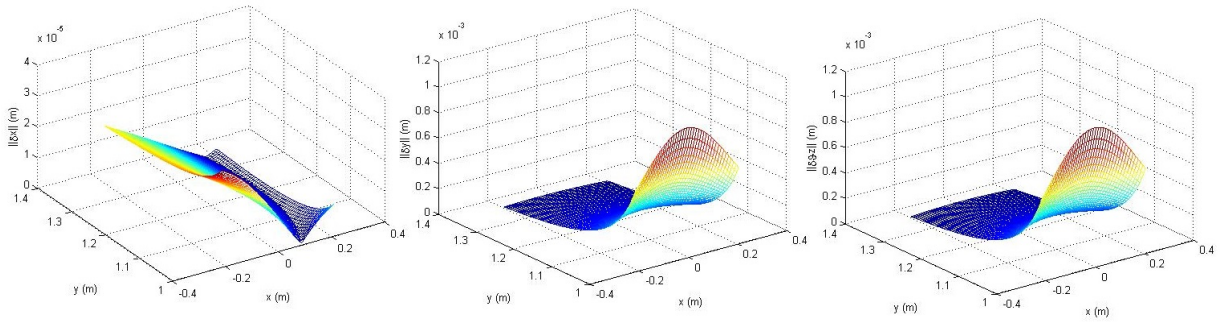

Fig. 4.21: Displacement Error of The RRRRR, Fx = 10N Fy = 10N Mz = 1Nm

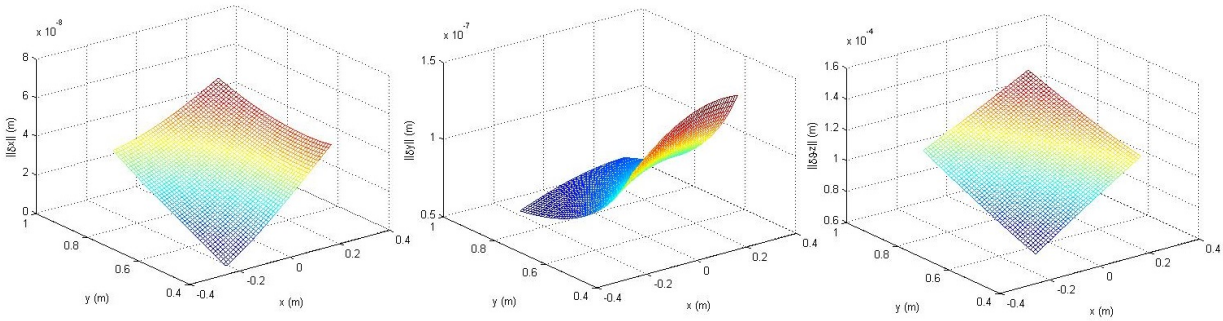

Fig. 4.22: Displacement Error of The RPRPR, Fx = 10N Fy = 10N Mz = 1Nm

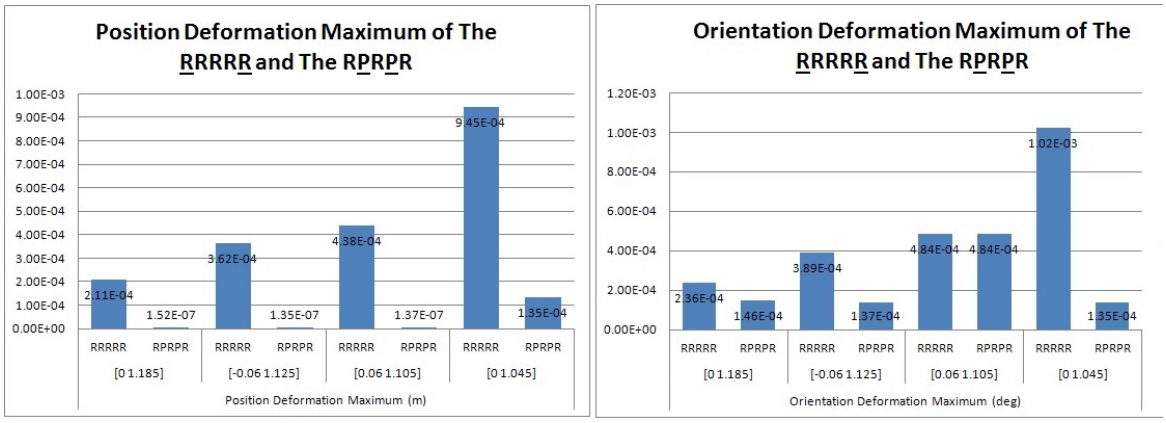

Fig. 4.23: The 2-DOF Comparison of Maximum Deformation at Several Points

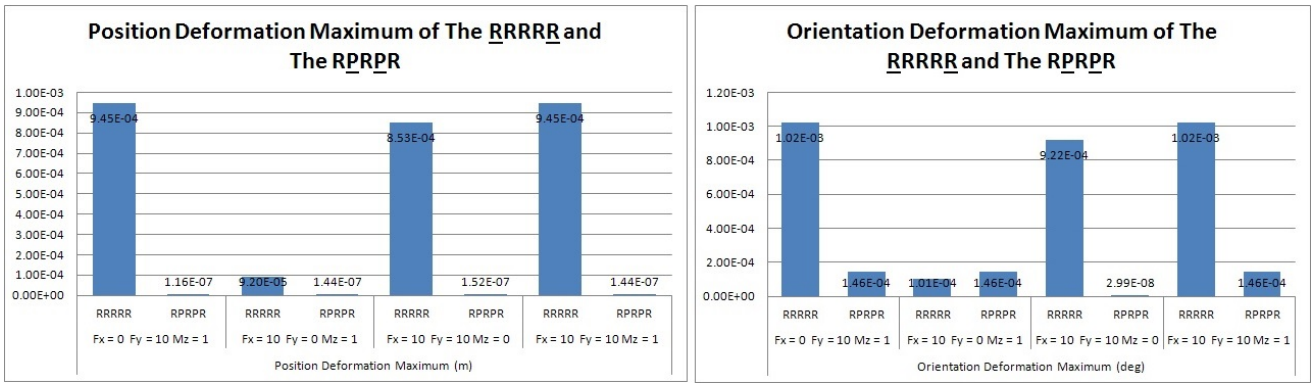

Fig. 4.24: The 2-DOF Comparison of Maximum Deformation for Several Wrench

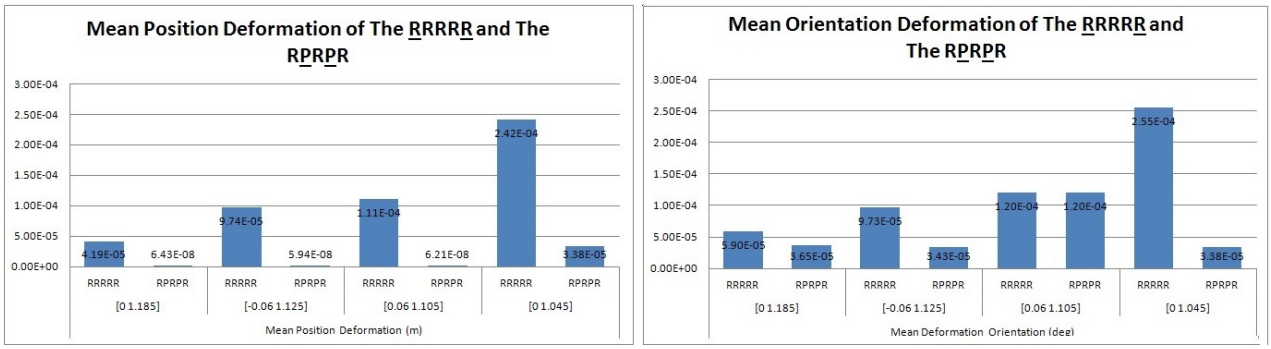

Fig. 4.25: The 2-DOF Comparison of Mean Deformation at Several Points

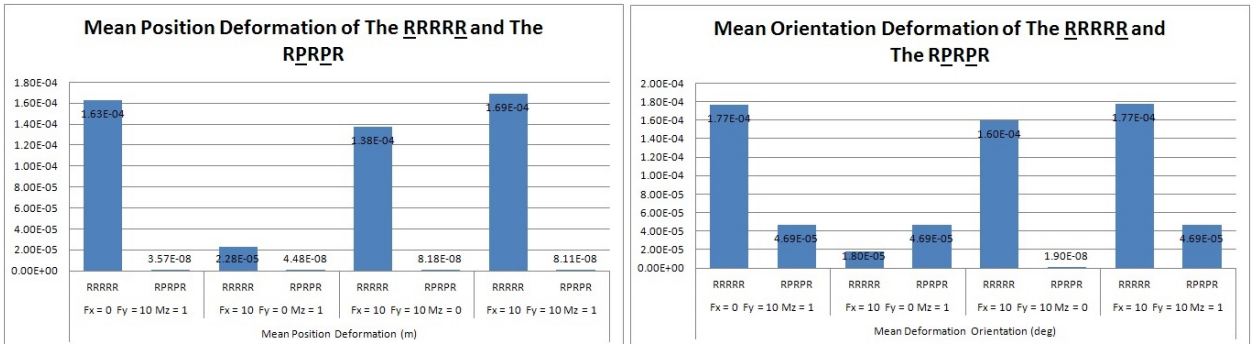

Fig. 4.26: The 2-DOF Comparison of Mean Deformation for Several Wrench

4.11 Displacement Comparison of 3-DOF Planar Parallel Manipulator

There are three 3-DOF planar parallel manipulators under study in this thesis: the 3-RRR, 3-RPR, and the 3-RPR manipulator. In this chapter, a displacement comparison is done for those three manipulators. The goal of this comparison is to determine which manipulator's architecture has a better stiffness.

Previous section already explained about the important of testing points determination. The selected testing points should lay inside the intersection workspace area of the three manipulators. Since this will guarantee that the points are reachable by those three manipulators.

Figure 4.20, 4.17, and 4.14 denote the workspace of these three manipulators as yellow area. By intersecting these areas, we can determine the testing points. In this case, four points inside the area are selected as shown in table 4.14.

Table 4.14, 4.15, and 4.16 shows the linear and rotation displacement at several points under subject of several combination of forces and moments. In addition, Table 4.17 and table 4.18 show the maximum and mean of displacement.

According to table 4.17, the 3-RRR manipulator has the smallest both linear and rotation displacements value comparing to the others. Similar condition is found for the mean deformation value. Therefore, the 3-RRR manipulator has a better architecture than the 3-RPR and the 3-RPR manipulators in the term of stiffness because it has smallest linear and rotation displacement value.

Table 4.10: Deformation Error of RPRPR Manipulator

Coordinate	Linear Displacement		Rotation Angle	
$[x\ y]^T$	δp_x δp_y δp_z	Norm	$\delta\varphi_x$ $\delta\varphi_y$ $\delta\varphi_z$	Norm
$F_x = 10\ F_y = 10\ M_z = 0$				
[0 1.185]	1.52E-07 1.08E-07 0.00E+00	1.86E-07	0.00E+00 0.00E+00 -2.99E-08	2.99E-08
[−0.06 1.125]	1.35E-07 1.05E-07 0.00E+00	1.71E-07	0.00E+00 0.00E+00 -2.46E-08	2.46E-08
[0.06 1.105]	1.37E-07 1.12E-07 0.00E+00	1.77E-07	0.00E+00 0.00E+00 -1.39E-08	1.39E-08
[0 1.045]	1.21E-07 1.11E-07 0.00E+00	1.64E-07	0.00E+00 0.00E+00 -7.46E-09	7.46E-09

Coordinate	Linear Displacement		Rotation Angle	
$[x\ y]^T$	δp_x δp_y δp_z	Norm	$\delta\varphi_x$ $\delta\varphi_y$ $\delta\varphi_z$	Norm
$F_x = 10\ F_y = 0\ M_z = 1$				
[0 1.185]	1.44E-07 4.50E-09 0.00E+00	1.44E-07	0.00E+00 0.00E+00 1.46E-04	1.46E-04
[−0.06 1.125]	1.31E-07 1.58E-09 0.00E+00	1.31E-07	0.00E+00 0.00E+00 1.37E-04	1.37E-04
[0.06 1.105]	1.28E-07 8.27E-09 0.00E+00	1.28E-07	0.00E+00 0.00E+00 1.44E-04	1.44E-04
[0 1.045]	1.15E-07 5.28E-09 0.00E+00	1.15E-07	0.00E+00 0.00E+00 1.35E-04	1.35E-04

Coordinate	Linear Displacement		Rotation Angle	
$[x\ y]^T$	δp_x δp_y δp_z	Norm	$\delta\varphi_x$ $\delta\varphi_y$ $\delta\varphi_z$	Norm
$F_x = 0\ F_y = 10\ M_z = 1$				
[0 1.185]	-7.49E-09 1.13E-07 0.00E+00	1.13E-07	0.00E+00 0.00E+00 1.46E-04	1.46E-04
[−0.06 1.125]	-1.07E-08 1.13E-07 0.00E+00	1.14E-07	0.00E+00 0.00E+00 1.37E-04	1.37E-04
[0.06 1.105]	-2.63E-09 1.14E-07 0.00E+00	1.14E-07	0.00E+00 0.00E+00 1.44E-04	1.44E-04
[0 1.045]	-6.03E-09 1.16E-07 0.00E+00	1.16E-07	0.00E+00 0.00E+00 1.35E-04	1.35E-04

Coordinate	Linear Displacement		Rotation Angle	
$[x\ y]^T$	δp_x δp_y δp_z	Norm	$\delta\varphi_x$ $\delta\varphi_y$ $\delta\varphi_z$	Norm
$F_x = 10\ F_y = 10\ M_z = 1$				
[0 1.185]	1.44E-07 1.13E-07 0.00E+00	1.83E-07	0.00E+00 0.00E+00 1.46E-04	1.46E-04
[−0.06 1.125]	1.28E-07 1.10E-07 0.00E+00	1.68E-07	0.00E+00 0.00E+00 1.37E-04	1.37E-04
[0.06 1.105]	1.31E-07 1.17E-07 0.00E+00	1.76E-07	0.00E+00 0.00E+00 1.44E-04	1.44E-04
[0 1.045]	1.15E-07 1.16E-07 0.00E+00	1.63E-07	0.00E+00 0.00E+00 1.35E-04	1.35E-04

Table 4.11: Deformation Error of RRRRR Manipulator

Coordinate	Linear Displacement		Rotation Angle	
$[x\ y]^T$	δp_x δp_y δp_z	Norm	$\delta\varphi_x$ $\delta\varphi_y$ $\delta\varphi_z$	Norm
$F_x = 10\ F_y = 10\ M_z = 0$				
[0 1.185]	1.99E-05 0.00E+00 0.00E+00	1.91E-04	0.00E+00 0.00E+00 2.13E-04	2.13E-04
[−0.06 1.125]	2.69E-05 3.28E-04 0.00E+00	3.29E-04	0.00E+00 0.00E+00 3.52E-04	3.52E-04
[0.06 1.105]	1.39E-05 3.88E-04 0.00E+00	3.88E-04	0.00E+00 0.00E+00 4.32E-04	4.32E-04
[0 1.045]	2.11E-05 8.53E-04 0.00E+00	8.54E-04	0.00E+00 0.00E+00 9.22E-04	9.22E-04

Coordinate	Linear Displacement		Rotation Angle	
$[x\ y]^T$	δp_x δp_y δp_z	Norm	$\delta\varphi_x$ $\delta\varphi_y$ $\delta\varphi_z$	Norm
$F_x = 10\ F_y = 0\ M_z = 1$				
[0 1.185]	2.02E-05 2.10E-05 0.00E+00	2.91E-05	0.00E+00 0.00E+00 2.59E-05	2.59E-05
[−0.06 1.125]	2.13E-05 4.09E-05 0.00E+00	4.61E-05	0.00E+00 0.00E+00 4.46E-05	4.46E-05
[0.06 1.105]	2.03E-05 3.68E-05 0.00E+00	4.20E-05	0.00E+00 0.00E+00 4.44E-05	4.44E-05
[0 1.045]	2.13E-05 9.20E-05 0.00E+00	9.45E-05	0.00E+00 0.00E+00 1.01E-04	1.01E-04

Coordinate	Linear Displacement		Rotation Angle	
$[x\ y]^T$	δp_x δp_y δp_z	Norm	$\delta\varphi_x$ $\delta\varphi_y$ $\delta\varphi_z$	Norm
$F_x = 0\ F_y = 10\ M_z = 1$				
[0 1.185]	2.61E-07 2.11E-04 0.00E+00	2.11E-04	0.00E+00 0.00E+00 2.33E-04	2.33E-04
[−0.06 1.125]	7.20E-06 3.56E-04 0.00E+00	3.56E-04	0.00E+00 0.00E+00 3.82E-04	3.82E-04
[0.06 1.105]	-7.19E-06 4.38E-04 0.00E+00	4.38E-04	0.00E+00 0.00E+00 4.84E-04	4.84E-04
[0 1.045]	1.83E-07 9.45E-04 0.00E+00	9.45E-04	0.00E+00 0.00E+00 1.02E-03	1.02E-03

Coordinate	Linear Displacement		Rotation Angle	
$[x\ y]^T$	δp_x δp_y δp_z	Norm	$\delta\varphi_x$ $\delta\varphi_y$ $\delta\varphi_z$	Norm
$F_x = 10\ F_y = 10\ M_z = 1$				
[0 1.185]	2.02E-05 2.11E-04 0.00E+00	2.12E-04	0.00E+00 0.00E+00 2.36E-04	2.36E-04
[−0.06 1.125]	2.77E-05 3.62E-04 0.00E+00	3.63E-04	0.00E+00 0.00E+00 3.89E-04	3.89E-04
[0.06 1.105]	1.35E-05 4.31E-04 0.00E+00	4.32E-04	0.00E+00 0.00E+00 4.80E-04	4.80E-04
[0 1.045]	2.13E-05 9.45E-04 0.00E+00	9.46E-04	0.00E+00 0.00E+00 1.02E-03	1.02E-03

Table 4.12: Comparison Maximum Deformation Error Between The RRRRR and The RPRPR Manipulator

Position Deformation Maximum (m)							
[0 1.185]		[-0.06 1.125]		[0.06 1.105]		[0 1.045]	
RRRRR	RPRPR	RRRRR	RPRPR	RRRRR	RPRPR	RRRRR	RPRPR
2.11E-04	1.52E-07	3.62E-04	1.35E-07	4.38E-04	1.37E-07	9.45E-04	1.35E-04

Position Deformation Maximum (m)							
Fx = 0 Fy = 10 Mz = 1		Fx = 10 Fy = 0 Mz = 1		Fx = 10 Fy = 10 Mz = 0		Fx = 10 Fy = 10 Mz = 1	
RRRRR	RPRPR	RRRRR	RPRPR	RRRRR	RPRPR	RRRRR	RPRPR
9.45E-04	1.16E-07	9.20E-05	1.44E-07	8.53E-04	1.52E-07	9.45E-04	1.44E-07

Orientation Deformation Maximum (deg)							
[0 1.185]		[-0.06 1.125]		[0.06 1.105]		[0 1.045]	
RRRRR	RPRPR	RRRRR	RPRPR	RRRRR	RPRPR	RRRRR	RPRPR
2.36E-04	1.46E-04	3.89E-04	1.37E-04	4.84E-04	4.84E-04	1.02E-03	1.35E-04

Orientation Deformation Maximum (deg)							
Fx = 0 Fy = 10 Mz = 1		Fx = 10 Fy = 0 Mz = 1		Fx = 10 Fy = 10 Mz = 0		Fx = 10 Fy = 10 Mz = 1	
RRRRR	RPRPR	RRRRR	RPRPR	RRRRR	RPRPR	RRRRR	RPRPR
1.02E-03	1.46E-04	1.01E-04	1.46E-04	9.22E-04	2.99E-08	1.02E-03	1.46E-04

Table 4.13: Comparison Mean Deformation Error Between The RRRRR and The RPRPR Manipulator

Mean Position Deformation (m)							
[0 1.185]		[-0.06 1.125]		[0.06 1.105]		[0 1.045]	
RRRRR	RPRPR	RRRRR	RPRPR	RRRRR	RPRPR	RRRRR	RPRPR
4.19E-05	6.43E-08	9.74E-05	5.94E-08	1.11E-04	6.21E-08	2.42E-04	3.38E-05

Mean Orientation Deformation (deg)							
[0 1.185]		[-0.06 1.125]		[0.06 1.105]		[0 1.045]	
RRRRR	RPRPR	RRRRR	RPRPR	RRRRR	RPRPR	RRRRR	RPRPR
5.90E-05	3.65E-05	9.73E-05	3.43E-05	1.20E-04	1.20E-04	2.55E-04	3.38E-05

Mean Position Deformation (m)							
Fx = 0 Fy = 10 Mz = 1		Fx = 10 Fy = 0 Mz = 1		Fx = 10 Fy = 10 Mz = 0		Fx = 10 Fy = 10 Mz = 1	
RRRRR	RPRPR	RRRRR	RPRPR	RRRRR	RPRPR	RRRRR	RPRPR
1.63E-04	3.57E-08	2.28E-05	4.48E-08	1.38E-04	8.18E-08	1.69E-04	8.11E-08

Mean Orientation Deformation (deg)							
Fx = 0 Fy = 10 Mz = 1		Fx = 10 Fy = 0 Mz = 1		Fx = 10 Fy = 10 Mz = 0		Fx = 10 Fy = 10 Mz = 1	
RRRRR	RPRPR	RRRRR	RPRPR	RRRRR	RPRPR	RRRRR	RPRPR
1.77E-04	4.69E-05	1.80E-05	4.69E-05	1.60E-04	1.90E-08	1.77E-04	4.69E-05

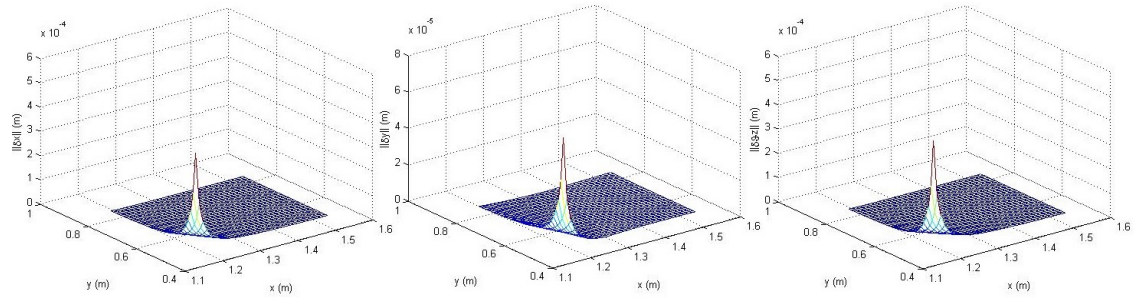

Fig. 4.27: Displacement Error of The 3-RRR, Fx = 10N Fy = 10N Mz = 1Nm

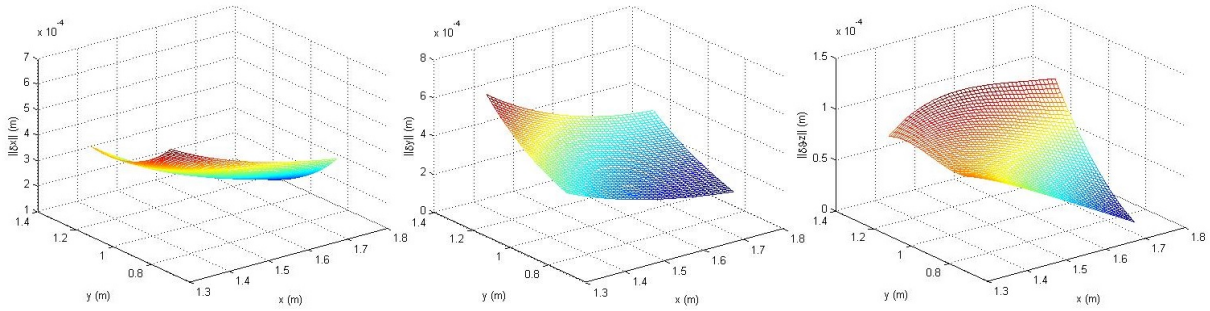

Fig. 4.28: Displacement Error of The 3-RPR, Fx = 10N Fy = 10N Mz = 1Nm

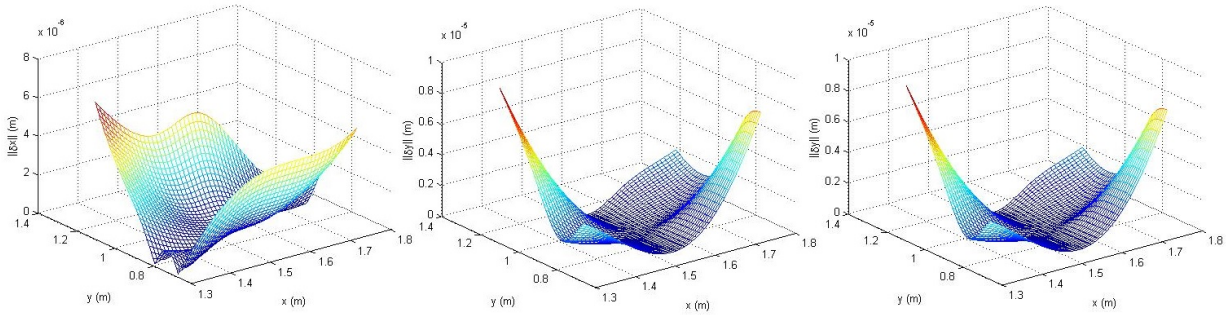

Fig. 4.29: Displacement Error of The 3-RPR, Fx = 10N Fy = 10N Mz = 1Nm

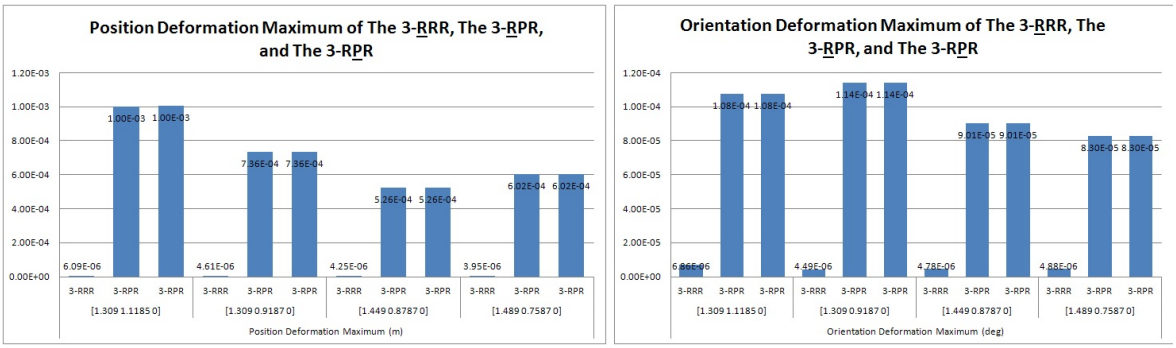

Fig. 4.30: The 3-DOF Comparison of Maximum Deformation at Several Points

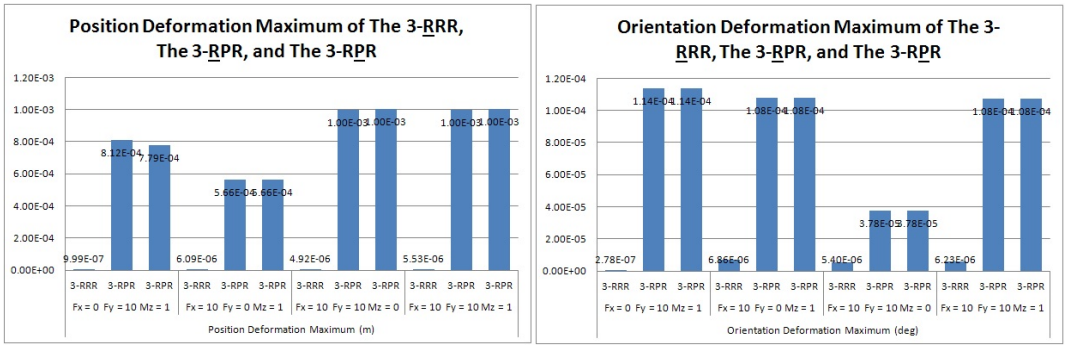

Fig. 4.31: The 3-DOF Comparison of Maximum Deformation for Several Wrench

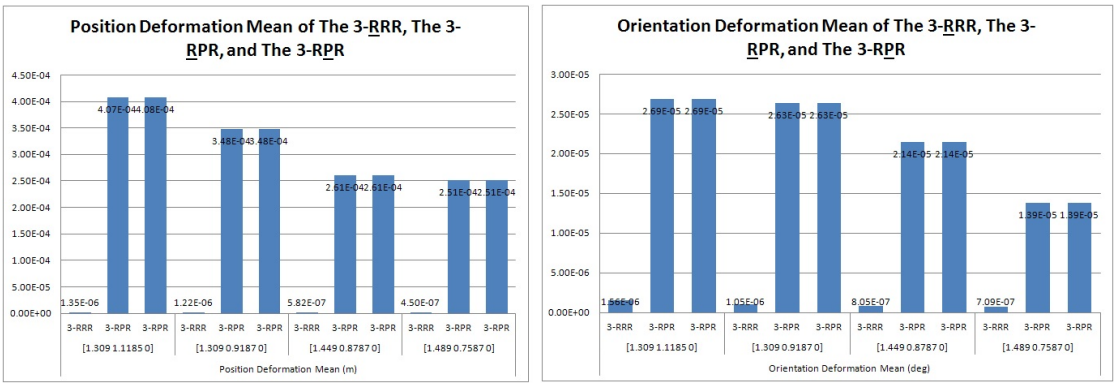

Fig. 4.32: The 3-DOF Comparison of Mean Deformation at Several Points

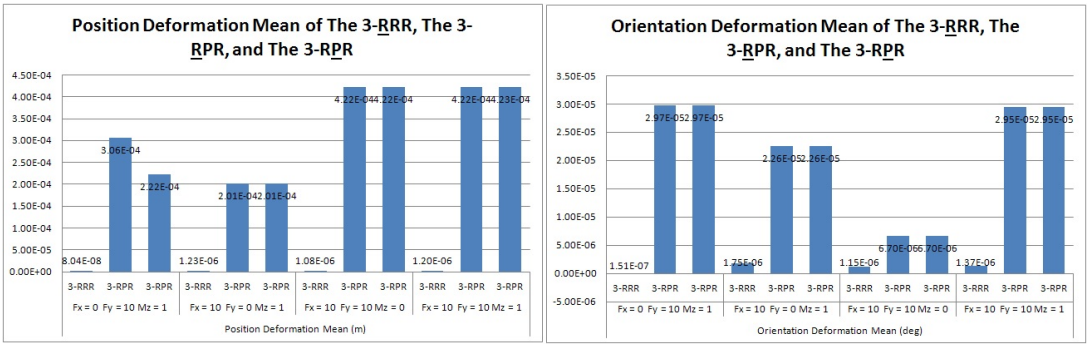

Fig. 4.33: The 3-DOF Comparison of Mean Deformation for Several Wrench

Table 4.14: Deformation Error of The 3-RRR Manipulator

Coordinate	Linear Displacement		Rotation Angle	
$[x\ y]^T$	δp_x δp_y δp_z	Norm	$\delta\varphi_x$ $\delta\varphi_y$ $\delta\varphi_z$	Norm
$F_x = 10\ F_y = 10\ M_z = 0$				
[1.309 1.11850]	4.92E-06 -6.20E-08 0.00E+00	4.92E-06	0.00E+00 0.00E+00 5.40E-06	5.40E-06
[1.309 0.91870]]	4.09E-06 4.09E-07 0.00E+00	4.11E-06	0.00E+00 0.00E+00 3.66E-06	3.66E-06
[1.449 0.87870]	2.46E-06 -3.89E-07 0.00E+00	2.49E-06	0.00E+00 0.00E+00 2.59E-06	2.59E-06
[1.489 0.75870]	1.96E-06 -3.72E-07 0.00E+00	1.99E-06	0.00E+00 0.00E+00 2.14E-06	2.14E-06

Coordinate	Linear Displacement		Rotation Angle	
$[x\ y]^T$	δp_x δp_y δp_z	Norm	$\delta\varphi_x$ $\delta\varphi_y$ $\delta\varphi_z$	Norm
$F_x = 10\ F_y = 0\ M_z = 1$				
[1.309 1.11850]	6.09E-06 -6.24E-07 0.00E+00	6.12E-06	0.00E+00 0.00E+00 6.86E-06	6.86E-06
[1.309 0.91870]]	4.61E-06 -1.56E-07 0.00E+00	4.62E-06	0.00E+00 0.00E+00 4.49E-06	4.49E-06
[1.449 0.87870]	4.25E-06 -1.53E-06 0.00E+00	4.52E-06	0.00E+00 0.00E+00 4.78E-06	4.78E-06
[1.489 0.75870]	3.95E-06 -1.78E-06 0.00E+00	4.33E-06	0.00E+00 0.00E+00 4.88E-06	4.88E-06

Coordinate	Linear Displacement		Rotation Angle	
$[x\ y]^T$	δp_x δp_y δp_z	Norm	$\delta\varphi_x$ $\delta\varphi_y$ $\delta\varphi_z$	Norm
$F_x = 0\ F_y = 10\ M_z = 1$				
[1.309 1.11850]	4.26E-08 4.36E-07 0.00E+00	4.38E-07	0.00E+00 0.00E+00 1.91E-07	1.91E-07
[1.309 0.91870]]	2.65E-07 5.10E-07 0.00E+00	5.75E-07	0.00E+00 0.00E+00 2.78E-07	2.78E-07
[1.449 0.87870]	-9.64E-07 8.33E-07 0.00E+00	1.27E-06	0.00E+00 0.00E+00 -9.27E-07	9.27E-07
[1.489 0.75870]	-1.16E-06 9.99E-07 0.00E+00	1.53E-06	0.00E+00 0.00E+00 -1.35E-06	1.35E-06

Coordinate	Linear Displacement		Rotation Angle	
$[x\ y]^T$	δp_x δp_y δp_z	Norm	$\delta\varphi_x$ $\delta\varphi_y$ $\delta\varphi_z$	Norm
$F_x = 10\ F_y = 10\ M_z = 1$				
[1.309 1.11850]	5.53E-06 -1.25E-07 0.00E+00	5.53E-06	0.00E+00 0.00E+00 6.23E-06	6.23E-06
[1.309 0.91870]]	4.48E-06 3.81E-07 0.00E+00	4.50E-06	0.00E+00 0.00E+00 4.22E-06	4.22E-06
[1.449 0.87870]	2.87E-06 -5.45E-07 0.00E+00	2.93E-06	0.00E+00 0.00E+00 3.22E-06	3.22E-06
[1.489 0.75870]	2.38E-06 -5.76E-07 0.00E+00	2.44E-06	0.00E+00 0.00E+00 2.83E-06	2.83E-06

Table 4.15: Deformation Error of The 3-RPR Manipulator

Coordinate	Linear Displacement		Rotation Angle	
$[x\ y]^T$	δp_x δp_y δp_z	Norm	$\delta\varphi_x$ $\delta\varphi_y$ $\delta\varphi_z$	Norm
$F_x = 10\ F_y = 10\ M_z = 0$				
[1.309 1.11850]	6.23E-04 1.00E-03 0.00E+00	1.18E-03	0.00E+00 0.00E+00 3.78E-05	3.78E-05
[1.309 0.91870]]	6.56E-04 7.32E-04 0.00E+00	9.82E-04	0.00E+00 0.00E+00 3.66E-05	3.66E-05
[1.449 0.87870]	5.26E-04 5.16E-04 0.00E+00	7.37E-04	0.00E+00 0.00E+00 1.83E-05	1.83E-05
[1.489 0.75870]	6.02E-04 4.05E-04 0.00E+00	7.25E-04	0.00E+00 0.00E+00 -1.23E-05	1.23E-05

Coordinate	Linear Displacement		Rotation Angle	
$[x\ y]^T$	δp_x δp_y δp_z	Norm	$\delta\varphi_x$ $\delta\varphi_y$ $\delta\varphi_z$	Norm
$F_x = 10\ F_y = 0\ M_z = 1$				
[1.309 1.11850]	4.02E-04 2.25E-04 0.00E+00	4.60E-04	0.00E+00 0.00E+00 1.08E-04	1.08E-04
[1.309 0.91870]]	4.74E-04 1.85E-04 0.00E+00	5.09E-04	0.00E+00 0.00E+00 6.01E-05	6.01E-05
[1.449 0.87870]	4.62E-04 6.62E-05 0.00E+00	4.66E-04	0.00E+00 0.00E+00 6.31E-05	6.31E-05
[1.489 0.75870]	5.66E-04 3.45E-05 0.00E+00	5.67E-04	0.00E+00 0.00E+00 4.02E-05	4.02E-05

Coordinate	Linear Displacement		Rotation Angle	
$[x\ y]^T$	δp_x δp_y δp_z	Norm	$\delta\varphi_x$ $\delta\varphi_y$ $\delta\varphi_z$	Norm
$F_x = 0\ F_y = 10\ M_z = 1$				
[1.309 1.11850]	2.29E-04 7.79E-04 0.00E+00	8.12E-04	0.00E+00 0.00E+00 6.97E-05	6.97E-05
[1.309 0.91870]]	1.80E-04 5.56E-04 0.00E+00	5.84E-04	0.00E+00 0.00E+00 1.14E-04	1.14E-04
[1.449 0.87870]	6.35E-05 4.54E-04 0.00E+00	4.59E-04	0.00E+00 0.00E+00 9.01E-05	9.01E-05
[1.489 0.75870]	3.02E-05 3.74E-04 0.00E+00	3.75E-04	0.00E+00 0.00E+00 8.30E-05	8.30E-05

Coordinate	Linear Displacement		Rotation Angle	
$[x\ y]^T$	δp_x δp_y δp_z	Norm	$\delta\varphi_x$ $\delta\varphi_y$ $\delta\varphi_z$	Norm
$F_x = 10\ F_y = 10\ M_z = 1$				
[1.309 1.11850]	6.27E-04 1.00E-03 0.00E+00	1.18E-03	0.00E+00 0.00E+00 1.08E-04	1.08E-04
[1.309 0.91870]]	6.55E-04 7.36E-04 0.00E+00	9.85E-04	0.00E+00 0.00E+00 1.05E-04	1.05E-04
[1.449 0.87870]	5.26E-04 5.18E-04 0.00E+00	7.38E-04	0.00E+00 0.00E+00 8.58E-05	8.58E-05
[1.489 0.75870]	5.99E-04 4.07E-04 0.00E+00	7.24E-04	0.00E+00 0.00E+00 5.54E-05	5.54E-05

Table 4.16: Deformation Error of The 3-RPR Manipulator

Coordinate	Linear Displacement		Rotation Angle	
$[x\ y]^T$	δp_x δp_y δp_z	Norm	$\delta\varphi_x$ $\delta\varphi_y$ $\delta\varphi_z$	Norm
$F_x = 10\ F_y = 10\ M_z = 0$				
[1.309 1.11850]	6.23E-04 1.00E-03 0.00E+00	1.18E-03	0.00E+00 0.00E+00 3.78E-05	3.78E-05
[1.309 0.91870]]	6.56E-04 7.32E-04 0.00E+00	9.82E-04	0.00E+00 0.00E+00 3.66E-05	3.66E-05
[1.449 0.87870]	5.26E-04 5.16E-04 0.00E+00	7.37E-04	0.00E+00 0.00E+00 1.83E-05	1.83E-05
[1.489 0.75870]	6.02E-04 4.05E-04 0.00E+00	7.25E-04	0.00E+00 0.00E+00 -1.23E-05	1.23E-05

Coordinate	Linear Displacement		Rotation Angle	
$[x\ y]^T$	δp_x δp_y δp_z	Norm	$\delta\varphi_x$ $\delta\varphi_y$ $\delta\varphi_z$	Norm
$F_x = 10\ F_y = 0\ M_z = 1$				
[1.309 1.11850]	4.02E-04 2.25E-04 0.00E+00	4.60E-04	0.00E+00 0.00E+00 1.08E-04	1.08E-04
[1.309 0.91870]]	4.74E-04 1.85E-04 0.00E+00	5.09E-04	0.00E+00 0.00E+00 6.01E-05	6.01E-05
[1.449 0.87870]	4.62E-04 6.62E-05 0.00E+00	4.66E-04	0.00E+00 0.00E+00 6.31E-05	6.31E-05
[1.489 0.75870]	5.66E-04 3.45E-05 0.00E+00	5.67E-04	0.00E+00 0.00E+00 4.02E-05	4.02E-05

Coordinate	Linear Displacement		Rotation Angle	
$[x\ y]^T$	δp_x δp_y δp_z	Norm	$\delta\varphi_x$ $\delta\varphi_y$ $\delta\varphi_z$	Norm
$F_x = 0\ F_y = 10\ M_z = 1$				
[1.309 1.11850]	2.29E-04 7.79E-04 0.00E+00	8.12E-04	0.00E+00 0.00E+00 6.97E-05	6.97E-05
[1.309 0.91870]]	1.80E-04 5.56E-04 0.00E+00	5.84E-04	0.00E+00 0.00E+00 1.14E-04	1.14E-04
[1.449 0.87870]	6.35E-05 4.54E-04 0.00E+00	4.59E-04	0.00E+00 0.00E+00 9.01E-05	9.01E-05
[1.489 0.75870]	3.02E-05 3.74E-04 0.00E+00	3.75E-04	0.00E+00 0.00E+00 8.30E-05	8.30E-05

Coordinate	Linear Displacement		Rotation Angle	
$[x\ y]^T$	δp_x δp_y δp_z	Norm	$\delta\varphi_x$ $\delta\varphi_y$ $\delta\varphi_z$	Norm
$F_x = 10\ F_y = 10\ M_z = 1$				
[1.309 1.11850]	6.27E-04 1.00E-03 0.00E+00	1.18E-03	0.00E+00 0.00E+00 1.08E-04	1.08E-04
[1.309 0.91870]]	6.55E-04 7.36E-04 0.00E+00	9.85E-04	0.00E+00 0.00E+00 1.05E-04	1.05E-04
[1.449 0.87870]	5.26E-04 5.18E-04 0.00E+00	7.38E-04	0.00E+00 0.00E+00 8.58E-05	8.58E-05
[1.489 0.75870]	5.99E-04 4.07E-04 0.00E+00	7.24E-04	0.00E+00 0.00E+00 5.54E-05	5.54E-05

Table 4.17: Comparison Maximum Deformation Error of The 3-RRR, The 3-RPR, and The 3-RPR Manipulators

Position Deformation Maximum (m)											
[1.309 1.1185 0]			[1.309 0.9187 0]			[1.449 0.8787 0]			[1.489 0.7587 0]		
3-RRR	3-RPR	3-RPR	3-RRR	3-RPR	3-RPR	3-RRR	3-RPR	3-RPR	3-RRR	3-RPR	3-RPR
6.09E-06	1.00E-03	1.00E-03	4.61E-06	7.36E-04	7.36E-04	4.25E-06	5.26E-04	5.26E-04	3.95E-06	6.02E-04	6.02E-04

Orientation Deformation Maximum (deg)											
Fx = 0 Fy = 10 Mz = 1			Fx = 10 Fy = 0 Mz = 1			Fx = 10 Fy = 10 Mz = 0			Fx = 10 Fy = 10 Mz = 1		
3-RRR	3-RPR	3-RPR	3-RRR	3-RPR	3-RPR	3-RRR	3-RPR	3-RPR	3-RRR	3-RPR	3-RPR
6.86E-06	1.08E-04	1.08E-04	4.49E-06	1.14E-04	1.14E-04	4.78E-06	9.01E-05	9.01E-05	4.88E-06	8.30E-05	8.30E-05

Position Deformation Maximum (m)											
[1.309 1.1185 0]			[1.309 0.9187 0]			[1.449 0.8787 0]			[1.489 0.7587 0]		
3-RRR	3-RPR	3-RPR	3-RRR	3-RPR	3-RPR	3-RRR	3-RPR	3-RPR	3-RRR	3-RPR	3-RPR
9.99E-07	8.12E-04	7.79E-04	6.09E-06	5.66E-04	5.66E-04	4.92E-06	1.00E-03	1.00E-03	5.53E-06	1.00E-03	1.00E-03

Orientation Deformation Maximum (deg)											
Fx = 0 Fy = 10 Mz = 1			Fx = 10 Fy = 0 Mz = 1			Fx = 10 Fy = 10 Mz = 0			Fx = 10 Fy = 10 Mz = 1		
3-RRR	3-RPR	3-RPR	3-RRR	3-RPR	3-RPR	3-RRR	3-RPR	3-RPR	3-RRR	3-RPR	3-RPR
2.78E-07	1.14E-04	1.14E-04	6.86E-06	1.08E-04	1.08E-04	5.40E-06	3.78E-05	3.78E-05	6.23E-06	1.08E-04	1.08E-04

Table 4.18: Comparison Mean Deformation Error of The 3-$\underline{R}$RR, The 3-R$\underline{P}$R, and The 3-$\underline{R}$PR Manipulators

Mean Position Deformation (m)											
[1.309 1.1185 0]			[1.309 0.9187 0]			[1.449 0.8787 0]			[1.489 0.7587 0]		
3-RRR	3-RPR	3-RPR	3-RRR	3-RPR	3-RPR	3-RRR	3-RPR	3-RPR	3-RRR	3-RPR	3-RPR
1.35E-06	4.07E-04	4.08E-04	1.22E-06	3.48E-04	3.48E-04	5.82E-07	2.61E-04	2.61E-04	4.50E-07	2.51E-04	2.51E-04

Mean Orientation Deformation (deg)											
Fx = 0 Fy = 10 Mz = 1			Fx = 10 Fy = 0 Mz = 1			Fx = 10 Fy = 10 Mz = 0			Fx = 10 Fy = 10 Mz = 1		
3-RRR	3-RPR	3-RPR	3-RRR	3-RPR	3-RPR	3-RRR	3-RPR	3-RPR	3-RRR	3-RPR	3-RPR
1.56E-06	2.69E-05	2.69E-05	1.05E-06	2.63E-05	2.63E-05	8.05E-07	2.14E-05	2.14E-05	7.09E-07	1.39E-05	1.39E-05

Mean Position Deformation (m)											
[1.309 1.1185 0]			[1.309 0.9187 0]			[1.449 0.8787 0]			[1.489 0.7587 0]		
3-RRR	3-RPR	3-RPR	3-RRR	3-RPR	3-RPR	3-RRR	3-RPR	3-RPR	3-RRR	3-RPR	3-RPR
8.04E-08	3.06E-04	2.22E-04	1.23E-06	2.01E-04	2.01E-04	1.08E-06	4.22E-04	4.22E-04	1.20E-06	4.22E-04	4.23E-04

Mean Orientation Deformation (deg)											
Fx = 0 Fy = 10 Mz = 1			Fx = 10 Fy = 0 Mz = 1			Fx = 10 Fy = 10 Mz = 0			Fx = 10 Fy = 10 Mz = 1		
3-RRR	3-RPR	3-RPR	3-RRR	3-RPR	3-RPR	3-RRR	3-RPR	3-RPR	3-RRR	3-RPR	3-RPR
-1.51E-07	2.97E-05	2.97E-05	1.75E-06	2.26E-05	2.26E-05	1.15E-06	6.70E-06	6.70E-06	1.37E-06	2.95E-05	2.95E-05

Chapter 5

Conclusions

The subject of this thesis was to analyze the manipulator's stiffness and to compare the manipulators in the term of their intrinsic stiffness properties. For this thesis, there are five manipulators under study, which are the RRRRR, the RPRPR, the 3-RRR, the 3-RPR, and the 3-RPR manipulators. Furthermore, stiffness models of these manipulator were successfully built with Virtual Joint Modeling method. Beside, the stiffness models of the manipulators were also constructed with RDM6 software for preliminary validation process. This validation process was done to verify if the developed stiffness models are correct or not.

Optimization of these five manipulators was conducted to find the optimum manipulator's parameters that meet two objective functions. In this case of study, the objective functions that aim to be realized, i.e., to minimize the total mass in motion and to minimize the compactness of the manipulator. In addition, the manipulators were also designed under the same specifications, which are the size of regular workspace, deformation maximum under a certain load, and the passive joint reactions.

Using their optimum design, the manipulators were compared in the term of their displacements with subject to a given forces and moments. For the 2-DOF manipulator, the comparison is conducted between the RRRRR and the RPRPR manipulator. The result of this comparison is the architecture of RPRPR manipulator was stiffer than the RRRRR manipulator. For the 3-DOF manipulator, the comparison is conducted among 3-RRR, the 3-RPR, and the 3-RPR manipulators. The result shows that the 3-RRR architecture has the lowest displacements value. This means that in the term of stiffness the 3-RRR architecture is the best among others.

Bibliography

[1] Vigen Arakelian, Sébastien Briot, and Victor Glazunov. Increase of singularity-free zones in the workspace of parallel manipulators using mechanisms of variable structure. *Mechanism and Machine Theory*, 43(9):1129–1140, September 2008.

[2] IA Bonev and CM Gosselin. Singularity loci of planar parallel manipulators with revolute joints. *2nd Workshop on Computational Kinematics*, 2001.

[3] Sébastien Briot, V Glazunov, and V Arakelian. Investigation on the Effort Transmission in Planar Parallel Manipulators. *Journal of Mechanisms and Robotics*, 5(1):011011, January 2013.

[4] Sebastien Briot, Anatol Pashkevich, and Damien Chablat. Optimal technology-oriented design of parallel robots for high-speed machining applications. *2010 IEEE International Conference on Robotics and Automation*, pages 1155–1161, May 2010.

[5] Stéphane Caro, Waseem Ahmad Khan, Damiano Pasini, and Jorge Angeles. The rule-based conceptual design of the architecture of serial Schönflies-motion generators. *Mechanism and Machine Theory*, 45(2):251–260, February 2010.

[6] Stéphane Caro, Raza Ur-Rehman, Damien Chablat, and Philippe Wenger. Multi-objective Design Optimization of 3-PRR Planar Parallel Manipulators. In *Global Product Development*, pages 1–10, 2010.

[7] JSZF Chu and ZJ Feng. Mobility of Spatial Parallel Manipulators, Parallel Manipulators, towards New Applications. Number April. InTech, huapeng wu edition, 2008.

[8] HR Mohammadi Daniali, P.J. Zsombor-Murray, and Jorge Angeles. Singularity analysis of planar parallel manipulators. *Mechanism and Machine Theory*, 30(5):665–678, 1995.

[9] 1930 Fu. *Robotics : control, sensing, vision, and intelligence / K.S. Fu, R.C. Gonzalez, C.S.G. Lee.* McGraw-Hill,, New York, internatio edition, 1987.

[10] G Gogu. *Structural Synthesis of Parallel Robots: Part 3: Topologies with Planar Motion of the Moving Platform*. Solid mechanics and its applications. Springer, 2010.

[11] Grigore Gogu. *Structural Synthesis of Parallel Robots*. Springer Netherlands, 2008.

[12] Tian Huang, Zhanxian Li, Meng Li, Derek G Chetwynd, and Clément M Gosselin. Conceptual design and dimensional synthesis of a novel 2-DOF translational parallel robot for pick-and-place operations. *Journal of Mechanical Design*, 126:449, 2004.

[13] X.-J. Liu and J. Wang. Some New Parallel Mechanisms Containing the Planar Four-Bar Parallelogram. *The International Journal of Robotics Research*, 22(9):717–732, September 2003.

[14] JP Merlet. *Parallel robots*. Springer, AA Dordrecht, 2nd edition, 2001.

[15] Leila Notash. A methodology for actuator failure recovery in parallel manipulators. *Mechanism and Machine Theory*, 46(4):454–465, April 2011.

[16] Anatol Pashkevich, Damien Chablat, and Philippe Wenger. Stiffness analysis of overconstrained parallel manipulators. *Mechanism and Machine Theory*, 44(5):966–982, May 2009.

[17] Anatol Pashkevich, Alexandr Klimchik, Damien Chablat, and Philippe Wenger. Stiffness Analysis of Multi-Chain Parallel Robotic System With Loading. *Automation, Mobile Robotics and Intelligent Systems*, 3(3):75–82, 2009.

[18] Tanio K Tanev. Kinematics of a hybrid (parallel ± serial) robot manipulator. *Mechanism and Machine Theory*, 35:1183–1196, 2000.